Studying the Fabrication of Electrically-conductive Nanocomposite Membranes for wastewater treatment

by

Zahra Zandi

A thesis submitted in partial fulfillment of the requirements for the degree of

Master of Science

Department of Mechanical Engineering
University of Alberta

Abstract

Membrane separation processes are crucial in separating various solutes from water sources, including ions, colloids, macromolecules, and organic matter. Among membrane technologies, ultrafiltration (UF) has emerged as a powerful method for effectively removing organic matter and macromolecules from wastewater treatment. Despite their efficacy, membrane fouling remains a significant challenge, impacting permeate flux, membrane lifespan, and energy consumption in widespread membrane technology applications for wastewater treatment. Surface modification is a crucial strategy in minimizing membrane fouling, offering a powerful technique to prevent fouling by altering membrane surface properties. This involves tuning the surface physicochemical properties (wettability, roughness, and charge) by various methods such as chemical grafting, coating, and plasma treatment. An innovative approach to mitigate fouling includes incorporating conductive elements like MXene nanosheets and silver nanoparticles onto the membrane surface. Applying electric potential to conductive membranes is an emerging electrochemical technique for fouling mitigation through various mechanisms, including electrochemical reactions, gas bubble generation, and electrostatic repulsive forces.

In the project's first phase, Ti_3C_2 MXene was employed to produce electro-conductive antifouling polyamide-imide (PAI) membranes. The fabrication involved the phase inversion technique for the PAI membrane and a pressure-assisted filtration method to coat MXene on the PAI membrane surface. Different Ti_3C_2 MXene and carboxymethyl cellulose (CMC, as a binder) concentrations were used to tune the physicochemical properties of PAI membrane surfaces. A cathodic potential was applied in an experimental electrochemical membrane cell, and the Ti_3C_2 MXene-modified PAI membrane with the highest MXene content exhibited maximum conductivity. Evaluating the membrane performance in cathodic electro-reduction (CER), using various aqueous solutions of humic acid (HA), sodium alginate (SA)/calcium chloride ($CaCl_2$), and bovine serum albumin (BSA) as model foulants, revealed significant improvement in flux decline ratio (FDR) and flux recovery ratio (FRR) with applied electric potential. For example, applying a 4V cathodic potential resulted in FDR and FRR less than 1% and 99.83%, respectively. Without voltage, the MXene-coated PAI membrane showed FDR and FRR of 45.56% and 92.51%, respectively.

In the second phase of this study, a silver nanoparticle ink was applied to the surface of PAI membranes. The impact of the highly conductive silver coating layer was examined to produce electroconductive UF membranes with enhanced antifouling and dye rejection properties. Using 3 mL of silver nanoparticle ink to coat a 1000 cm^2 area of a PAI membrane resulted in a membrane that demonstrated exceptional resistance to fouling when subjected to SA/$CaCl_2$ as a model foulant. The modified Ag-coated PAI membrane exhibited a FDR of 42.94% and a high flux FRR of 80.41%, outperforming the pristine PAI membrane, which had a 59.58% FDR and a 49.14% FRR. This represents an improvement of approximately 16.6% in FDR and 31% in FRR. The enhanced antifouling properties of the modified Ag-coated membrane can be attributed to the high electrostatic repulsion between the Ag-coated PAI membrane and foulants facilitated by the high negative surface charge induced by the cathodic potential applied to the membrane surface.

This study showcases the considerable potential of conductive elements in tackling antifouling challenges, improving dye removal, and generating value-added solutions for water treatment. It introduces a groundbreaking approach to developing high-performance membranes by integrating conductive materials, thus paving the way for innovative advancements in water treatment.

Keywords: Ti_3C_2 MXene; Silver nanoparticles; Electroconductive membranes; ultrafiltration; nanofiltration; surface modification; fouling; dye removal; wastewater treatment

Preface

This dissertation is an original work by Zahra Zandi. No part of this thesis has been previously published.

This thesis highlights the first applications of lab-fabricated PAI membranes for synthesizing electro-conductive membranes utilizing various conducting elements to treat wastewater by improving the antifouling performance of the membrane in the presence of the applied electrical potential.

Specifically, a version of chapter 2 of this thesis, "Development of Electro-Conductive Ti_3C_2 MXene Multilayered Membranes: Dye Removal and Antifouling Performance," has been submitted to the "*Advanced Functional Materials"* journal. I was responsible for performing all experiments, data collection and analysis as well as the manuscript composition. Mohtada Sadrzadeh and Masoud Rastgar were the supervisory authors and involved with concept formation and manuscript composition. Mojtaba Mohseni, Waralee Dilokekunakul, and Mathias Wessling assisted with some electrochemical analysis. Ahmad Rahimpour, Mostafa Dadashi Firouzjaei, and Babak Anasori contributed to manuscript edits.

Additionally, a version of chapter 3, entitled "Developing Electrically-Conductive Silver-Coated Polyamide-imide membranes for Sustainable Dye Removal and Antifouling Performance" has been prepared for submission. I was responsible for performing all experiments, data collection and analysis as well as the manuscript composition. Mostafa Dadashi Firouzjaei and Mehrasa Yassari contributed to the manuscript formation and edits.

I am the first author of these two works mentioned above.

Dedicated to my parents and my husband,

Masoumeh, Ahmad, and Hadi

For their endless love and support.

I always love you.

Acknowledgement

Completing my M.Sc. studies at the University of Alberta had always been one of my cherished dreams and this achievement would not have been possible without the unwavering support and help of some incredible persons, to whom I would like to express my heartfelt appreciation.

First and foremost, I would like to thank my supervisor, Prof. Mohtada Sadrzadeh. You have always been more than a supervisor to all of us. Your endless support, motivation, enthusiasm, and guidance in both academic and personal life always inspired me and made me persevere. I am truly proud to have the privilege to collaborate with you and learn from you.

My gratitude extends to my committee members, Dr. Benjamin Cheung, and Dr. Ge Li, for their guidance and support. I would like to take the opportunity and thank Prof. Ahmad Rahimpour and Dr. Masoud Rastgar for their treasured support, mentorship, tremendous encouragement and understanding.

I also appreciate all the support that I received from Dr. Pooria Karami, Dr. Mehrasa Yassari, Mizanul MD. Mizan, Farah Rahman Omi, Amirhossein Taghipour, Sadegh Aghapour Aktij, Fatima Seyedpour Taji, Amir Aghaei, Afrouz Yousefi, Nazanin Chitgar, Kazem Moradi, and Amir Aghaei. Thank you all!

I can not express enough thanks to my family for their unconditional love, care, and support. You have always been there for me, and I feel secure knowing that you will always have my back. Undoubtedly, without your help and love, the fulfillment of this study was impossible.

Table of Contents

List of Tables

List of Figures

Abbreviation

AFM	Atomic force microscopy
AOP	Advanced oxidation processes
BSA	Bovine serum albumin
CER	Cathodic electro-reduction
CMC	Carboxymethyl cellulose
CNT	Carbon nanotube
CV	Cyclic voltammetry
DI	Deionized
DET	Direct electron transfer
DMAc	N, N-dimethylacetamide
ECM	Electro-conductive membrane/ Electrically-conductive membranes
EDX	Energy-dispersive X-ray
EIPS	Evaporation induced phase separation
FESEM	Field emission scanning electron microscopy
GA	Glutaraldehyde
GO	Graphene oxide
HA	Humic acid
HER	Hydrogen evolution reaction
ICP-OES	Inductively coupled plasma-optical emission spectroscopy
LBL	Layer-by-layer
LIG	Laser induced graphene
LMH	L m^{-2} hr^{-1}
LSV	Linear sweep voltammetry
MD	Membrane distillation
MF	Microfiltration
MMMs	Mixed Matrix Membranes
MO	Methyl orange
MW	Molecular weight
MWCO	Molecular weight cut-off
NF	Nanofiltration

NIPS	Nonsolvent induced phase separation
OER	Oxygen evolution reaction
PAI	Polyamide-imide
PANI	Polyaniline
PEG	Polyethylene glycol
PPy	Polypyrrole
PSF	Polysulfone
PVC	Polyvinyl Chloride
PVP	Polyvinylpyrrolidone
RB	Reactive black
rGO	Reduced graphene oxide
RO	Reverse osmosis
ROS	Reactive oxygen species
RR120	Reactive red 120
SA	Sodium alginate
SAD	Surface area difference
SHE	Standard hydrogen electrode
TEM	Transmission electron microscopy
TIPS	Temperature induced phase separation
Ti_3C_2	Titanium carbide
TMP	Transmembrane pressure
TOC	Total organic carbon
UF	Ultrafiltration
UWOCA	Under-water oil contact angle
UV	Ultraviolet
VIPS	Vapor induced phase separation
WCA	Water contact angle
XDLVO	Extended Derjaguin, Landau, Verwey and Overbeek
XPS	X-ray photoelectron spectroscopy

Nomenclature

A_m	Effective filtration area of membrane
Ag	Silver
c_i	Concentration of component *i*
C_f	Total organic carbon concentration of feed
$C_{i,p}$	Solute concentration in the permeate solution
$C_{i,f}$	Solute concentration in the feed solution
C_f	Concentration of dye in feed solution
C_p	Concentration of dye in permeate solution
dP/dx	Pressure gradient across a porous membrane
FDR_t	Total flux decline ratio
FRR	Flux recovery ratio
J_i	Transfer rate of component *i* across the membrane
J_w	Pure water flux in dye removal tests
J_{w1}	Initial pure water flux of fouling tests
J_{wf}	Permeate flux of foulant solution
J_{w2}	Recovered pure water flux after washing step of membrane fouling test
k	Mass transfer coefficient
m	Permeate mass
R_t	Total resistance of the membrane
R_m	Inherent hydrodynamic resistance of the membrane
R_c	Membrane resistance caused by the cake layer formation
R_{cp}	Membrane resistance caused by the concentration polarization
R_{avg}	Average surface roughness
R_{rms}	Root mean square roughness
r	Wenzel roughness ratio
r_p	Pore radius
T	Absolute temperature
ΔP	Transmembrane pressure
$\Delta\pi$	Transmembrane osmotic pressure
Δt	Time interval

ΔG	Free energy of adhesion
ρ	Water density
μ	dynamic viscosity
θ	Contact angle

Superscripts

AB	Acid-base
LW	Lifshitz-van der Waals
EL	Electrostatic
CO	Cohesion
TOT	Total
$+$	Electron acceptor
$-$	Electron donor

Subscripts

m	Membrane
l	Liquid
f	Foulant
s	Solid surface (membrane)

Chapter 1

Introduction

1.1 Water demand

Water scarcity is a critical global challenge that has attracted significant attention recently due to its far-reaching implications for human well-being, environmental sustainability, and socio-economic development. The scarcity of freshwater resources, exacerbated by factors such as population growth, climate change, and unsustainable water management practices, poses a critical challenge for numerous regions worldwide. According to the United Nations, nearly half of the world's population will be living in areas of high water stress by 2030 [1]. This alarming statistic underscores the urgency of addressing water scarcity and implementing effective strategies to ensure access to safe and sufficient water resources for all humans. The consequences of water scarcity are multifaceted and wide-ranging. From an environmental standpoint, dwindling water supplies disrupt ecosystems, impair biodiversity, and degrade aquatic habitats [2]. Moreover, water scarcity intensifies the vulnerability of agricultural systems as farmers struggle to meet crop irrigation needs, resulting in reduced yields and food insecurity [3].

In addition to water contamination issues, global water demand is estimated to increase by 20-30% by 2050 [4]. Over 7% of the global population will face at least one month of water scarcity annually [4]. Moreover, Canada grapples with increasing water demands and potential risks to water quality. This concerning trend is driven by population growth, climate change, industrial and agriculture activities, leading to concerns about overconsumption and escalating water shortages. To ensure the long-term availability of freshwater, it becomes crucial to implement sustainable allocation strategies and promote efficient water use[5].

Nowadays, human beings are struggling with water-related challenges, such as the contamination and scarcity of freshwater resources [6,7]. To address such pressing issues, researchers worldwide are actively exploring novel technologies that can efficiently eliminate contaminants from water while minimizing energy consumption [8,9]. Nations can take practical steps toward sustainable development by implementing cost-effective and energy-efficient techniques for treating, recycling, and reusing industrial, agricultural, and domestic wastewater. This holistic approach to water management contributes to preserving precious water resources and addresses the main goals of environmental protection and sustainable growth.

Among the various techniques being proposed thus far, advanced oxidation processes (AOPs) such as the Fenton reaction [10], ozone/UV [11], and photocatalysis [12], along with membrane-based technologies [13], stand out as highly promising approaches. Advanced oxidation processes involve generating highly reactive species that can effectively degrade and remove contaminants in water [14]. The Fenton reaction, for instance, utilizes a combination of hydrogen peroxide and ferrous ions to generate hydroxyl radicals, which exhibit strong oxidative capabilities. Ozone/UV technology involves the application of ozone and ultraviolet (UV) light, which produce hydroxyl radicals and other reactive species that can break down pollutants. Photocatalysis utilizes semiconductors, such as titanium dioxide (TiO_2), to generate electron-hole pairs under light irradiation, enabling the degradation of organic pollutants [15]. In addition to AOPs, membrane-based technologies, e.g., reverse osmosis (RO) and nanofiltration (NF), offer effective filtration and separation of contaminants based on their size and molecular properties [16]. Membranes can remove particles, ions, and dissolved organic compounds, ensuring high-quality treated water. Researchers aim to achieve efficient and sustainable water treatment solutions for various applications by harnessing the potential of oxidation processes and membrane technology.

1.2 Membrane technology for wastewater treatment applications

Recent advancements in membrane design and fabrication have paved the way for innovative membrane materials, thereby positioning membranes as a superior option for water treatment compared to alternative methods [17,18]. Membrane technologies offer distinct advantages such as high selectivity, scalability, and ease of operation [19]. Developing new membrane materials, including polymeric, ceramic, and composite membranes, has significantly enhanced their performance and durability [12,13]. For instance, incorporating nanomaterials and advanced surface modifications has improved membrane properties such as permeability, fouling resistance, and antimicrobial activity [20,21]. These advancements have resulted in membranes that exhibit superior performance in terms of contaminant removal, energy efficiency, and cost-effectiveness compared to conventional water treatment methods.

Membrane separation processes have emerged as promising technologies for water purification, offering several advantages over conventional processes such as lime softening, ion exchange, distillation, and evaporation [22–24]. One key advantage is the ability of membrane processes to provide high-quality filtrate, ensuring the effective removal of contaminants, particles, and dissolved substances [25,26]. The selective permeability of membranes allows for precise separation, resulting in purified water that meets stringent quality standards. In addition to high filtrate quality, membrane separation processes offer lower operating expenses and a compact design [21,26]. Membrane systems can be modular and easily scaled up or down to meet specific water treatment needs, providing flexibility and cost-effectiveness [22,24]. The compact design of membrane modules enables efficient space utilization, making them suitable for both centralized and decentralized water treatment applications [22,24]. Moreover, membrane separation processes have smaller environmental footprints and require less energy than traditional processes [16,19]. Conventional methods often involve using chemicals, large infrastructure, and energy-intensive operations, leading to higher environmental impacts. In contrast, membrane separation processes operate based on physical filtration mechanisms, reducing the need for chemical additives and minimizing energy consumption [19]. These advantages make membrane separation processes more sustainable and environmentally friendly options for water purification. Consequently, membranes are increasingly recognized as a preferred choice for various applications, including desalination, wastewater treatment, and drinking water purification, supporting the achievement of sustainable and reliable water supplies.

The required driving force for filtration in membrane processes can be classified into different categories: pressure, electric field, concentration gradient, and temperature [27,28]. Among these, pressure-driven membrane processes are widely utilized to treat liquids containing dissolved or dispersed contaminants. Among these, pressure-driven membrane processes, such as MF, UF, NF, and RO, are widely utilized to treat liquids containing dissolved or dispersed pollutants due to their ability to selectively remove particles, ions, colloids, and macromolecules based on their size and charge [15,27–29]. The selection of a membrane process for a certain application depends on the size of the solutes that need to be removed [30]. MF membranes typically have an average pore size ranging from 0.05 μm to 10 μm. These membranes effectively retain large particulate matter and colloidal organic substances [31]. They are commonly used in industrial water treatment processes to remove suspended solids, turbidity, and certain microorganisms. UF membranes have pore diameters typically ranging from 100 nm to 10 μm in the top layer. These membranes are extensively employed to eliminate bacteria, organic molecules, and macromolecules such as proteins [32]. UF membranes are used in various applications, including drinking water production, wastewater treatment, and food and beverage processing. NF membranes have an average pore size of 1 to 10 nm [15]. These membranes are particularly suitable for water softening and separating divalent ions from wastewater streams. NF membranes can selectively remove ions while allowing smaller molecules and monovalent ions to pass through, offering effective water treatment and ion separation. RO membranes have the smallest pore size, less than 1 nm, making them the densest membranes available. RO membranes are primarily used for desalination, separating monovalent ions, and producing high-quality drinking water from seawater or brackish water. The high-pressure applied in RO processes helps remove dissolved salts, organic compounds, and other contaminants, resulting in purified water [33–35].

1.3 Membrane fabrication techniques for porous and dense membranes

The fabrication of polymeric membranes involves various techniques which are chosen based on the desired properties of the membranes. **Figure 1.1** classifies membrane fabrication techniques by bulk morphology and internal free volume of membranes. Among these techniques, phase inversion is the most versatile fabrication technique widely used to synthesize both isotropic and anisotropic porous membranes [33,36]. The phase inversion technique offers several advantages for membrane fabrication, including simplicity, versatility, and the ability to control pore size and morphology. By adjusting the composition of the polymer solution and the process conditions, such as temperature and evaporation rate, the properties of the resulting membrane can be tailored to meet specific requirements [35]. This technique has been widely employed in producing porous polymeric membranes for various applications, including water treatment and gas separation [33].

As the term phase separation implies, during this fabrication process, a one-phase casting liquid solution is precipitated into two separate phases: a solid (polymer-rich phase that forms the membrane matrix) and a liquid (polymer-poor phase that creates the membrane pores). Therefore, this separation process relies on the separation of solvent and non-solvent in a polymer solution, forming a porous polymer film [33,35]. During the phase inversion process, precipitation of the liquid polymer solution can be performed through multiple methods. Precipitation can be achieved by immersing the polymer solution in a non-solvent bath, typically a water bath (nonsolvent-induced phase separation or NIPS) [33]. Precipitation can also occur by exposing the polymer solution to water vapor from a humid atmosphere (vapor-induced phase separation or VIPS) [37]. Another precipitation method entails casting a film from a high-temperature polymer solution and subsequently lowering the temperature to initiate the precipitation (temperature-induced phase separation or TIPS) [33]. An additional precipitation method is casting a polymer solution, which may not necessarily be at high temperature and includes a volatile solvent along with a non-solvent (typically water) (evaporation-induced phase separation or EIPS) [37]. As the volatile solvent evaporates, the cast film becomes increasingly enriched in the non-solvent, leading to eventual precipitation.

Among these methods, NIPS is the most widely used technique for fabricating porous membranes. In the NIPS method, a homogeneous polymer solution is first cast onto a flat surface and then placed into a container filled with a nonsolvent called the coagulation bath. The phase inversion process is controlled by the diffusion of low molecular weight constituents, which include the solvent and the nonsolvent, typically water. As the polymer film is immersed in the coagulation bath, the solvent in the polymer solution is gradually replaced by the nonsolvent. This results in changes in the composition of the polymer film until the composition of the polymer-rich phase reaches the glass transition composition, leading to solidification. Once solidified, the film's structure is fixed, and a polymer membrane with a porous or dense structure is formed [33,37]. The NIPS method offers several advantages, such as simplicity, scalability, and the ability to control the morphology and pore size of the resulting membranes. It has been widely utilized in various applications, including water treatment, gas separation, and biomedical fields [33].

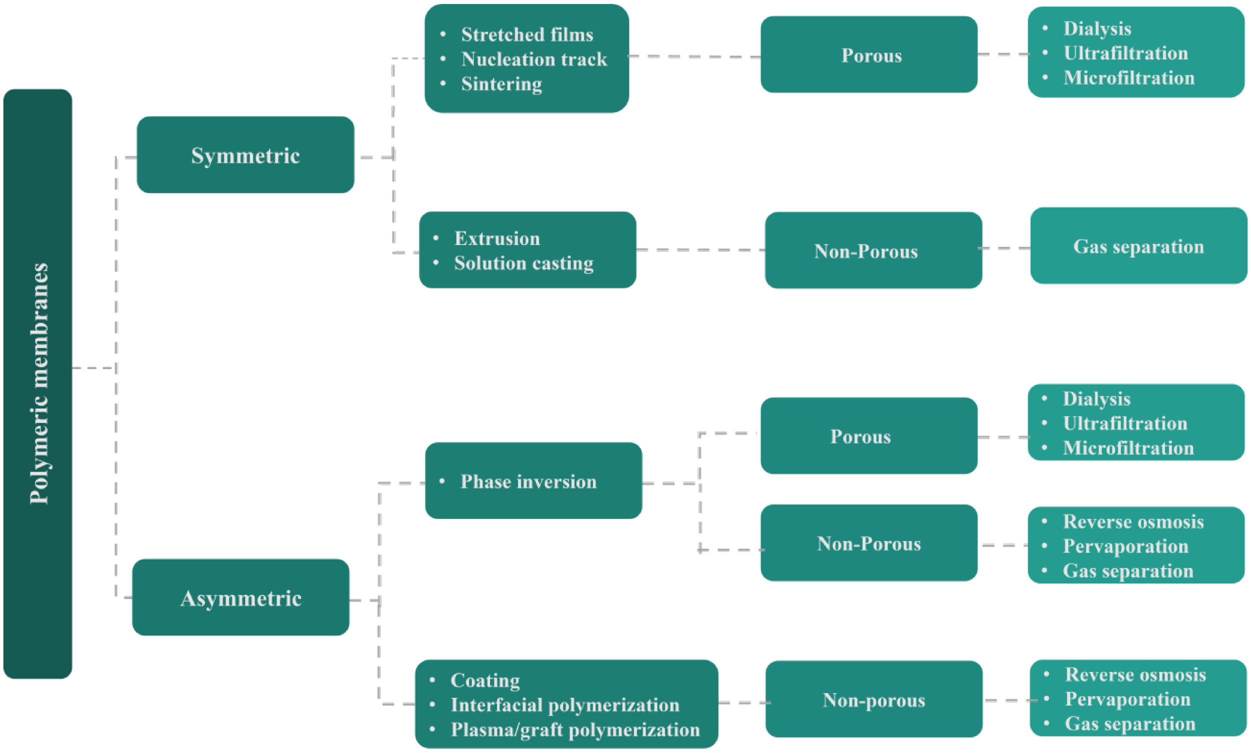

Figure 1.1: Classification of polymeric membranes based on their overall structure, fabrication method, and applications [33,37].

1.4 Theoretical background on transport phenomena in membrane processes

The theory of mass transport through membranes is essential in understanding membrane separation processes. The primary and most important characteristic of a membrane process is the capability of the membrane to control the permeation of various components within the feed solution. In microporous membranes, separation occurs through a molecular sieving mechanism based on the shape and the size of the solutes compared to the membrane pores. In this mechanism, some of the permeants are prevented from entering the membrane pores while others can pass through [33]. Surface pores in these membranes are smaller than some particles in the feed solution, leading to the accumulation of these particles on the membranes' surface [33].

The chemical potential gradient drives the permeation of a component through a membrane and can be described by **Equation 1.1**, which relates the component flux (J_i) to the chemical potential gradient $\frac{d\mu_i}{dx}$ and a proportionality coefficient (L_i). Different driving forces, such as pressure, concentration, electrical potential, and temperature differences, are associated with the chemical potential gradient.

$$J_i = -L_i \frac{d\mu_i}{dx} \qquad 1.1$$

For pressure-assisted membrane processes, the pore-flow model describes the permeation mechanism in a porous medium [33]. According to this model, the permeants are transferred through a membrane by pressure-driven convective flow across tiny pores [33]. Darcy's law (**Equation 1.1**) is the basic equation for describing transport in porous media relating the flux (J_i) to the pressure gradient across the membrane ($\frac{dp}{dx}$), a coefficient representing the structural factors of the porous medium (K'), and c_i represents the concentration of component i [37–39]. Darcy's law explains the membrane transport phenomenon in that the pores are relatively large, fixed, and attached to one another [33]. For these membranes, the pores do not oscillate in volume or location on the permeant motion timescale [33]. **Equation 1.2** governs the flow in porous media for the pressure-assisted membrane process.

$$J_i = -K' c_i \frac{dp}{dx} \qquad 1.2$$

Where $\frac{dp}{dx}$ is the pressure gradient across the membrane, k' is a coefficient representing the nature of medium and c_i is the concentration of component i.

The Darcy's law equation can also be expressed as **Equation 1.3**, where the transmembrane pressure (ΔP), dynamic viscosity of the permeate (μ), and hydrodynamic resistance of the membrane (R_m) are considered.

$$J_w = \frac{\Delta P}{\mu R_m} \qquad 1.3$$

The hydrodynamic resistance of the membrane (R_m) can be determined using the Hagen-Poiseuille equation (**Equation 1.4**) for MF/UF membranes. According to **Equation 1.4**, the transport through the membrane is directly proportional to the fourth power of the pore radius.

$$R_m = \frac{8\delta_m}{n_p \pi r_p^4} \qquad 1.4$$

The resistance to water crossing through membranes in membrane processes includes the hydrodynamic resistance of the membrane in the absence of foulants, the resistance due to foulants accumulation on the membrane surface (cake formation, fouling), and the resistance resulting from the accumulation of low molecular weight solutes at the membrane surface, known as concentration polarization [40].

Concentration polarization is characterized by the transmembrane osmotic pressure ($\Delta\pi$), which diminishes the effective pressure driving force for solvent transport. In the context of fouling experiments, Darcy's law can be modified to incorporate the impact of concentration polarization. The modified equation is given as **Equation 1.5**.

$$J = \frac{\Delta P_t - \Delta \pi}{\mu \, R_t} \qquad 1.5$$

Where J represents the flux observed in fouling experiments, ΔP_t denotes the transmembrane pressure difference, $\Delta\pi$ signifies the transmembrane osmotic pressure, μ represents the dynamic viscosity of the permeate, and R_t denotes the total resistance against mass transfer. This equation captures the effect of concentration polarization, which reduces the effective pressure driving force, on the water flux during fouling experiments.

In the context of UF, the osmotic pressure, $\Delta\pi$, is often considered negligible as the primary contribution to osmotic pressure comes from low molecular weight solutes capable of passing through the UF membrane. Furthermore, since the concentration of these solutes is typically the same on both the feed and permeate sides, the osmotic pressure difference is negligible [37].

In membrane processes like UF, the total resistance is composed of multiple factors, including the inherent hydrodynamic resistance of the membrane, the resistance caused by the cake layer, the resistance due to concentration polarization, and potentially other contributing factors. These resistances collectively affect the overall mass transfer through the membrane. Therefore, the total resistance, R_t, in **Equation 1.6** is described as follows.

$$R_t = R_m + R_c + R_{cp} + \cdots \qquad 1.6$$

Where R_m is the inherent hydrodynamic resistance of the membrane, R_c represents the resistance caused by the cake layer that forms and accumulates on the membrane surface, and R_{cp} denotes the resistance attributed to concentration polarization. Another crucial parameter for evaluating membrane separation performance is the membrane's rejection. The rejection of a membrane can be expressed as **Equation 1.7**.

$$R_j = 1 - \frac{C_{i,p}}{C_{i,f}} \qquad 1.7$$

Where $C_{i,p}$ and $C_{i,f}$ represent the solute concentration in the permeate and feed solutions, respectively. The rejection value indicates the extent to which the membrane prevents the passage of a specific solute, with higher rejection values indicating more effective separation. It is important to note that the rejection is typically influenced by various factors, including the properties of the solute, membrane characteristics, operating conditions, and fouling/cake layer formation on the membrane surface. Thus, the rejection value provides valuable information about the membrane's separation efficiency and its suitability for specific applications.

1.5 Filtration configurations

In membrane filtration setups, there are two process configurations: dead-end filtration and cross-flow filtration. In dead-end filtration, the feed stream is directed perpendicularly to the membrane surface. As filtration progresses, the retained particles accumulate, forming a cake layer on the membrane surface. The thickness of the cake layer increases over time, resulting in a reduction in the permeation rate. Dead-end filtration is characterized by a decreasing flux as the cake layer thickness grows.

On the other hand, in cross-flow filtration, the feed flow is parallel to the membrane surface. This configuration offers several advantages compared to dead-end filtration. Cross-flow filtration exhibits improved fouling tolerance, as the flow helps to continuously sweep away particles from the membrane surface, minimizing cake formation. It allows for higher sustainable flux rates since the cross-flow helps prevent complete blockage of the membrane by the retained particles. Cross-flow filtration requires less frequent cleaning and can extend the membrane's lifetime by reducing fouling. Therefore, these benefits make cross-flow filtration a preferred configuration in many applications, especially when dealing with complex feed streams.

1.6 Membrane fouling

As a cost-effective alternative to conventional water treatment methods, the membrane separation technique should not only provide a fast rate of high-quality permeate but also need to maintain a consistently high production rate over an extended period. Therefore, fouling is the major challenge of membrane technology, significantly impeding its widespread application. The term “fouling” describes the undesired deposition of colloids, particles, and macromolecules on the surface of the membrane and inside the pores [41,42]. As fouling occurs, the permeation flux declines, necessitating higher operating pressure or increased energy consumption to achieve the desired throughput.

Organic fouling on membranes is a multifaceted phenomenon that arises from specific and nonspecific interactions between foulants and the membrane surface [43]. Specific interactions involve covalent bonding and coordination between specific functional groups, such as metal-carboxyl and amino-carboxyl groups. Nonspecific interactions include van der Waals forces, hydrophobic interactions, hydrogen bonding, and electrostatic interactions [44]. Various physical and chemical parameters can influence membrane fouling, including membrane properties (surface roughness, charge, hydrophobicity/hydrophilicity, surface functional groups, and pore size distribution), feed compositions (foulant type, concentration, pH, and ionic strength), and hydrodynamic conditions (cross-flow velocity, temperature, flux, and transmembrane pressure).

Based on the operational characteristics of the membrane and the chemical composition of foulants, various types of fouling can happen in a membrane system. Fouling can be classified as particulate/colloidal fouling, inorganic fouling or scaling, organic fouling, and biofouling [45]. Colloidal fouling refers to attaching suspended and colloidal particles with sizes from a few nanometers up to a few micrometers to the membrane surfaces [30]. The formation of scale is caused by increasing the concentration of minerals and divalent ions above their solubility limits, leading to the ultimate precipitation of these materials on the membrane surface [41]. Organic fouling occurs by depositing organic compounds such as humic substances, proteins, and polysaccharides at the membrane surface [31]. Biologically active organisms cause biofouling, including the colonization and growth of microbial organisms, leading to the formation of microbial biofilms at the membrane surface [30,41].

Various characteristics of the membrane surface, including hydrophilicity, roughness, and charge, are known to strongly affect the fouling tendency of membranes. The literature has a consensus that hydrophilic surfaces are less prone to fouling. The hydrogen bonding between water molecules and the membrane hydrophilic functional groups forms a thin layer of bounded water on the membrane surface. This layer prevents or decreases the undesirable adsorption/adhesion hydrophobic interactions of foulants to the membrane surface [33]. The surface roughness of membranes also strongly affects their fouling tendency. A higher surface roughness provides more surface area on membranes to attach foulants. Additionally, the ridge-and-valley structure of rough membranes favors the accumulation of foulants in the valley regions [33]. Therefore, it is likely that the membranes with rougher surfaces are more susceptible to fouling [34]. Also, the surface charge of membranes plays an important role in their antifouling properties. It is common to employ a membrane with the same surface electric charge as the foulants so that the electrostatic repulsion forces between the foulant and the membrane surface prevent the deposition of foulants on the membrane and thus mitigate the fouling [41].

1.7 Literature review

Membranes have experienced continuous growth since their first synthesis in 1907, primarily due to their wide range of practical applications. Extensive research efforts have been dedicated to improving membrane performance regarding permeation, rejection, and fouling resistance. A trade-off relationship exists between permeability and selectivity in conventional membranes, wherein high water flux membranes often exhibit low rejection rates and vice versa. However, enhanced membrane surface properties can impede fouling. Consequently, a key objective of membrane research has consistently been the development of high-flux membranes with excellent separation efficiency and low fouling propensity.

The field of membrane technology has witnessed significant advancements aimed at improving membrane fabrication processes [46,47], developing nanocomposite membranes by using multifunctional nanomaterials [48–51], exploring new polymeric materials for support layers [52], and improving the surface properties of membranes [53,54]. Researchers have focused on optimizing the manufacturing processes to improve membrane fabrication processes. This includes refining the casting methods, modifying the composition of casting solutions, and controlling the parameters involved in membrane fabrication [46,47]. Fabrication of nanocomposite membranes by incorporating multifunctional nanomaterials into membrane matrices has also gained significant attention. These nanomaterials offer unique properties that can enhance membranes' bulk and surface properties. They can improve hydrophilicity, antifouling properties, mechanical strength, and selectivity [48–51]. Various nanomaterials, including metal oxides, graphene, carbon nanotubes, and MXenes, have been explored for their potential to improve membrane performance. Furthermore, improving the surface properties of composite membranes has been a key area of research. By modifying the surface characteristics, such as roughness, charge, and hydrophobicity/hydrophilicity, researchers could effectively enhance membrane performance in terms of fouling resistance, flux, and selectivity [53,54]. Surface modification techniques, including surface grafting, coating, and functionalization, have been employed to achieve the desired membrane surface properties. Despite successful results in the literature [55–58], the achieved impact on fouling reduction during long-term operations remains insufficient [59–62]. Researchers have, therefore, been actively exploring the development of advanced smart membranes that can effectively modulate membrane water flux and improve membrane fouling performance in practical applications. The application of an electric filed has attracted significant attention due to its precision, and practical implementation, and ease of control. As a result, ECMs have emerged as promising solutions for mitigating fouling issues. Over the past decade, applications of conductive membranes have attracted significant attention in membrane-based water treatment technologies, driven by their potential in membrane fouling mitigation and membrane selectivity performance. Researchers have explored the potential of electrically conductive membranes for a wide range of applications, including fouling mitigation [63–65]. These membranes, known as electro-conductive or electrically active membranes, possess unique properties that make them suitable for various purposes.

ECMs exhibit various action mechanisms depending on the type of applied potentials (cathodic, anodic, or alternating potential). Under anodic conditions, dominant action mechanisms against various foulants include direct oxidation, translational motion, and reduction in local pH might occur. Conversely, cathodic conditions result in electrostatic repulsion, indirect oxidation due to reactive oxygen species (ROS) generation, and local pH change as the primary action mechanisms. Using alternating potential can enhance fouling mitigation efficiency by combining the action mechanisms of both anodic and cathodic potentials. The major reported mechanisms for ECMs are the Joule heating effect, piezoelectric vibration, and bubble generation. Recent studies have demonstrated that the accumulation of charged particles on the membrane surface can be reduced to some extent by applying a constant electric potential to the electrically conductive membrane through electrostatic repulsion and electrochemical reactions [66,67]. Moreover, using an electromagnetic field can minimize fouling by altering the physicochemical properties of the feed solution, such as pH and ionic strength, and by disrupting the adhesion of foulants to the membrane surface [68–70]. This strategy offers the advantage of leveraging the dual effects of electrostatic repulsion and gas bubble generation [71] as well as the electrochemical oxidation/reduction of foulants on the membrane surface [71–74]. The application of an electric field induces electrostatic repulsion forces between the foulants and the membrane surface, preventing their adhesion and reducing fouling propensity. Additionally, the electric field promotes the formation of gas bubbles on the membrane surface, which can further hinder foulant deposition by creating a physical barrier. Furthermore, electrochemical processes induced by the electric field can facilitate the oxidation or reduction of foulants, thereby enhancing their removal from the membrane surface. These mechanisms collectively contribute to the fouling control capabilities of electro-conductive membranes. Several studies have investigated the effectiveness of this approach, demonstrating its potential for mitigating fouling in various membrane systems [71–74].

ECMs have been effectively fabricated from various materials, encompassing organic and inorganic materials such as conductive polymers, carbon-based nanomaterials, and metals, using multiple fabrication techniques [75–80]. **Table 1.1** summarizes all conductive elements that have been used so far to fabricate ECMs. Extensive research in electro-conductive membranes has led to significant progress in developing fabrication techniques and material designs to enhance their performance. Various methods have been employed, including electrospinning, interfacial polymerization, and the integration of conductive nanoparticles or polymers [60]. These strategies enable the production of membranes with customized properties, such as desired conductivity levels, improved stability, and enhanced selectivity for specific applications. As a result, conductive membranes can be tailored to meet the diverse requirements of different industries, including water treatment, energy storage, and sensing applications. An early approach involved incorporating conductive polymers, such as polyaniline (PANI), with porous supports [77]. Other various methods have been reported for the fabrication of ECMs, including immersing cellulose fibers in aniline followed by surface polymerization [78], depositing polyaniline (PANI) on PVC membrane surfaces through in situ polymerization [79], depositing carbon nanotubes (CNTs) on bucky papers [80], employing ion-enhanced metallization for PANI and polypyrrole (PPy) fabrication [77], and coating CNTs on electrospun nylon-6 [81]. Additional methods for fabricating ECMs include casting polymeric films containing nanoparticles, synthesizing polymeric films on conductive meshes, and embedding platinized titanium electrodes on the membrane surface [82–86]. In the blending process of fabricating conductive mixed matrix membranes (MMMs), the use of non-conductive polymers can limit membrane conductivity [87]. It has been suggested that controlling the membrane formulation, specifically the polymer-to-solvent ratio, could provide an effective means of achieving optimal electrical conductivity [88]. In addition to employing conductive polymers, some studies have explored utilizing conductive elements such as carbon nanotubes (CNTs), graphene, MXene, silver, and their derivatives to fabricate ECMs [51,89]. Early research involved incorporating metallic nanoparticles and multi-walled carbon nanotubes into various polymer matrices, forming nanocomposite ultrafiltration and nanofiltration membranes [90–92]. These nanocomposite membranes not only exhibited improved fouling resistance but also showed enhancements in pure water flux and salt rejection when an optimal amount of CNTs was added to the polymer solution [93]. Moreover, investigations into incorporating functionalized CNTs into membrane polymers demonstrated that such modifications could induce changes in hydrophilicity, morphology, and surface charge, leading to enhanced permeability, selectivity, and fouling resistance [94,95]. Jing et al. [96] investigated the lamellar MXene nanofiltration membranes for electrostatic modulation of molecular permeation and separation improvement. Qian et al. [97] developed conductive MXene ultrafiltration membranes, which improved antifouling ability and great potential in advanced water treatment under electrochemical assistance. Chang et al. [98] reported a nano-channeled $Ti_3C_2T_X$ MXene membrane that enabled an efficient controlled rejection/permeation of inorganic ions and organic dye molecules under applied electrical potential. These advancements in membrane technology have paved the way for the development of electro-conductive Ti_3C_2-MXene multilayered membranes, which exhibit promising potential for dye removal and antifouling performance.

Table 1.1: Summary of ECMs' applications using different conductive elements

Conductive elements	Applications	Ref.
CNTs, rGO/CNTs, GO/PANI, GO/MWCNTs	Fouling mitigation	[88,99–101]
Stainless steel mesh/PPy, PANI/CNTs, SSS, PANI/MWCNTs, Functionalized CNTs	Electro-chemical cleaning	[102–106]
Nano-zeolite/CNTs, Silver nitrate, RGO/MXene, MXene/PANI,go/Ni, MXene/CNT	Dye/salt Rejection	[107–112]
LIG,Silver/CNTs, PPy-Ag	Antibacterial activity	[113–115]
ILs, CNTs/rGO, GO	Heavy metal removal	[116–118]
CNT-COOH, PANI-PSS/MWCNTs	Improved ion rejection	[119,120]

Developing electrically conductive composite membranes, simply made by coating a conductive layer on top of a polymeric membrane, offers several advantageous properties. One notable benefit is the enhanced recovery of membrane flux after cleaning procedures, as fouling typically occurs on the membrane surface rather than within the pores [112,121,122]. Coating is a physical modification technique during which hydrophilic components are deposited on the surface of the membrane [123]. The deposition mechanism takes place through the adsorption/adhesion mechanism [123]. In this mechanism, the coating layer is physically attached to the base polymer, which leads to the major obstacle of this technique, the instability of the coating layer [124]. However, in the surface coating process for making conductive membranes, the stability of coated conductive layers for membrane applications is compromised as they are prone to be easily scratched off from their supports [125]. Numerous studies have been investigated to enhance the durability of these conductive layers, often involving additional complex processing steps [87]. In this research, we proposed facile approaches to attach electroconductive materials firmly to the surface of membranes.

1.8 Research objectives

The main objective of the research was to develop Ti_3C_2 MXene-coated PAI and silver-coated PAI nanocomposite membranes for a more efficient water pretreatment process with improved fouling resistance characteristics, particularly when exposed to various model foulants. The aim was to harness the hydrophilic, electrical, and molecular sieve properties of these nanomaterials to enhance the performance of the base membrane, creating nanocomposite membranes with enhanced antifouling and separation capabilities.

Ti_3C_2 MXene and silver (Ag ink) were chosen as coating materials due to their remarkable chemical stability, hydrophilicity, electrical conductivity, and environmental friendliness [126,127]. These properties offered the tremendous potential for fabricating nanocomposite membranes with high chemical stability, strong hydrophilicity, and excellent antifouling and separation properties. Incorporating Ti_3C_2 MXene and silver coatings onto the PAI membrane aimed to impart several desirable characteristics. The hydrophilic nature of Ti_3C_2 MXene and silver coatings enhanced the membrane's performance in terms of fouling caused by organic foulants [128,129]. The hydrophilic surfaces discouraged foulant adhesion, leading to easier fouling removal and increased membrane lifespan. Additionally, the electrical conductivity of Ti_3C_2 MXene and silver coatings offered advantages in fouling control by applying an external electric field [130]. This enabled electrostatic repulsion forces to hinder foulant adhesion and generate gas bubbles that physically prevented foulants from accumulating on the membrane surface. Moreover, the molecular sieve properties of Ti_3C_2 MXene and silver coatings allowed for precise separation and rejection of unwanted contaminants. These coatings' nanoscale dimensions and unique structure provided selective transport pathways, facilitating the separation of different solutes and foulants [9,30]. This enhanced selectivity contributed to improved water quality and reduced fouling issues. The goals pursued in this research are outlined below:

(i) The first goal of this research was to develop novel and highly efficient nanocomposite membranes by laminating Ti_3C_2 MXene nanomaterials as a conductive coating layer on a base PAI support layer using a pressure-assisted technique. By coating the PAI membrane with Ti_3C_2, this conductive membrane could acquire different electrical charges when external potentials were applied. As a result, it could repel charged foulants through electrostatic repulsion forces, minimizing their deposition on the membrane surface. Furthermore, electrochemical reactions occurring on the conductive membrane could degrade the chemical structure of certain foulants partially or entirely. In addition, generating gas bubbles at specific potential ranges over the conductive membrane could help mitigate organic fouling. Therefore, it was expected to improve dye rejection and prevent fouling through controlled surface charge and electric field. Another objective was to investigate the fouling behavior of different organic model foulants on the lab-fabricated PAI membrane. This was achieved by employing an extended Derjaguin, Landau, Verwey, and Overbeek (XDLVO) interaction energy analysis. The XDLVO analysis allowed for the evaluation of fundamental interactions (such as van der Waals, electrostatic, and acid-base interactions) that contribute to organic fouling. Surface tension parameters derived from contact angle measurements were used to calculate the free energy of adhesion between the membrane and foulants, providing insights into the variations in flux decline.

(ii) A novel and durable electro-conductive silver-coated membrane was fabricated using the facile “spray-cure” technique, where a thin film of Ag ink was employed on the surface of the PAI membrane. This conductive membrane could mitigate fouling and increase dye rejection in the presence of cathodic electric potential. As a result, it could repel charged foulants through strong electrostatic repulsion forces and gas formation, minimizing the foulants' deposition on the membrane surface.

1.9 Thesis structure

The thesis is structured as follows:

Chapter 1 of this thesis comprehensively introduces the existing water treatment methods. It highlights the shortcomings associated with current water treatment techniques. Moreover, membrane-based separation processes, specifically electro-conductive membranes, are introduced as a viable alternative to overcome these limitations. This chapter also concludes with a literature review focusing on composite membranes and a clear outline of the research objectives pursued in this work.

Chapter 2 of this thesis was constructed around a previously prepared article, providing a detailed analysis of the research conducted. This chapter is dedicated to presenting the findings of a series of systematic studies investigating the effects of Ti_3C_2 MXene-coated PAI membranes. The main objective of these studies was to assess the impact of incorporating Ti_3C_2 MXene layer on polymeric PAI membrane and the overall separation and fouling performance of the prepared electro-conductive membranes in the presence of cathodic electric potential. A cross-flow filtration setup was employed to evaluate the performance of membranes. In addition to performance evaluation, the membranes were subjected to various characterization techniques to gain insights into their properties. Contact angle measurements were carried out to determine the wettability of the membranes, while zeta potential measurements provided information about their surface charge. Advanced imaging techniques such as field emission scanning electron microscopy (FESEM), transmission electron microscopy (TEM), and atomic force microscopy (AFM) were utilized to examine the morphological characteristics of the membranes at different scales. Furthermore, X-ray photoelectron spectroscopy (XPS) analysis was conducted to investigate the chemical composition of the membranes. These comprehensive characterizations allowed for a thorough understanding of the membrane properties, enabling the researchers to assess the improvements in antifouling performance and separation efficiency resulting from the incorporation of the Ti_3C_2 MXene coating layer. In this chapter, the research also delves into a study focusing on the adsorption behavior of organic substances on the optimized modified membrane, using XDLVO interaction energy analysis. To explain the differences in flux decline observed in the cross-flow filtration setup, the free energy of adhesion between the membrane and foulant material was calculated using surface tension components derived from contact angle measurements. By combining these surface energetics analyses and experimental results, this chapter provides valuable insights into the antifouling performance of the MXene-modified nanocomposite membranes, shedding light on their potential for practical applications in mitigating fouling issues in separation processes.

Chapter 3 presents the results of developing electro-conductive Ag-PAI membranes with enhanced antifouling and dye separation performances by applying electric potential. The effects of different applied cathodic potentials were investigated, and the permeation, separation, and antifouling performances of the silver-coated PAI membranes were evaluated. The separation performance of the membrane was examined using two dyes, specifically reactive red 120 (RR120) and reactive black (RB) aqueous solutions, and SA/$CaCl_2$ was used as a model foulant for evaluating the antifouling performance of the synthesized membranes.

Chapter 4 summarizes the main outcomes of this research and provides a concluding discussion. Furthermore, suggestions and recommendations for future research are provided.

Chapter 2

Development of Electro-Conductive Ti_3C_2 MXene Multilayered Membranes: Dye Removal and Antifouling Performance

2.1 Introduction

Human beings are struggling with water-related challenges, including contamination and scarcity of freshwater resources [131–133]. To address such issues, researchers worldwide are actively exploring novel technologies that can efficiently eliminate contaminants from water while minimizing energy consumption [134,135]. In this context, implementing cost-effective and energy-efficient techniques for treating, recycling, and reusing industrial, agricultural, and domestic wastewater represents a practical approach toward achieving sustainable development for nations [136]. Among the various techniques proposed thus far, advanced oxidation processes (AOPs), such as Fenton, ozone/UV, photocatalysis, and membrane-based technologies, stand out as highly promising approaches [137]. These techniques offer high treatment efficiency, minimal footprint, and versatility across various water streams, often without toxic chemical additives [134]. Recent advancements in the design and fabrication of novel membranes have positioned membrane technology as a superior option for water treatment compared to conventional methods [138]. However, sustainable membrane operations face significant technical hurdles, such as fouling, which must be addressed to ensure up-scaled feasibility [139].

Membrane fouling, caused by the adsorption of undesired substances on the membrane surface or within its pores [140], significantly hampers the performance and lifespan of membranes in separation technologies [141]. Consequently, addressing fouling challenges, especially in harsh environments, has become critical [142,143]. One approach to address membrane fouling is modifying the membrane surface using hydrophilic materials [13]. However, the achieved impact on fouling reduction during long-term operations remains insufficient [59–62]. To overcome this, researchers are delving into developing advanced smart membranes [144,145] responsive to external stimuli such as pH [146], temperature [147,148], pressure [149,150], ionic strength [151], ultrasonication [152], magnetic field [153], and electric field [154–156]. Among these, applying an electric field has garnered significant interest due to its precision and controllability. Recent studies have demonstrated that the accumulation of charged particles on the membrane surface can be adjusted by applying a constant electric potential to the electrically conductive membrane through electrostatic repulsion and electrochemical reactions [66,67,112,121,122]. Another mechanism involves electrochemical reactions that alter the molecular structure of foulants. Applying an electric potential to electroconductive membranes generates oxidizing species, such as hydroxyl radicals, that react with large macromolecular foulants, breaking them down into smaller compounds and thus preventing their attachment to the membrane surface [66,67]. Electromagnetic fields also play a role by modifying feed solution properties, such as pH and ionic strength, and disrupting foulant adhesion [68–70]. Furthermore, higher potential differences in electrochemical systems can induce water electrolysis reactions, generating oxygen and hydrogen gases. Gas bubbles on the membrane surface contribute to fouling mitigation by disrupting interactions between the membrane and foulants [69].

Electroconductive membranes have been fabricated by depositing electrically conductive materials onto the surface of traditional membranes. Notable materials include copper [157], nickel [158], platinum [159], indium tin oxide [160], antimony tin oxide [161], graphene [66,67], and carbon nanotubes (CNTs) [162,163], applied through methods like electrophoretic deposition, plasma deposition, chemical vapor deposition, spin coating, chemical and electrochemical reactions, and layer-by-layer assembly [164]. Among these materials, two-dimensional (2D) nanomaterials, particularly graphene, stand out for their conductivity and unique stacking structures that enhance selectivity for water solute removal. Integrating 2D nanomaterials into membranes holds promise for both conductivity and improved selectivity in water treatment applications [163–165]. MXenes, a recently discovered class of 2D nanomaterials, has never been used to fabricate electroconductive membranes. The general MXene formula is $M_{n+1}X_nT_x$, where M represents elements such as Ti, Zr, and V, interleaved with n layers of carbon or nitrogen (denoted as X), and T denotes surface terminal functions, e.g., O, OH, F, and/or Cl. Ti_3C_2 MXene, the most studied MXene, exhibits high hydrophilicity, specific surface area, flexibility, mechanical strength, stability, and electrical and thermal conductivities, making it highly attractive for developing high-performance membranes for water purification [165,166]. Stacking 1-nm-thick 2D flakes of Ti_3C_2 MXene creates interconnected and densely packed nanochannels arising from relatively uniform interlayer spacings at the sub-nanometer scale within the laminar membranes. This unique feature gives the membranes a high surface-to-volume ratio and can significantly enhance the water/solute selectivity [167–170]. Furthermore, functional groups on Ti_3C_2 MXene 2D flake surfaces enable covalent bonding, hydrogen dipole-dipole attractions, and electrostatic interactions between the host polymer and MXene nanostructures, facilitating uniform dispersion within composite membranes. A remarkable feature is Ti_3C_2 MXene's high electrical conductivity (up to 24000 S/cm), making it ideal for various electronic and energy-related applications.

We successfully fabricated a novel Ti_3C_2 MXene-coated membrane in this study using a simple pressure-assisted filtration technique. To enhance the chemical and mechanical stabilities of the MXene coating, carboxymethylcellulose (CMC) was incorporated into the MXene solution, followed by crosslinking the MXene/CMC coated membranes with the glutaraldehyde (GA) solution in the subsequent step. The Ti_3C_2 MXene-coated membrane exhibited remarkable improvements in rejection rates compared to the pristine polyamide-imide (PAI) membrane, achieving rejection rates exceeding 99.71%, 97.95%, and 68.91% for RR120, RB, and MO, respectively. We further demonstrated that the antifouling performance of the membrane could be easily enhanced by applying a low voltage between a multilayer Ti_3C_2 MXene-coated membrane and a stainless-steel electrode. By maintaining the desired level of antifouling performance, this membrane is a potential platform capable of controlled fouling behavior. During fouling experiments, surface energy analysis was also used to investigate the physicochemical interactions between foulants and the membrane surface. This analysis provides valuable insights into the affinity and adhesion mechanisms governing fouling behavior and contributes to developing effective membrane fouling control strategies.

2.2 Materials and methods

2.2.1 Materials

The etched multilayered Ti_3C_2-MXene powder was obtained from Luoyang Advanced Material Company (China). Carboxymethyl cellulose sodium salt (CMC), N,N−dimethylacetamide (DMAc, >99.9%), calcium chloride ($CaCl_2$), sulfuric acid (H_2SO_4), and acetone were provided by Fisher Scientific. Also, polyvinylpyrrolidone (PVP, 360 kDa), poly (ethylene glycol) (PEG), triton X-100, glutaraldehyde (GA, 25 wt% in water), humic acid (HA), sodium alginate (SA), glacial acetic acid (ReagentPlus, 99.0%), potassium hexacyanoferrate (III) ($K_4Fe(CN)_6$), and sodium nitrate ($NaNO_3$) were purchased from Sigma-Aldrich. PAI (Torlon 4000 THV) was supplied by Solvay Advanced Polymers. Reactive red 120 (RR120, MW: 1774.15 Da), reactive black (RB, MW: 991.82 Da), and methyl orange (MO, MW: 327.33 Da) dyes were obtained from Sigma-Aldrich and utilized as organic contaminants in water. Bovine Serum Albumin (BSA) was purchased from ChemCruz. Fouling experiments were conducted on aqueous solutions of HA, SA/$CaCl_2$, and BSA. Deionized water was used throughout this research.

2.2.2 Membrane preparation

2.2.2.1 Fabrication of PAI support layer

The fabrication of PAI support layers was carried out using the nonsolvent-induced phase separation (NIPS) technique. For this purpose, PAI polymer, known for its exceptional thermal, mechanical, and chemical resistances, as well as superior hydrophilicity, was selected as the main polymer. PVP and PEG were employed as additives to optimize the membrane porosity. DMAc served as the solvent in this process. To prepare a homogeneous polymer solution, PAI (9 wt%), along with the appropriate amounts of additives, was dissolved in the DMAc solvent. The mixture was stirred at a speed of 350 rpm and maintained at a temperature of 40 °C for 24 hours. After stirring, the homogeneous solution was allowed to rest in a vacuum oven for 15 minutes to eliminate any air bubbles. Next, the PAI membrane layers were fabricated by using a film applicator to cast the solution onto a non-woven polyester fabric. The casting speed was set to 20 mm/s, and the gap height between the applicator and base plate was fixed at 120 μm. Finally, the cast film was submerged in a coagulation bath containing deionized water overnight to ensure the complete removal of the solvent from the polymer matrix.

2.2.2.2 Preparation of Ti_3C_2 MXene-coated PAI membranes

To purify the MXene powder and remove impurities, 1 g of multilayered Ti_3C_2 MXene powder was washed three times. A stock solution of MXene was then prepared by suspending multilayer Ti_3C_2 MXene (1 g) in 50 mL of deionized water. The solution was then well-dispersed in a sonication bath for 1 h. This stock solution was used to make the coating layer of each membrane. **Table 2.1** shows three membranes with three different chemical compositions of the coating layers.

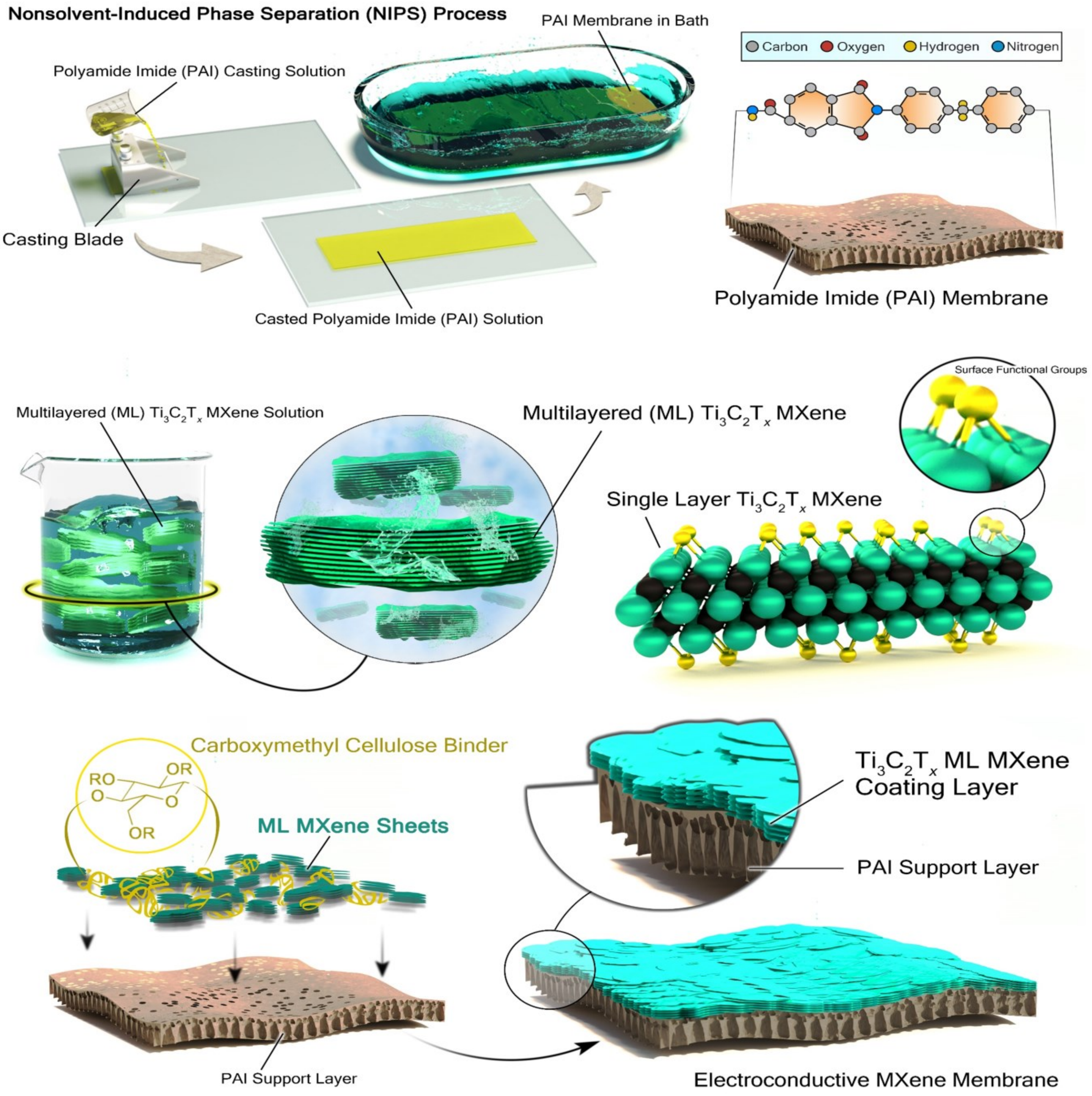

Figure 2.1. Schematic illustration of PAI membrane fabrication and MXene-coated PAI electroconductive membrane

Table 2.1: Chemical composition of different coating layers of membranes

Membrane ID	MXene (mg)	CMC (mg)	GA cross-linking time (min)
ECM1	80 mg	4	30
ECM2	40 mg	4	30
ECM3	40 mg	2	30

CMC was utilized as a binder to establish a strong and durable attachment of Ti_3C_2 MXene layers to the PAI membrane surface. We prepared three coatings by varying the amount of CMC binder and MXene. In all samples, deionized water was added to reach a total volume of 50 mL for the MXene coating solution. This coating solution was then subjected to sonication in a water bath for an additional 30 minutes. Next, each coating solution was passed through the microporous PAI membrane using a dead-end filtration cell, with a nitrogen gas pressure of 5 psi applied. Following filtration, the membrane was heat-treated in an oven at 50 °C for 15 minutes. Subsequently, the membrane was immersed in a 12%wt glutaraldehyde (GA) solution for 30 minutes to facilitate cross-linking. Finally, the Ti_3C_2 MXene coated membrane was dried for 15 minutes at 50 °C in the oven in preparation for further experiments. **Figure 2.1** shows the schematic illustration of the membrane fabrication process.

2.2.3 Physicochemical Characterizations of Membranes

2.2.3.1 Contact angle measurements

The hydrophilicity of the Ti_3C_2 MXene-coated PAI membranes was assessed using a contact angle analyzer (DSA100, Krüss GmbH, Germany). To conduct the measurements, small pieces of each air-dried membrane were affixed to glass slides with the active surface facing upward. A 2 μL droplet of distilled water was carefully dispensed onto the membrane surface using a syringe, and the contact angle was measured using the sessile drop technique. To evaluate the oleophobicity of the membranes, the underwater oil contact angle (UWOCA) was measured using the same contact angle analyzer, employing the captive bubble method. The membranes were secured on a 2 cm wide plastic holder using double-sided tape and then inverted in a quartz cuvette filled with deionized water. To initiate the measurement, 6 μL of n-hexadecane oil was deposited on the membrane surface using a J-shaped needle connected to a syringe. Three different locations on the membrane surface were selected for WCA and UWOCA measurements.

2.2.3.2 Field Emission Scanning Electron Microscopy (FESEM) and Energy-Dispersive Spectroscopy (EDS)

The top surface and cross-section morphology of the Ti_3C_2 MXene-coated PAI membranes were examined using a field emission scanning electron microscope (FESEM, Zeiss Sigma 300 VP) at an acceleration voltage of 25 kV. For cross-section SEM imaging, the membrane layers were separated from the polyester support and carefully fractured after being immersed in liquid nitrogen. The resulting fractured membranes were then placed on SEM stub holders using carbon tape. A thin layer of gold (approximately 2 nm in thickness) was sputter-coated onto the samples before SEM imaging to enhance conductivity and minimize charging effects during imaging.

2.2.3.3 Transmission electron microscopy (TEM)

The thickness and integrity of the Ti_3C_2-MXene coating on the PAI substrate were evaluated using the transmission electron microscopy (TEM, Philips/FEI Morgagni 268, Eindhoven, Netherlands) technique. The membrane samples underwent a staining process using a solution of uranyl acetate and lead citrate to enhance contrast. Subsequently, the samples were embedded in Spurr's resin to provide stability during the slicing process. Afterward, an ultramicrotome (Reichert-Jung Ultracut E, USA) was used to slice ultrathin sections of the samples, which were then observed using the TEM device.

2.2.3.4 X-ray photoelectron spectroscopy (XPS) analysis

To determine the chemical bonding and elemental composition of the Ti_3C_2-MXene coating layer, the X-ray photoelectron spectroscopy (XPS) was performed using a Kratos AXIS ULTRA XPS equipped with a monochromatic Al Kα X-ray source. The data were collected from 1 to 10 nm thickness of the surface layer in the 0-1100 eV range using 0.1 eV high-resolution scans.

2.2.3.5 Raman spectroscopy

Raman spectra were acquired at room temperature using the InVia Reflex Renishaw instrument, with a 532 nm laser serving as the excitation source. The measurements were conducted over a frequency range of 300 to 2000 cm^{-1}.

2.2.3.6 Zeta potential measurement

The zeta potential analysis of the Ti_3C_2-MXene coated samples was conducted using a Surpass^{TM} 3 Electrokinetic analyzer (Anton Paar, Graz, Austria) at different pH levels. Two pieces of membranes were securely placed in sample holders and immersed in a 1 mM KCl solution. The gap between the two flat membrane surfaces was adjusted to 100 µm. The pH of the solution was controlled using sodium hydroxide and hydrochloric acid to achieve the desired values within the pH range of 4-9. Streaming potential and current measurements were performed at various pH values. The surface zeta potential was then determined based on these measurements. Three separate measurements were conducted, and the reported zeta potential values are the average of these measurements.

2.2.3.7 Membranes' stability tests

The leaching rate of titanium ions from the membrane samples was examined to evaluate the stability of the Ti_3C_2-MXene coating layer. Membrane samples with a surface area of 45.34 cm^2 were immersed in deionized water and placed on magnetic stirrers rotating at a rate of 120 rpm for 3 weeks. To determine the concentration of leached ions, water samples were collected periodically after 7, 14, and 21 days of immersion and analyzed using ICP-OES (Thermo iCAP6300 Duo ICP-OES) following the modified EPA 6010d analysis method. To assess the chemical stability of the Ti_3C_2-Mxene coated membranes, small membrane pieces were soaked in acidic (pH=2), neutral (pH=7), and basic solutions (pH=12) as well as various organic solvents, including acetone and ethylene glycol. After immersing the membrane pieces in these solutions for 48 hours, the change in the appearance and physical properties of the membranes was evaluated. The UWOCA was also measured as an indicator of the membrane's chemical stability.

2.2.3.8 Membranes' surface roughness measurements

The surface topography of the fabricated membranes was examined using atomic force microscopy (AFM) with a Veeco Digital Instrument. The AFM measurements were performed in tapping mode under ambient conditions. The scanning area for each membrane was 10 µm × 10 µm, and three different regions of each membrane were analyzed. Average surface roughness (R_a) and root mean square roughness (R_{rms}) for all membranes were reported.

2.2.4 Membranes' surface energy measurements

The surface energy of the ECM1 membrane was evaluated using the extended Young–Dupré and van Oss equation [171]. Based on the van Oss equation, the total surface tension $\gamma^{TOT}$of a medium can be expressed as the sum of the nonpolar (Lifshitz–van der Waals, γ^{LW}) and the polar (acid-base, γ^{AB}) surface tension components [172]. The polar acid-base component takes into account the contribution of hydrogen bonding to the surface tension component. The value of "γ^{TOT}" is calculated using **Equation 2.1.**

$$\gamma^{TOT} = \gamma^{LW} + \gamma^{AB} \tag{2.1}$$

To implement this methodology, it is necessary to determine the surface tension components of both the membranes and the foulants using a three-probe liquid approach. The surface tension parameters for water, glycerol, and diiodomethane, with their corresponding nonpolar (Lifshitz-van der Waals) and polar (acid-base) surface tension components, can be found in **Table 2.2** [172].

Table 2.2: Surface tension components (mJ/m^2)

Probe Liquid	γ^{LW}	γ^{+}	γ^{-}	γ^{AB}	γ^{TOT}
Ultrapure water	21.8	25.5	25.5	51.0	72.8
Glycerol	34.0	3.9	57.4	30.0	64.0
Diiodomethane	50.8	0.0	0.0	0.0	50.8

First, the contact angles of three probe liquids (water, glycerol, diiodomethane), with known values of LW, negative (–), and positive (+) surface tension components, were measured [171,173].

The measured contact angles were then substituted into **Equation 2.2** to calculate the nonpolar (γ^{LW}) and polar (γ^{+} and γ^{-}) surface tension components of the solid surface.

$$\gamma^{TOT}\left(1 + \frac{\cos\theta}{r}\right) = 2(\sqrt{\gamma_s^{LW}\gamma_l^{LW}} + \sqrt{\gamma_s^{+}\gamma_l^{-}} + \sqrt{\gamma_s^{-}\gamma_l^{+}}) \tag{2.2}$$

where θ is the contact angle, s and l refer to a solid surface (membrane) and liquid, respectively. Superscripts LW, –, and + represent the nonpolar (Lifshitz-van der Waals), electron donor, and electron acceptor components of surface energy, respectively. Also, r is the Wenzel roughness factor, which represents the ratio of the actual surface area to the planar area. This factor is computed using the following **Equation 2.3** [174].

$$r = 1 + SAD \qquad 2.3$$

where SAD is the surface area difference and represents the percentage increase in surface area due to roughness. SAD value was obtained from AFM results. Also, the polar surface tension is made up of electron donor (–) and electron acceptor (+) components, which are calculated using **Equation 2.4** [171,173].

$$\gamma^{AB} = 2\sqrt{\gamma^{+}\gamma^{-}} \qquad 2.4$$

The nonpolar and polar surface tension components are used to calculate the nonpolar and polar free energy of adhesion between the membrane surface and different foulants using **Equation 2.5** and **Equation 2.6**, respectively [171,173].

$$\Delta G_{mlf}^{LW} = 2(\sqrt{\gamma_l^{LW}} - \sqrt{\gamma_s^{LW}})(\sqrt{\gamma_f^{LW}} - \sqrt{\gamma_l^{LW}} \qquad 2.5$$

$$\Delta G_{mlf}^{AB} = 2\sqrt{\gamma_l^{+}}\left(\sqrt{\gamma_s^{-}} + \sqrt{\gamma_f^{-}} - \sqrt{\gamma_l^{-}}\right) + 2\sqrt{\gamma_l^{-}}\left(\sqrt{\gamma_s^{+}} + \sqrt{\gamma_f^{+}} - \sqrt{\gamma_l^{+}}\right) - 2(\sqrt{\gamma_s^{+}\gamma_f^{-}} + \sqrt{\gamma_s^{-}\gamma_f^{+}}\,) \qquad 2.6$$

Consequently, the total interfacial energy of adhesion between the membrane surface and foulants can be calculated by summing up the nonpolar and polar components of adhesion-free energy using **Equation 2.7** [171,173].

$$\Delta G_{mlf}^{TOT} = \Delta G_{mlf}^{LW} + \Delta G_{mlf}^{AB} \qquad 2.7$$

In this study, water and glycerol were selected as polar liquids, while diiodomethane was used as a nonpolar liquid to calculate the polar and nonpolar surface tension components.

2.2.5 Membranes' electrochemical characterizations

To analyze the electrical conductivity of membranes, the resistance values of the Ti_3C_2-MXene coating layers were measured using a probe station in a four-point probe configuration. The prepared membranes were first cut into small pieces, and then a DC potential was applied to the dried surface of the membrane. The resulting current developed across the surface of the membrane was measured, allowing for the determination of resistance. Cyclic voltammetry (CV) and linear sweep voltammetry (LSV) experiments were conducted using a standard flow-through module generously provided by Flex-X-Cell GmbH for the purpose of electrolysis tests. The experimental setup employed a three-electrode configuration, wherein MXene-coated electroconductive membranes (5x5 cm^2) were designated as the working electrode, Pt-coated titanium expanded metal (4.5x5 cm^2) served as the counter electrode, and $Hg/HgSO_4$ saturated with potassium sulfate (-0.64 V vs. SHE) was chosen as the reference electrode. To maintain consistency, a separation distance of 3 mm between the cathode and anode was upheld, and the reference electrode was positioned external to the module, within the inlet stream. The background electrolyte solution consisted of 100 mL of 50 mM Na_2SO_4, supplemented with 200 mg/L of the target foulants (HA, SA/$CaCl_2$, and BSA). Throughout the experiments, the module's flow rate was set at 50 mL/min, and all CV and LSV measurements were conducted with a uniform scan rate of 15 mV/s.

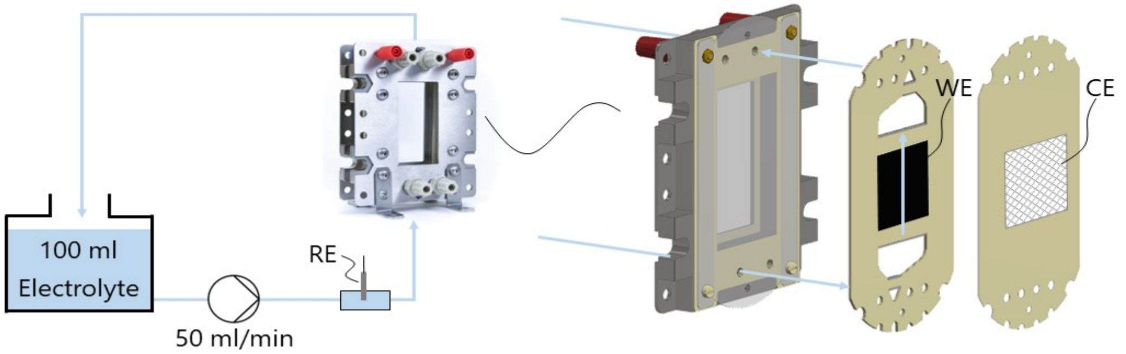

Figure 2.2. The experimental setup used in LSV and CV experiments. Electrolytes with different foulants were circulated with a flow rate of 50 mL/min through a standard electrochemical cell (Flex-E-Cell, Germany). The reference electrode (RE) was placed outside the cell in the inlet stream. MXene-coated membranes and a titanium expanded metal coated with Pt served as the working electrode (WE) and counter electrode (CE), respectively.

2.2.6 Membranes' permeation, dye rejection, and molecular weight cut-off (MWCO) measurements

The membrane separation performance was assessed in terms of rejection and flux by filtering various dye solutions using a bench-scale cross-flow filtration setup, which had an effective membrane area of approximately 20.25 cm^2. The tests were conducted under experimental conditions of 20 psi pressure and a cross-flow rate of 2.4 L/min. Each membrane was compacted until a steady flux was achieved under 30 psi pressure. The weight of the permeate was measured at regular time intervals using a weighing balance (ME4002, Mettler Toledo, USA). The pure water flux was calculated using **Equation 2.8** [161].

$$J_w = \frac{\Delta m}{\rho A_m \Delta t} \tag{2.8}$$

where J_w is pure water flux, Δm is permeate mass, ρ is water density, A_m is the effective membrane surface area, and Δt is filtration time. Also, the rejection performance of the pristine PAI membrane and all modified membranes was evaluated using aqueous solutions of RR120, RB, and MO dyes with a concentration of 20 mg L^{-1} as feed solutions. Dye rejection was determined by the **Equation 2.9**.

$$R(\%) = \left(1 - \frac{C_p}{C_f}\right) \times 100 \tag{2.9}$$

where C_p and C_f represent the dye concentration in permeate and feed solutions, respectively, which were measured by UV–vis spectrophotometer. In addition, the MWCO of the ECM1 membrane was determined by filtering 200 ppm PEG solutions with different molecular weights under a pressure of 20 psi. To determine the MWCO, the PEG concentrations in the permeate solutions were measured using a Shimadzu TOC-L CPH Model total organic carbon (TOC) Analyzer from Jiangsu, China. The MWCO of the ECM1 membrane is determined by measuring the molecular weight of solutes that are rejected by the membrane with 90% efficiency. This can be achieved by plotting the percentage of solute rejection against their molecular weight in Daltons. From this plot, the MWCO can be calculated as the molecular weight of the solutes that are effectively rejected by the modified membrane.

2.2.7 Fouling experiments procedure

To evaluate the fouling behavior of the prepared ECM1 membrane, fouling tests were conducted, and the effects of applying an electric field on the membrane's fouling performance were studied. The fouling experiments were carried out using a cross-flow filtration setup with a pressure of 20 psi and a feed cross-flow rate of 2.4 L/min. The cathodic electro-reduction (CER) reactions were carried out by connecting the membrane’s top surface to the cathode output of a DC power supply. A rectangular piece of stainless steel (7.54 cm^2) with a smaller size than the membrane was used as the anode, and a distance of 1.4 mm was adjusted between the anode and the cathode. The electroactivity of the coated membranes was investigated by applying different electric potentials to the membrane surface. A three-step experimental approach was used to evaluate the fouling behavior of the membranes with an applied electric potential. First, a deionized water filtration experiment was performed for 20 min, and the permeate flux was allowed to stabilize before the foulant was added to the feed solution. The water that passed through the membrane was collected on a digital balance (ME4002, Mettler Toledo), and the data was then automatically recorded on a computer at 15 seconds intervals. After measuring the pure deionized water flux, the feed solution was replaced with a 200 mg L^{-1} foulant solution, and the permeate flux of the foulant solution (J_{wf}) was measured for 20 minutes. Following the fouling step, the membrane surface was washed by stirring with distilled water for 10 minutes at the same operational flow rate used during the fouling step, with no applied pressure. Ultimately, the pure water flux of the cleaned membrane (J_{w2}) was recorded after cleaning the membrane surface with deionized water. To evaluate the antifouling property of the membranes, the total flux decline ratio (FDR) and flux recovery ratio (FRR) were determined as follows.

$$FDR = 1 - \frac{J_{wf}}{J_{w1}} \tag{2.10}$$

$$FRR = \frac{J_{w2}}{J_{w1}} \tag{2.11}$$

where J_{w1} is the pure deionized water flux, J_{wf} is the permeate flux of the foulant solution, and J_{w2} is the pure water flux of the cleaned membrane. It is worth noting that, during the cleaning step, the membrane surface was subjected to the same DC electrical potential applied during the fouling step. While literature studies have shown that AC voltage is more effective in cleaning than DC, we applied DC voltage here to mitigate the oxidation and gradual dissolution of Ti.

2.3 Results and discussion

2.3.1 Characterizations of fabricated membranes

The wettability of the membrane surface was assessed through water contact angle (WCA) and underwater oil contact angle (UWOCA) analyses. The surface roughness and chemistry of the membrane are crucial factors influencing wettability [175,176]. **Figure 2.3(A)** demonstrates that the initial WCA of the pristine PAI support was approximately 41°, which reduced to zero within 30 seconds. Also, the pristine PAI support exhibited an average UWOCA of around 124° **(Figure 2.3(C))**. However, all Ti_3C_2 MXene-coated membranes displayed an apparent WCA of 0° immediately upon contact with water droplets. This exceptional hydrophilicity of the MXene-modified membranes can be attributed to the presence of hydrophilic functional groups on Ti_3C_2 MXene, enabling hydrogen bonding between Ti_3C_2 MXene and water molecules. Additionally, the UWOCA analysis of the ECM1 sample was conducted to assess the oil-repelling properties of the MXene-coated membrane. As depicted in **Figure 2.3(B),** the oil droplet adhered to the surface of ECM1 when immersed in water. However, upon pressure release, the droplet no longer adhered to the surface and reverted to its original spherical shape, indicating easy separation from the membrane's surface.

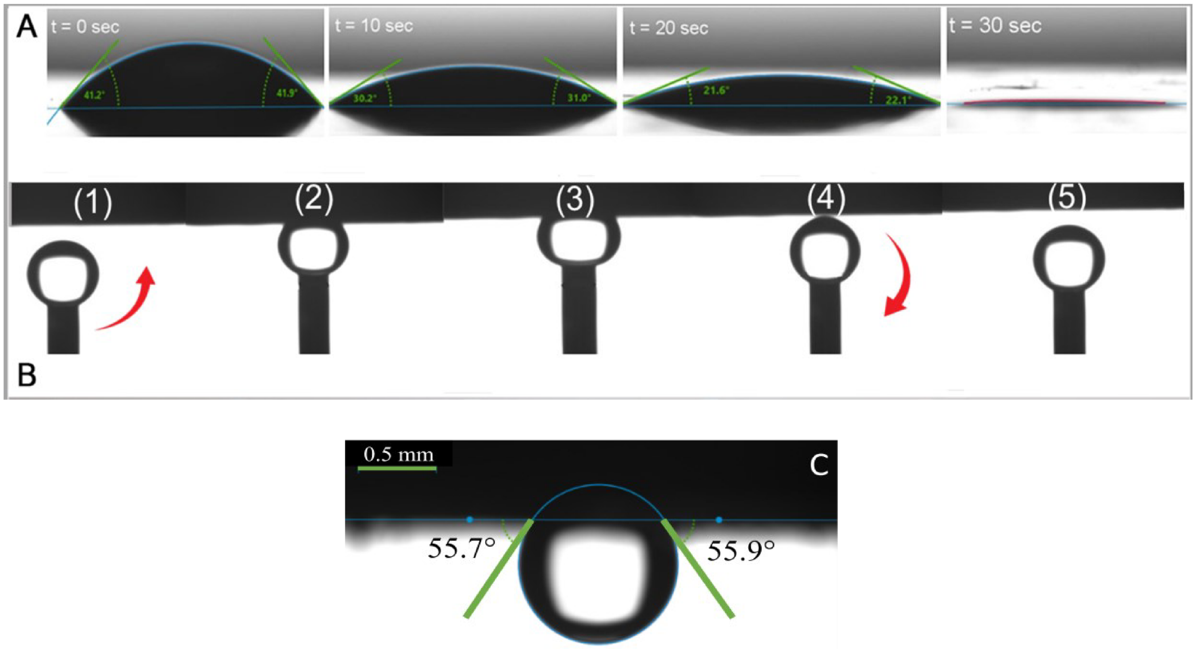

Figure 2.3. Dynamic water contact angles of pristine PAI membrane in 30 sec. The initial WCA of the pristine PAI support is around 41°, then drops to 0° in 30 seconds. All Ti_3C_2 MXene-coated membranes, on the other hand, exhibit an immediate WCA of 0° upon contact with water, which is attributed to hydrophilic functional groups on Ti_3C_2 MXene allowing strong hydrogen bonding with water molecules. The average UWOCA for the pristine PAI support is around 124°. (B) Different steps of n-hexadecane droplet interactions with the surface of ECM1 under DI water. Steps include (1) n-hexadecane droplet approaching, (2) touching and (3) forcing to the ECM1 surface, (4) pressure release, and (5) full detachment of n-hexadecane droplet from the ECM1 surface. When immersed in water, oil droplets initially adhere to the membrane's surface but easily separate upon pressure release, returning to their spherical shape. (C) the UWOCA of pristine PAI membrane.

Moreover, the oil-repelling capability of the MXene-coated membranes under underwater conditions was evaluated using both light oil (n-hexane) and heavy oil (dichloromethane). As shown in **Figure 2.4(A)**, when the oil came into contact with the ECM1 membrane surface, the light oil droplets were quickly expelled and floated on the water without adhering to the membrane surface. Similarly, when heavy oil droplets contacted the membrane surface **(Figure 2.4(B)**), they formed spherical droplets that easily slid down to the bottom of the beaker. Consequently, upon removing the membrane from the bottom of the beaker, no noticeable oil adhesion was observed on the membrane surface, confirming the underwater oil-repelling behavior of the modified membrane. When a hydrophilic membrane comes into contact with water, the hydrophilic surface creates a thin hydration layer that acts as a solid-water interface. As a result, oil interacts with the membrane-water interface rather than directly with the membrane surface, leading to reduced oil adhesion. Incorporating hydrophilic Ti_3C_2 MXene onto the polymeric PAI membrane facilitates the formation of the hydration layer, resulting in higher oil-repelling properties.

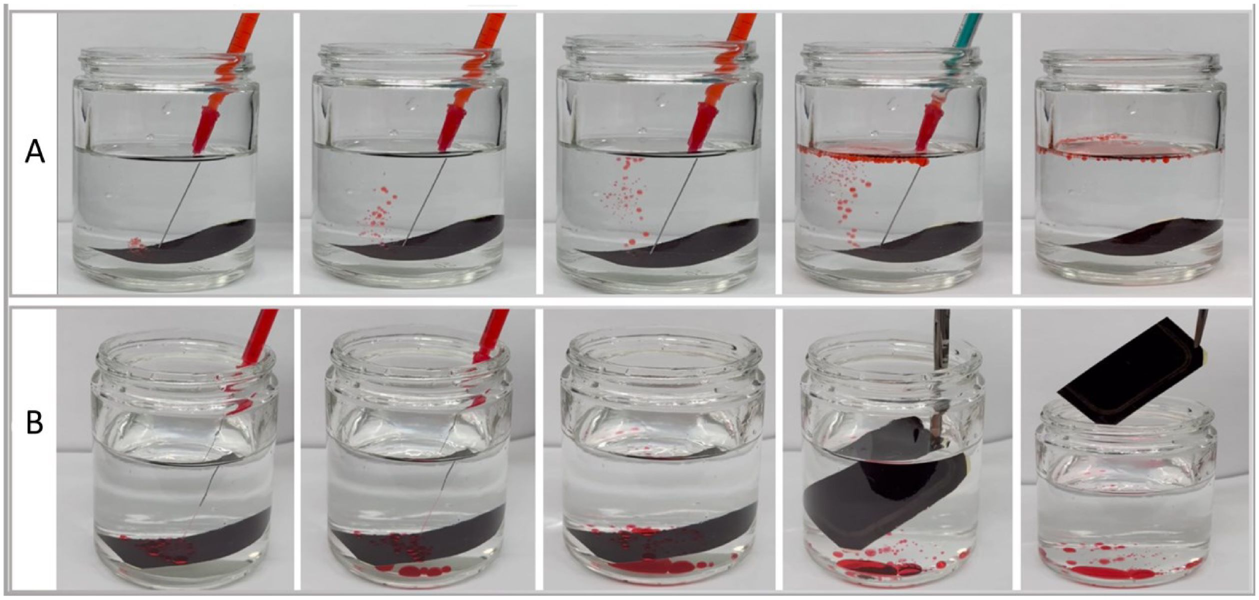

Figure 2.4. (A) The oil-repelling property of ECM1 in a light oil (n-hexane), fast repelling of the oil-injected droplets from the surface, and (B) in a heavy oil (dichloromethane). Further testing of underwater oil repellence shows that both light (n-hexane) and heavy (dichloromethane) oil droplets are ejected from the ECM1 membrane surface. These droplets float on the water and form spherical shapes, confirming the modified membrane's exceptional underwater oil-repellency.

Figure 2.5(A) and **Figure 2.6(A_1, B_1, and C_1)** display the optical images of the pristine and MXene-coated membranes, respectively. The Ti_3C_2-MXene/CMC nanocomposites are firmly attached to the yellowish surface of the PAI membrane without any visible detachment or pinholes. FESEM image of the top surface of the PAI support (**Figure 2.5 (B)**) reveals the membrane surface without any visible pores. The top FESEM images of the MXene-modified membranes (**Figure 2.6, A_2, B_2, and C_2**) confirm the successful coating of MXene particles made of 2D sheets of Ti_3C_2 MXene distributed over the modified membrane surface. In **Figure 2.5(C),** the cross-sectional view of the PAI support layer demonstrates straight finger-like open pores that enhance membrane permeability by facilitating the passage of permeated water. SEM results show that the average thickness of the PAI support is approximately 50 µm.

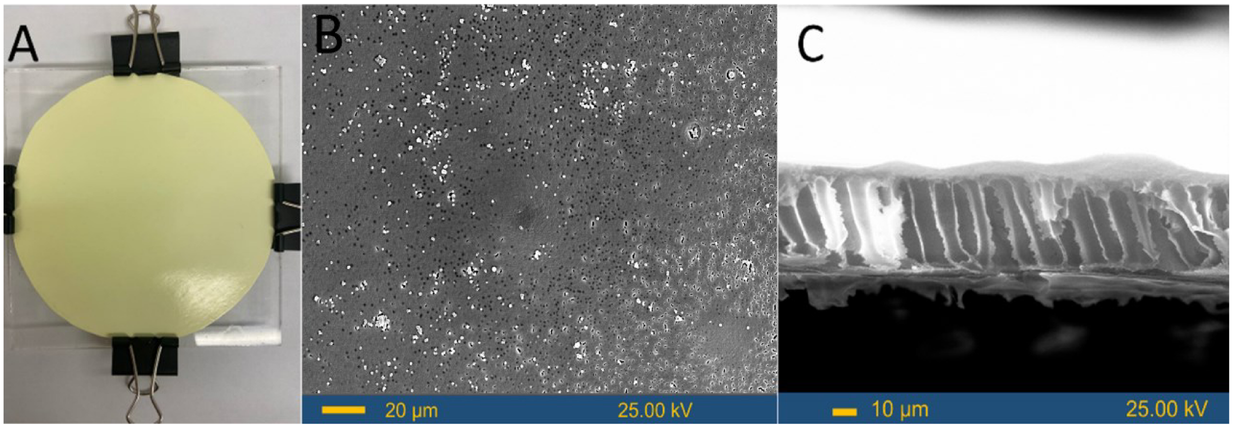

Figure 2.5. (A) The optical image (B) top and (C) cross-sectional FESEM of the prepared PAI support layer.

The third row of **Figure 2.6** presents the cross-sectional views of the MXene-modified membranes. The thickness of MXene coating layer varied across different spots on the membrane surface, but its average thickness is about 7 µm. EDX mappings were also conducted in the same positions to assess the distribution of three elements: carbon (C), titanium (Ti), and fluorine (F) in the cross-sectional slicing of the membrane. The resulting EDX mapping images are shown in the last three rows of **Figure 2.6**. Carbon is present in both the PAI and MXene coating layers, while Ti and F are exclusively found in the top multilayer MXene layer. The EDX mapping images validate the deposition of MXene nanosheets across the membrane surfaces. The EDX elemental composition and EDX spectra of Ti_3C_2 MXene-coated membranes are provided in **Table 2.3** and **Figure 2.7**.

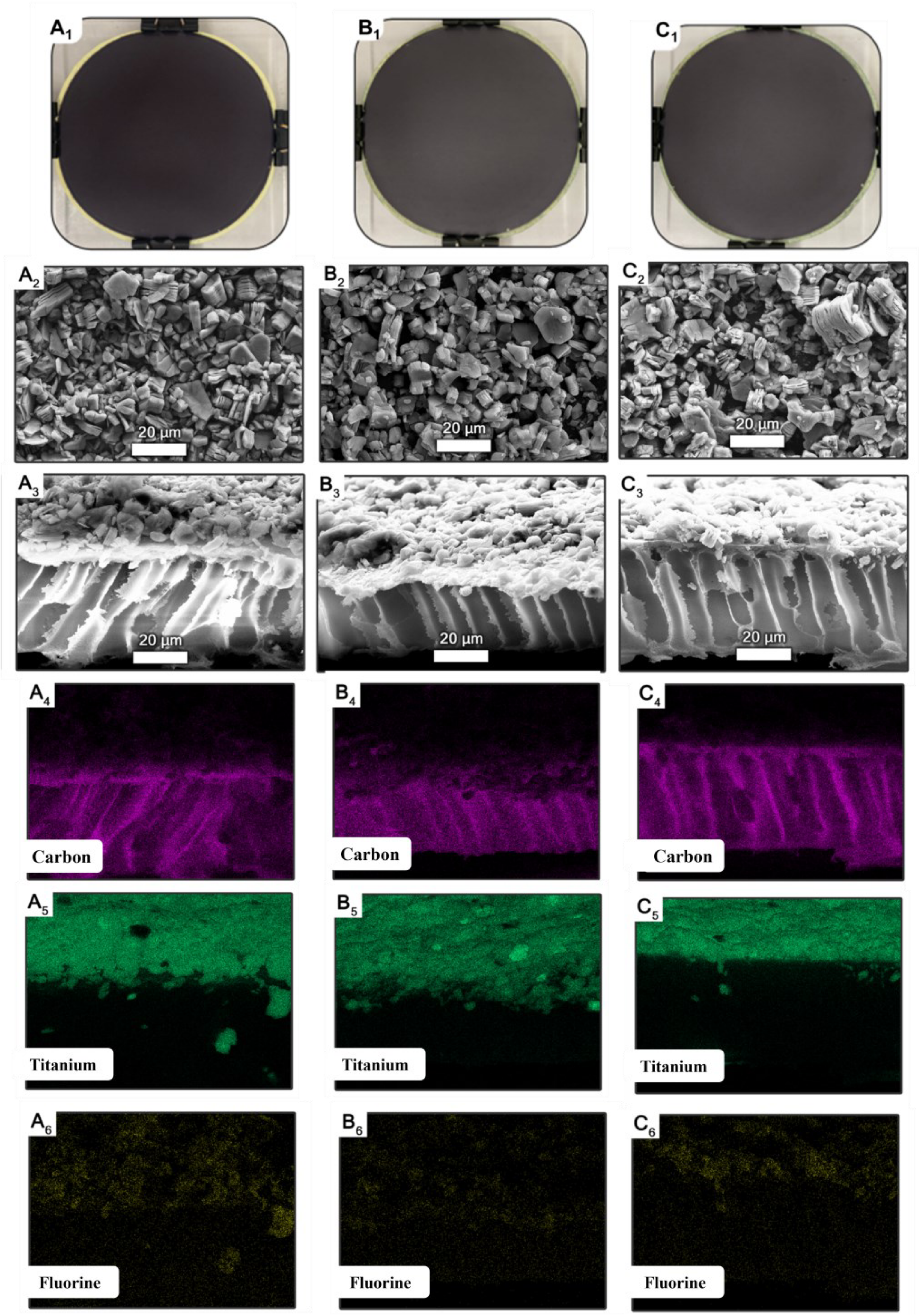

Figure 2.6. (A_1-A_6) Characterization of ECM1, (B_1-B_6) ECM2, and (C_1-C_6) EMC3. A_1, B_1, and C_1 : Optical depictions from the top surfaces. The second and third rows are top and cross-sectional FESEM images membranes. The three last rows demonstrate the EDX mapping analyses for three elements from the corresponding cross-section.

Table 2.3. EDX elemental compositions for three Ti3C2 MXene-coated membranes ECM1, ECM2, and ECM3. All values are reported in percentages and averaged over three sample locations at medium magnification (1 KX).

Chemical elements	**Weight % from EDX analysis**		
	ECM1	**ECM2**	**ECM3**
Ti	62.25	49.50	58.90
Al	2.42	2.76	2.59
C	8.76	17.97	10.94
F	13.50	12.26	13.24
O	13.04	17.48	14.31

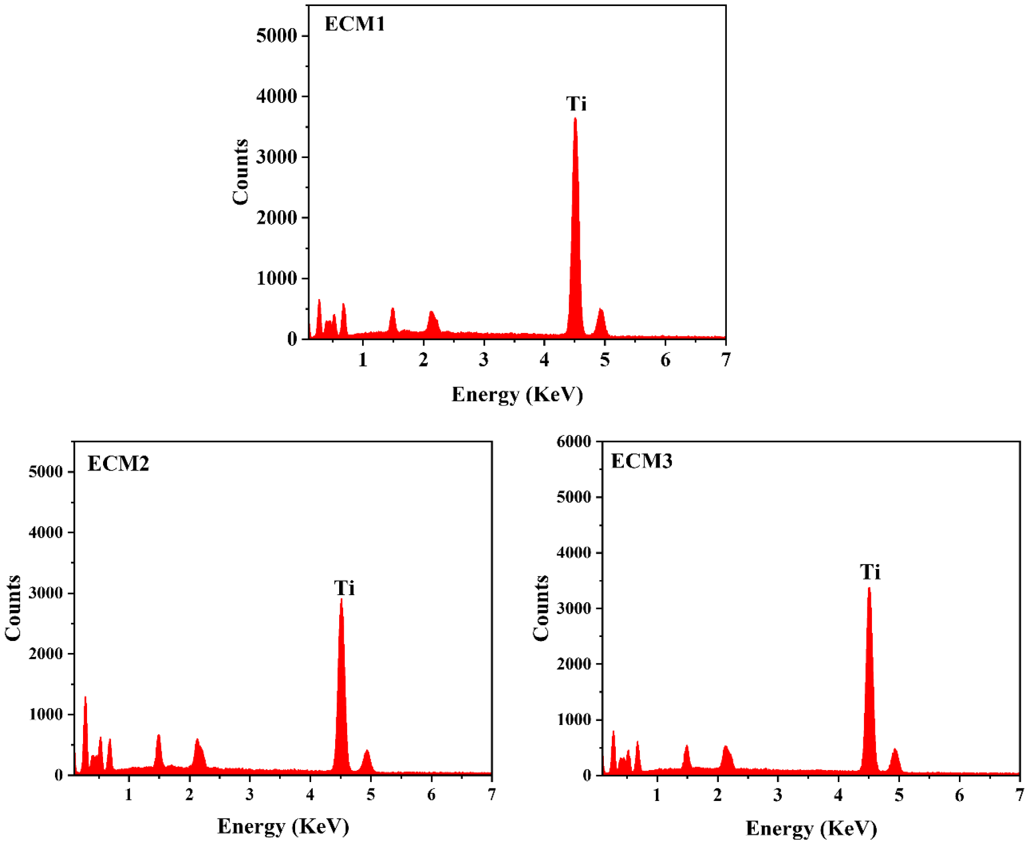

Figure 2.7. EDX spectra of three Ti_3C_2 MXene -coated membranes ECM1, ECM2, and ECM3.

Figure 2.8(A) presents transmission electron microscopy (TEM) images of three different MXene-coated membranes. These images reveal the presence of accordion-like Ti_3C_2 particles on the top surface of all three MXene-coated membranes, indicating the successful coating of multilayered Ti_3C_2 nanosheets onto the porous PAI support. To assess the effect of MXene coating on surface roughness, atomic force microscopy (AFM) was employed (**Figure 2.8(B) and (C)**). For comparison, 2D/3D AFM images of the pristine PAI support layer are shown in **Figure 2.9**.

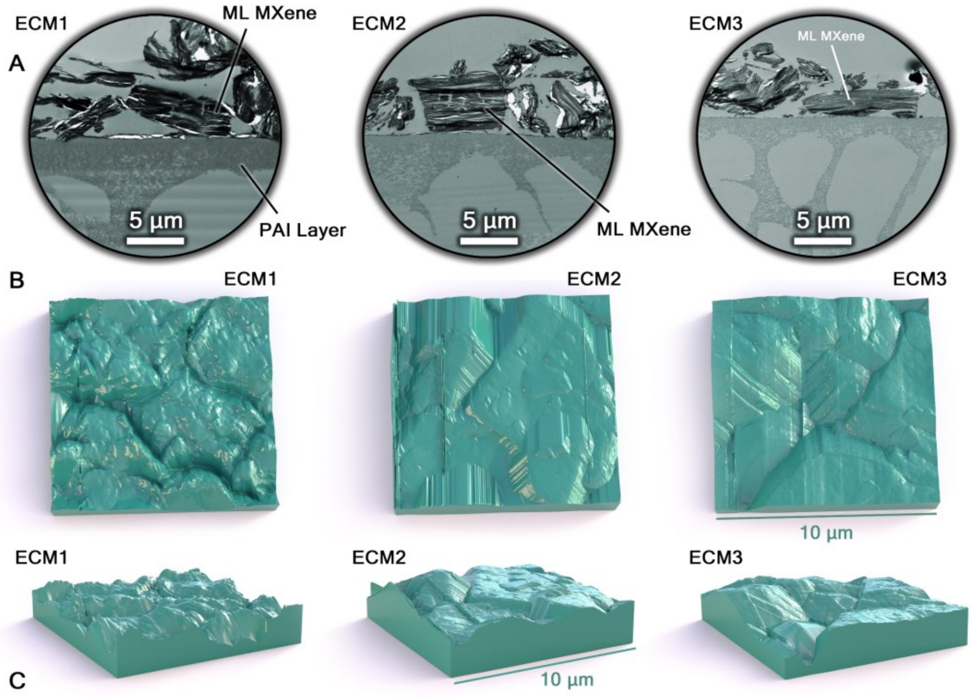

Figure 2.8. (A) Cross-sectional TEM images for ECM1, ECM2, and ECM3, (B) 2D AFM images of ECM1, ECM2, and ECM3, and (C) 3D AFM images of ECM1, ECM2, and ECM3.

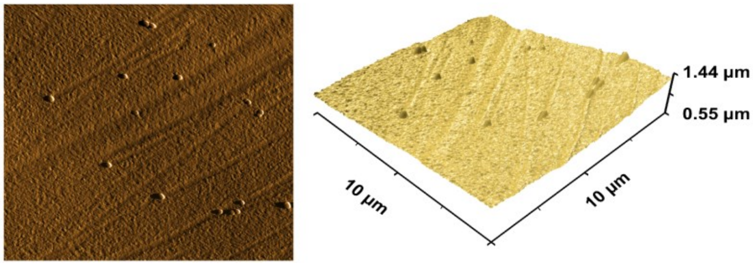

Figure 2.9. 2D/3D AFM images of pristine PAI membrane

The surface roughness values, including average roughness (R_{avg}), RMS roughness (R_{rms}), and Wenzel roughness ratio (1+SAD), are provided in **Table 2.4**. Upon MXene coating, the R_{avg} and R_{rms} of the MXene nanocomposite membrane increased by more than five folds from 35.89 and 45.05 nm for the pristine PAI membrane to 195.5 and 252.5 nm for ECM1, respectively. The reduction in MXene concentration in ECM2 and ECM3 resulted in greater MXene multilayer inhomogeneity and an increased number of surface cavities, leading to increasing average roughness values from 195.5 nm for ECM1 to 594.6 and 912.0 nm for ECM2 and ECM3, respectively. The Wenzel roughness, which represents the ratio between the actual and projected solid surface area, increased from 1.384 for ECM1 up to 1.885 and 1.813 for ECM2 and ECM3 membranes, respectively.

Table 2.4. Surface roughness parameters from the AFM analyses with a scan size of 10 µm ×10 µm.

Membrane	Average roughness (R_{avg})	RMS roughness (R_{rms})	Wenzel roughness-ratio (r=*1+SAD*)
PAI	35.89 nm	45.05 nm	1.113
ECM1	195.5 nm	252.5 nm	1.384
ECM2	594.6 nm	798.2 nm	1.885
ECM3	912.0 nm	1176 nm	1.813

Figure 2.10(A) depicts the results of the zeta potential study conducted on the MXene-coated membranes, as well as the PAI support, at various pH values. The results show that the surface of the PAI support layer is negatively charged across the entire pH range, which can be attributed to the deprotonation of carboxyl and hydroxyl groups present on the surface. The negative charge density on the membrane surface was significantly enhanced upon coating the MXene layer on ECM1, ECM2, and ECM3. The negative charge of the MXene layer can be attributed to the presence of functional groups such as C=O, –OH, and –F, which carry negative charges [165].

The electrical conductivities of the Ti_3C_2-MXene coating layers were measured using a four-point probe resistivity measurement (

Figure 2.10(B)).

ECM1 exhibited the highest electrical conductivity of 174 ± 0.16 S/m among all the prepared membranes, while ECM2 and ECM3 coated membranes showed electrical conductivities of 27 ± 0.32 S/m and 15 ± 0.13 S/m, respectively. The higher conductivity of ECM1 compared to those of ECM2 and ECM3 suggest that higher amount of MXene (doubling the MXene amount) leads to an approximate tenfold increase in conductivity. This observed conductivity enhancement with a higher MXene coating can be attributed to the improved connectivity within the coating layer. A thicker coating with more MXene particles provides a more continuous conductive network between the particles with fewer gaps and voids, facilitating electron transport throughout the membrane. The higher conductivity of ECM1 implies that by adding more MXene we can enhance the electrical conductivity which is beneficial for our membrane use. However, increasing the MXene concentration will decrease the membrane flux, because a denser MXene particles network could hinder the passage of molecules through the membrane. Thus, while a higher MXene coating thickness can enhance conductivity, there are practical considerations, such as flux reduction, that need to be considered when optimizing the MXene concentration.

Figure 2.10(C) illustrates the dynamic electrical conductivity of ECM1 over 40 days exposure to the ambient air. It can be observed that the electrical conductivity of ECM1 decreased rapidly in the first 15 days. However, after 30 days, the reduction in electrical conductivity reached a plateau and stabilized around 16 S/m. This trend reveals the oxidation of the MXene coating layer in the initial days after membrane fabrication.

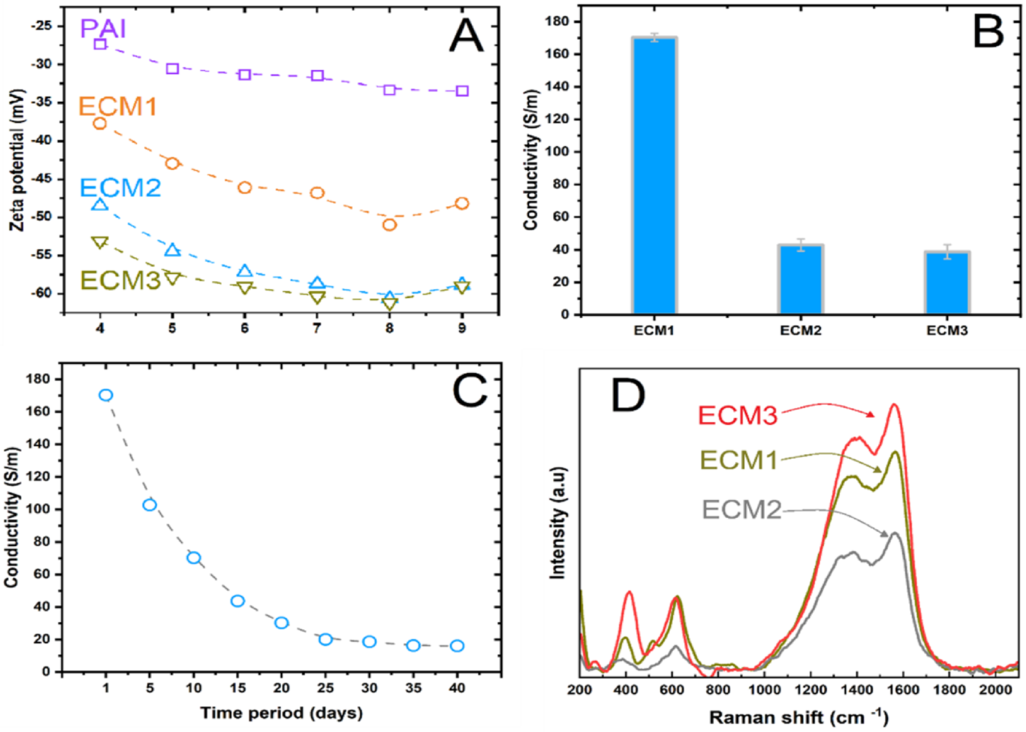

Figure 2.10. (A) Surface zeta potential of pristine PAI membrane (M0), ECM1, ECM2, and ECM3, (B) electrical conductivities of three fabricated membranes (ECM1, ECM2, and ECM3), (C) Trend of electrical conductivities of the ECM1 in 40 days, (D) Raman spectra of three MXene-coated membranes ECM1, ECM2, and ECM3.

The Raman spectra of the prepared Ti_3C_2-MXene membranes, including various modes with distinct vibrational frequencies, are shown in

Figure 2.10(D). The peak at 201 cm^{-1} wavenumber is specifically assigned to the A_{1g} (Ti, O, C) mode, which represents the out-of-plane vibrations of Ti atoms [177]. The strong peak at 403 cm^{-1} corresponds to the E_g group vibrations of surface functional groups attached to Ti atoms. Another characteristic peak exists at 617 cm^{-1} wavenumber, which relates to both E_g and A_{1g} vibrations of carbon.

Surface chemical compositions of the prepared membranes were investigated through XPS analyses, and the XPS survey scan spectrums are shown in **Figure 2.11(A)**. The important peaks corresponding to C 1s (~284 eV), O 1s (~455 eV), Ti 2P (~532 eV), and F 1s (~685 eV) of Ti_3C_2 MXene are marked on the plot [178]. The Ti concentration in all samples, as determined by XPS analysis, was approximately 48 wt.%, a close match to the composition of the coating solution at around 50%. The deconvoluted C 1s region for ECM1 is presented in **Figure 2.11(B)**. The prominent peak at a binding energy of 281.5 eV corresponds to the C−Ti−x bond, while the other two dominant peaks at 284.7 eV and 286.3 eV relate to graphitic C−C (or C−H) and C−O, respectively [179]. These chemical bonds exist in the structure of CMC and GA. Two smaller peaks centered at 287.5 eV and 289.2 eV correspond to the carbon bonds existing in the carbonyl and carboxyl functional groups, respectively. The fractional percentage of each specific chemical bond was determined by measuring the peak area, and the resulting values for three different membranes are presented in **Table 2.5**. It is evident from the table that ECM1 exhibited the highest fraction of Ti−C−Ti, with a percentage of 14.28%. **Figure 2.11(C)** illustrates the Ti 2P region for ECM1, where the peaks at 455.5, 456.2, 457.3, and 458.0 eV can be attributed to Ti−C, Ti(II), Ti(III), and Ti(IV) or TiO_2, respectively [180]. Moreover, a prominent peak at 459.6 eV corresponds to $TiO_{2-x}F_x$ chemical bonds. The O 1s region of ECM1 was also analyzed through deconvolution, as shown in **Figure 2.11(D)**. This analysis revealed five fitting peaks at 530.0 eV (TiO2), 530.7 eV (C−O), 531.9 eV (C=O), 533.9 eV (C−Ti−O or C−Ti−OH), and 534.2 eV (O−H) [181].

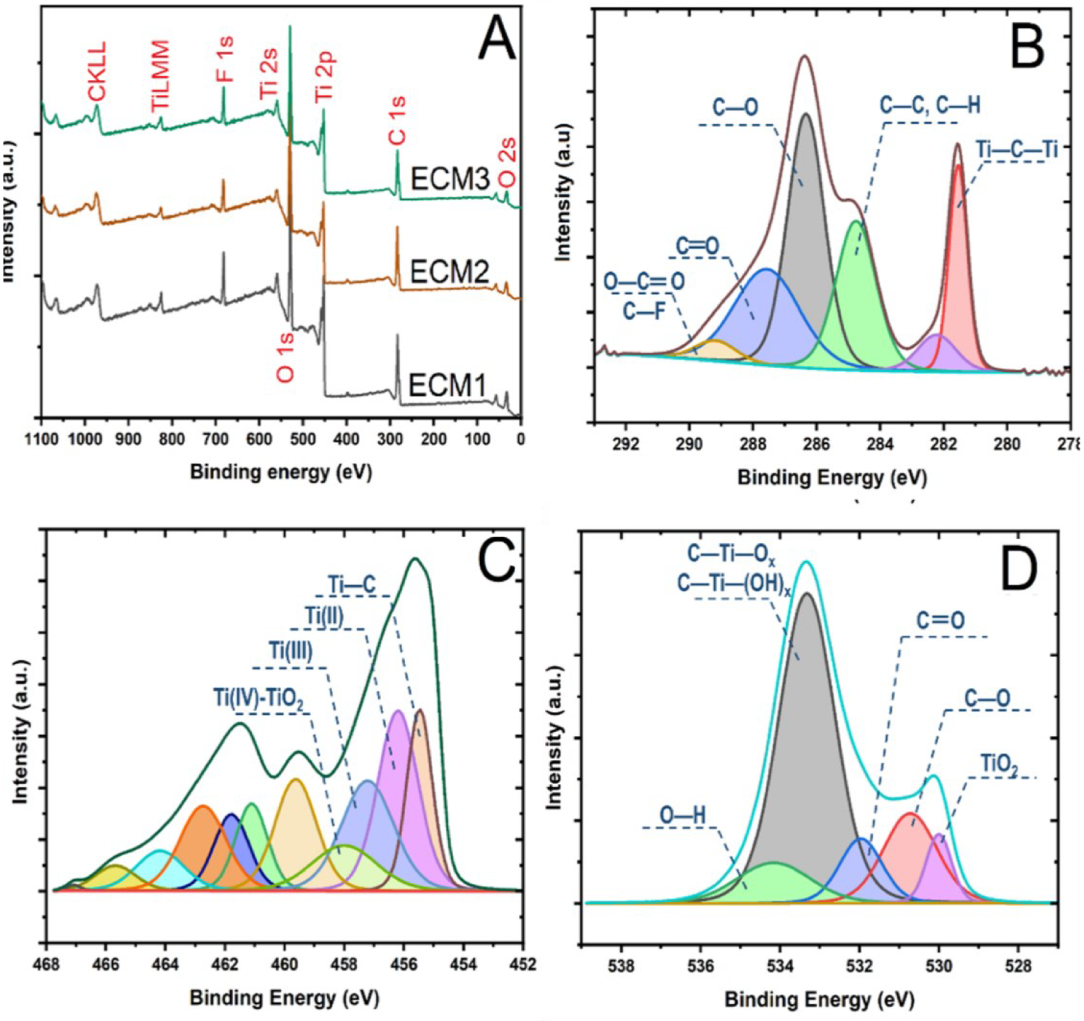

Figure 2.11. (A) XPS survey scan spectrums for ECM1, ECM2, and ECM3. Regions (B) C 1s, (C) Ti 2p, and (D) O 1s for ECM1 membrane.

Table 2.5. Fractional percentage of each specific chemical bond in deconvoluted C 1s

Name	Position (eV)	Percentage atomic concentration (%)		
		ECM1	ECM2	ECM3
C-O	286.36	37.71	43.74	34.08
Ti-C-Ti	281.54	14.28	10.97	13.66
C=O	287.78	11.2	10.06	22.56
C 1s	284.81	27.61	25.18	21.56
C-M (metal carbide)	282.34	4.93	4.1	5.11
O-C=O, C-F	289.12	4.28	5.96	3.04

The physical stability of the modified membranes' coated layer was assessed by measuring the presence of Ti ions in the immersed solution. For this purpose, membranes with an effective surface area of 45.34 cm^2 were immersed in DI water and stirred at 100 rpm for three weeks [160]. The leaching rate of Ti ions served as an indicator of the stability of the Ti_3C_2 MXene coating layer. **Figure 2.12(A)** demonstrates the higher Ti leaching rate for ECM1 membrane compared to the other two membranes (EC2 and ECM3). This observation could be attributed to the higher MXene content in the ECM1 membrane. The leaching rates for the first 7 days, first 14 days, and first 21 days are 0.029 mg/d, 0.011 mg/d, and 0.006 mg/d, respectively. Considering an average Ti leaching rate of 0.00291 mg/d during the initial 21-day period, we can estimate that the coating lifetime, until complete removal of the MXene coating layer (80 mg MXene for ECM1), is at least 36529 days. It is important to note that this estimation assumes a linear trend in leaching over time with a relatively constant leaching rate. However, in reality, the leaching rate tends to decrease over time. Consequently, the actual coating lifetime is expected to be longer as the leaching rate decreases over time.

To evaluate the chemical stability of the modified membranes, various corrosive solutions, and organic reagents (NaOH, HCl, ethylene glycol, and acetone) were employed. Optical images of the ECM1 membrane after 48 hours of immersion in various pH solutions and organic solvents are presented in **Figure 2.13**. With the exception of the alkali solution with a pH of 13, all solutions appear clear, and no physical detachment can be observed on the surfaces of the tested membrane pieces. Exposure of MXene-modified membranes to harsh alkali solutions appears to weaken the covalent bonds between CMC and GA binders, leading to the peeling off of entrapped MXene nanosheets from the PAI surface. Subsequently, the UWOCA of the ECM1 was measured after these experiments, and the obtained values are reported in **Figure 2.12(B)**. The MXene-coated membrane exhibited the UWOCA of approximately 180° after 48 hours of immersion in acetone and ethylene glycol solutions. A similar UWOCA was measured for the ECM1 membrane after immersing it in an HCl acid solution.

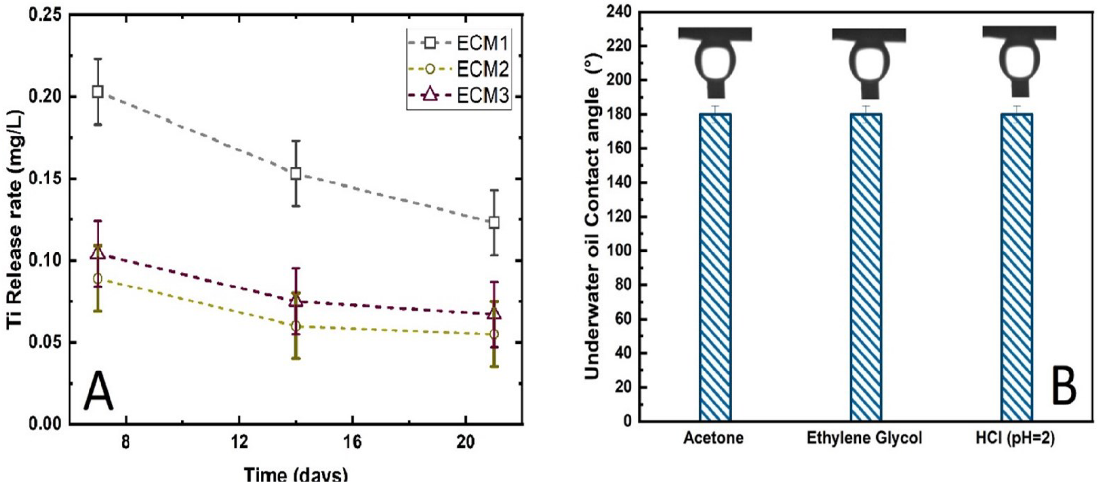

Figure 2.12. (A) The concentrations of Ti from the surfaces of three different membranes in the immersed solutions. The samples were taken on different days, and the released Ti concentration was measured through the ICP method. (B) UWOCA of the ECM1 after 48 h immersion in acetone, ethylene glycol, and HCl acidic solution.

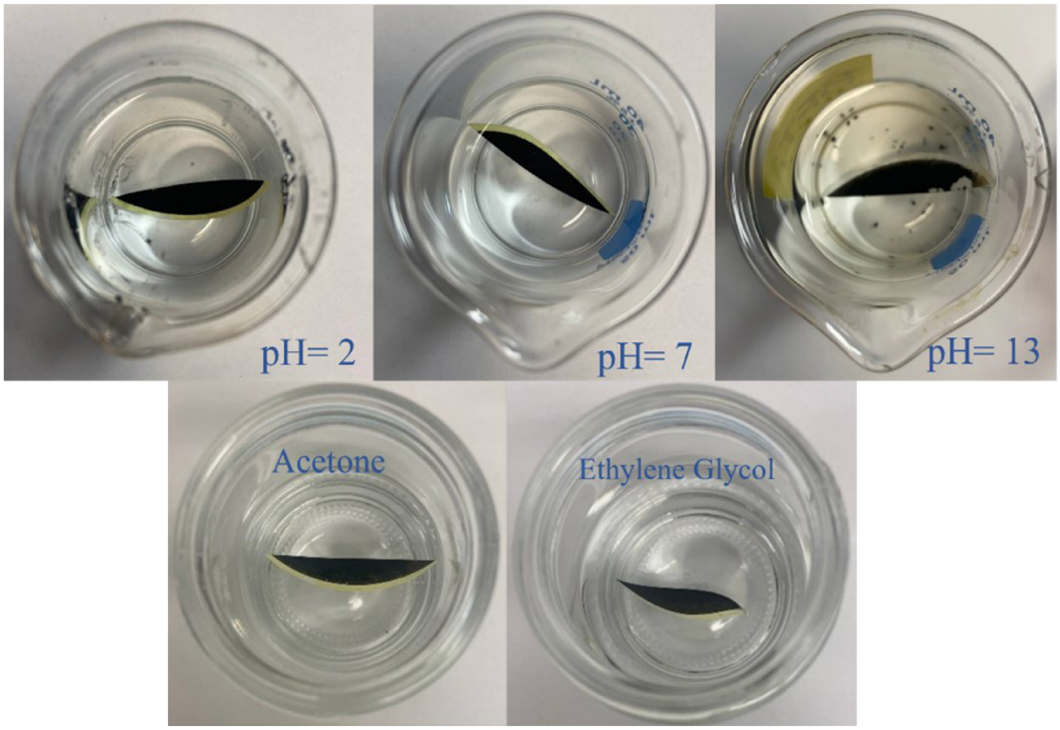

Figure 2.13. Membrane images after immersing in various organic solvents, acidic and alkali solutions after 48 hours.

2.3.2 Dye separation performance of Ti_3C_2 MXene-modified membranes

The water flux and dye rejection performance of PAI and all modified membranes were assessed using a cross-flow filtration setup. As shown in **Figure 2.14(A)**, coating the membrane surface with Ti_3C_2-MXene resulted in a decline in water flux from 1400 LMH to 57 LMH, 80 LMH, and 140 LMH for ECM1, ECM2, and ECM3, respectively, at 20 psi transmembrane pressure. However, the efficacy of the membrane in dye rejection significantly increased. The performance of all fabricated membranes for rejecting three different dyes, namely RR120 (MW: 1774.15 Da), RB (MW: 991.82 Da), and MO (MW: 327.33 Da), was evaluated.

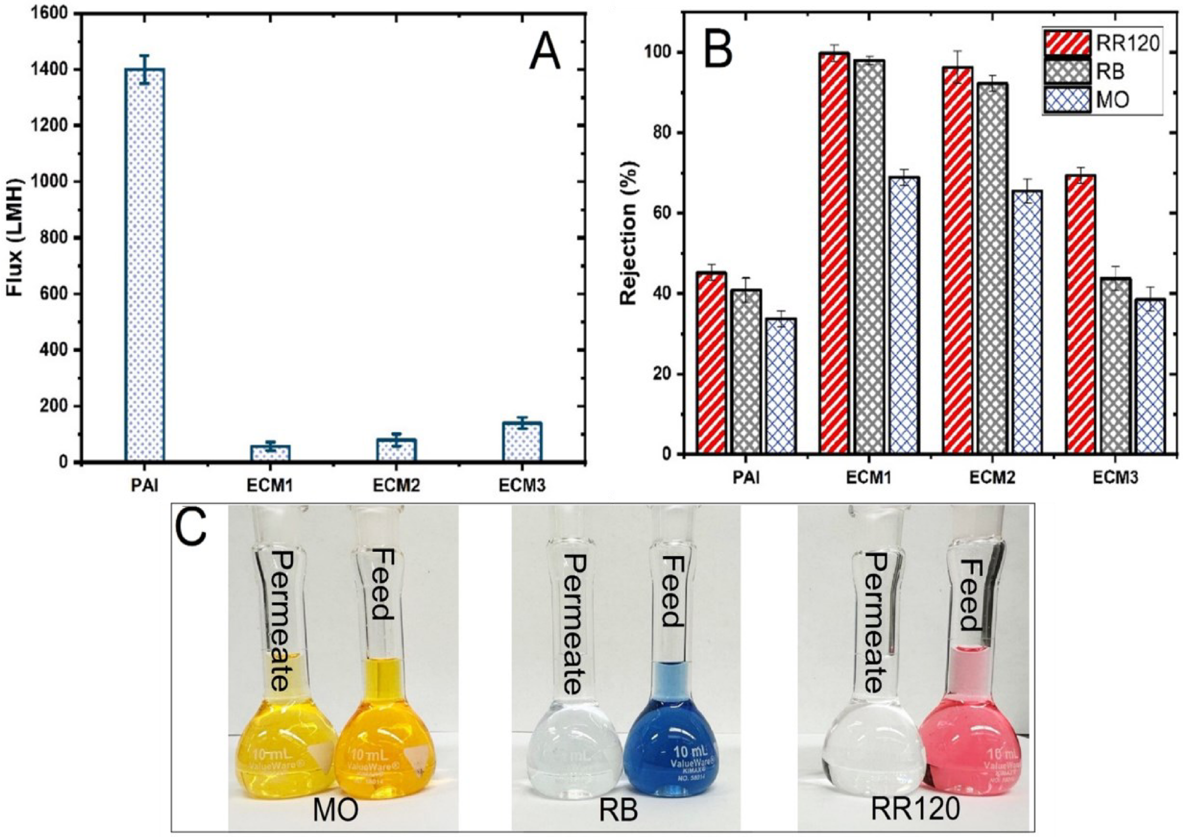

Figure 2.14. (A) pure water flux, and (B) RR120, RB, and MO dye rejection performances of all synthesized membranes. (C) Optical images of ECM1 membrane performance in the rejections of three different dyes.

The chemical characteristics of these dyes are provided in **Table 2.6**. Based on the experimental results shown in **Figure 2.14(B)**, the coating of the MXene layer on the ECM1 membrane surface improved the dye rejection performance from 45.2% to 99.71% for RR120, from 40.81% to 97.95% for RB, and from 33.65% to 68.91% for MO. Optical images of the feed solutions for the three different dyes, as well as the permeated solutions passed through ECM1, are displayed in **Figure 2.14(C)**. The coating of Ti_3C_2 MXene followed by CMC/GA cross-linking effectively reduced the membrane surface pore size (~20 times), as evidenced by the MWCO and flux results (**Figure 2.14(A)** and **Figure 2.15**), leading to enhanced dye rejection. It is conceivable that the higher concentration of Ti_3C_2 MXene on ECM1 might lead to a reduction in its pore size and surface cavities compared to the other two fabricated membranes, resulting in more effective dye rejection by ECM1. Comparing the dye rejection results between ECM2 and ECM3, it can be concluded that the concentration of CMC as a binder can also impact the membrane separation performance. Reducing the CMC concentration in ECM3 led to a slight decline in membrane dye rejection performance. Another factor contributing to such a dye rejection performance could be the high electrostatic repulsion between negatively charged dye molecules and the negatively charged modified membrane surfaces.

MWCO experiments were conducted on the ECM1 using 200 ppm of PEG with different molecular weights, and the obtained data are illustrated in **Figure 2.15**. The results reveal that the MWCO of the ECM1 membrane is approximately 6,200 Da, indicating that the membrane is capable of rejecting >90% of solutes with a molecular weight of this magnitude. Since the molecular weights of the studied dyes are significantly lower than 6,200 Da, it was expected that the membrane would have a very low rejection capacity for these dyes. It is important to note that while MWCO indicates the membrane's sieving capability based on size, it does not fully capture the complex interactions between the membrane and the dye molecules, which can affect rejection performance. Membrane surface interactions due to surface charge, hydrophilicity/hydrophobicity, presence of functional groups, and electrostatic interactions can contribute in dye rejection. Therefore, MXene-coated membranes, specifically ECM1 with higher amounts of MXene, showed high rejection rate even for dyes with lower than 6,200 Da.

Table 2.6. Some of the chemical characteristics of used dyes in the water filtration tests.

Name	Chemical structure	Molecular formula	Weight (g/mol)
RR120	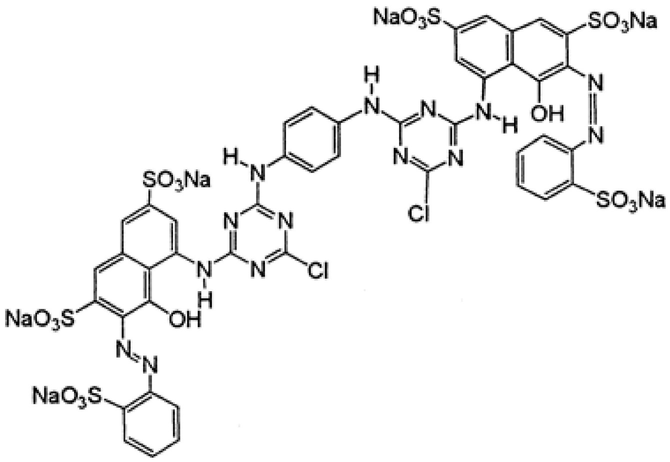	$C_{44}H_{24}Cl_2N_{14}Na_6O_{20}S_6$	1469.98
RB	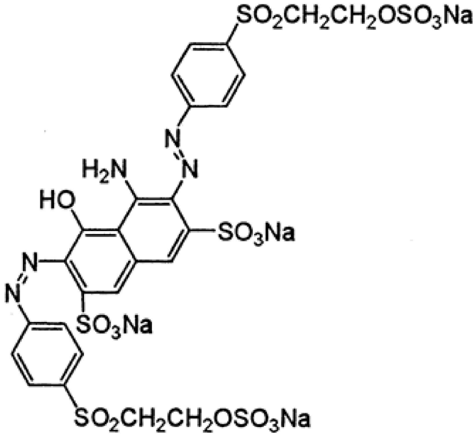	$C_{26}H_{21}N_5Na_4O_{19}S_6$	991.82
MO	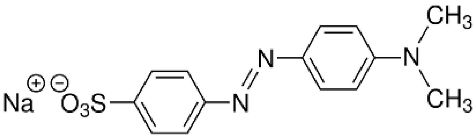	$C_{14}H_{14}N_3NaO_3S$	327.33

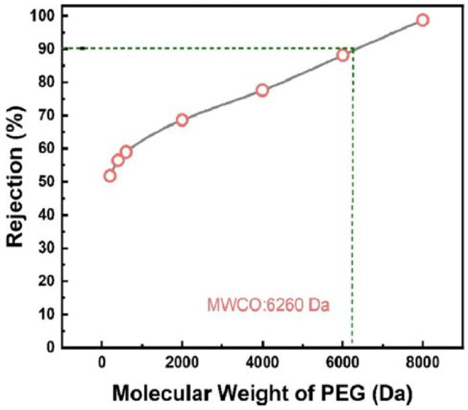

Figure 2.15. MWCO for the ECM1 membrane

Figure 2.16 illustrates the electrochemical assessment of MXene-coated membranes within a flow-through electrochemical cell, utilizing LSV methodology. The current response indicates an incremental trend in all three electrolytes as the potential decreases, indicative of the hydrogen evolution reaction (HER). However, the attained current response remains modest, peaking at a maximum value of -0.22 mA/cm² with an applied potential of -1.9 V vs. SHE in a H_2SO_4 solution. Among the tested electrolytes, i.e., NaOH, Na_2SO_4, and H_2SO_4, the latter, owing to its higher proton concentration, establishes a more conducive milieu for HER. The LSV outcomes aptly showcase the conductivity and operational efficacy of the in-house fabricated membranes functioning as electroconductive substrates.

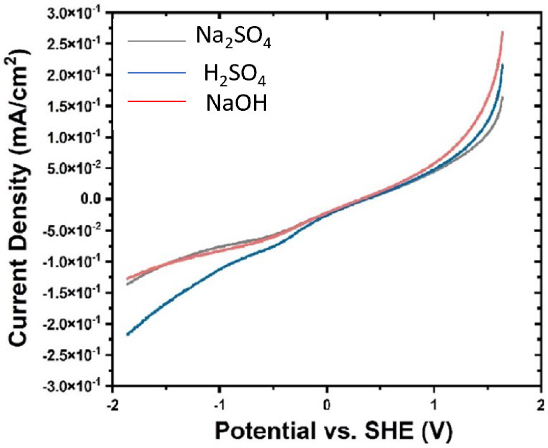

Figure 2.16. LSV curve for ECM1

Cyclic voltammetry tests were performed to assess the electrochemical activity of the Ti_3C_2-modified membranes in reduction and oxidation processes. As shown in **Figure 2.17(A)** , the ECM1 membrane exhibited two prominent peaks related to redox reactions when exposed to potassium hexacyanoferrate. The cathodic peak at approximately -0.92 V and the anodic peak at approximately -0.1 V versus SHE corresponded to the reduction and oxidation of the $Fe(CN)_6^{3-}/Fe(CN)_6^{4-}$ redox pair species, respectively. The observed peak currents for both the cathodic and anodic peaks indicating the electrochemical activity of the Ti_3C_2 MXene membrane surface. Furthermore, three additional CV tests were conducted using ECM1 as a working electrode in the presence of model foulants, and the results are depicted in **Figure 2.17(B-D)**. All these CV results indicate no significant difference between the voltammogram of the baseline electrolyte (Na_2SO_4) and those infused with 200 mg L^{-1}. As depicted in **Figure 2.17(B)** and **Figure 2.17(C)**, neither SA nor HA engages in discernible interactions with the MXene-coated surface within the range of applied potentials (-1.9 V to 1.6 V vs. SHE). The CV data for BSA (**Figure 2.17(D)**) spans an expanded potential spectrum, encompassing -3.3 V to 3.6 V vs. SHE. However, similar to the behaviors of HA and SA, BSA exhibits no distinct peaks corresponding to reduction or oxidation in comparison to the background electrolyte.

2.3.3 Study of membranes' fouling behavior in an electrochemical cell

The fouling potential of the MXene-modified membrane (ECM1) and its corresponding FRR were assessed through three-step dynamic cross-flow filtration experiments with feed solutions containing HA, SA/$CaCl_2$, and BSA. To evaluate the impact of the electric potential application on the membrane's FDR and FRR in the fouling tests, distinct cathodic potentials were applied and the normalized water flux versus time was recorded. **Figure 2.18(A)** illustrates the water flux through the ECM1 membrane for the HA solution over time, aiming to evaluate the organic fouling. When negative potentials of 2V and 4V were applied to the ECM1 membrane surface, the FRR increased from 92.52% to 95.63% and 99.83%, respectively. Simultaneously, the FDR decreased from 45.56% to 23.13% and <1% with the application of 2V and 4V negative potentials, respectively. These results demonstrate that the antifouling property of the ECM1 membrane significantly improved with higher negative potentials applied.

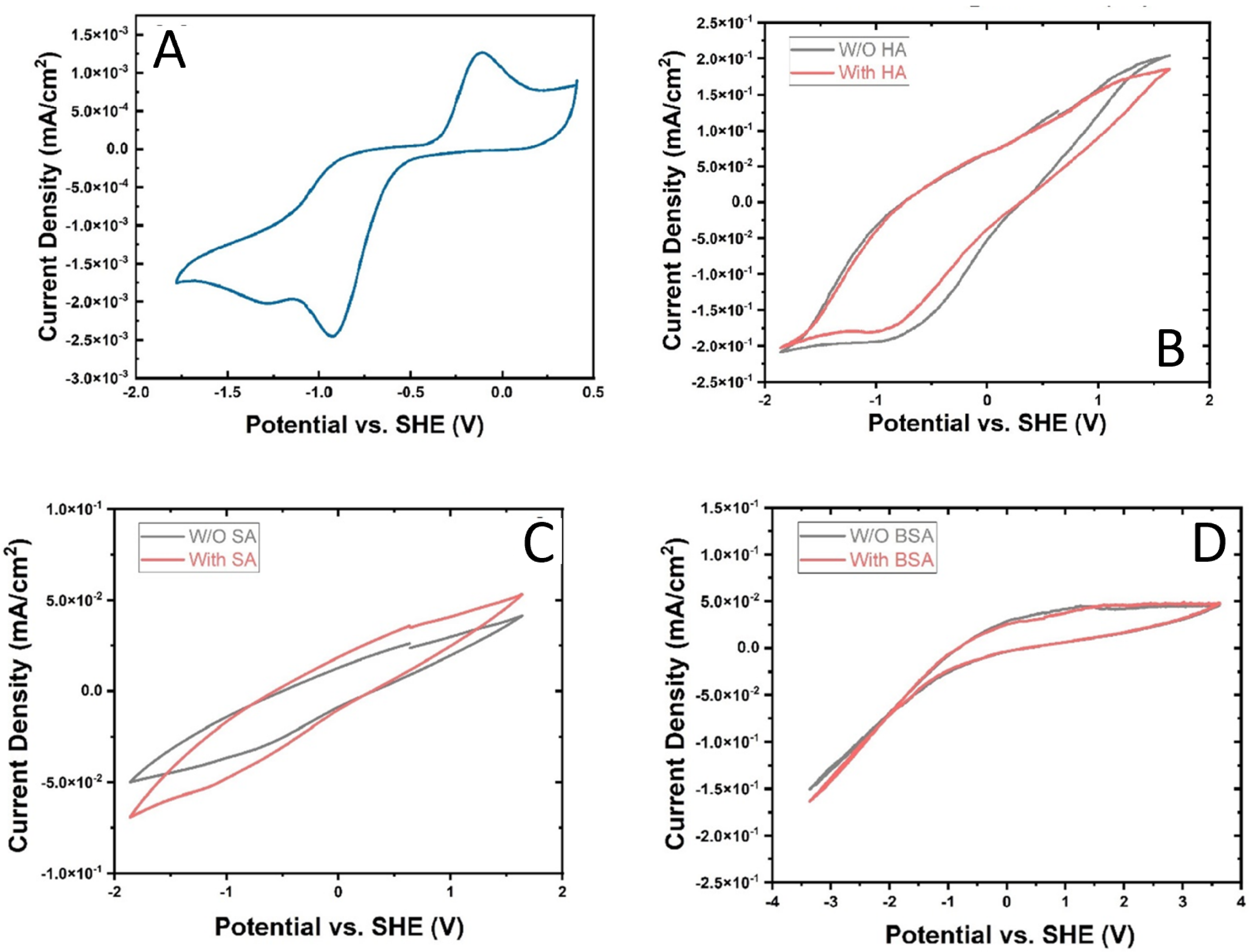

Figure 2.17. CV curves of ECM1 membrane (A) in the mixture of $K_4Fe(CN)_6$ (0.01 M)/$NaNO_3$ (0.1 M) solution with a potential range from –1.77 to 0.41 V vs SHE with a scan rate of 15 mV/sec. (B-D) CV curves for the ECM1 in the lack and presence of different model foulants with different potential ranges

The MXene-modified membrane's performance in resisting organic fouling was further evaluated using a feed solution containing SA/$CaCl_2$ in the same three consecutive steps as before. **Figure 2.18(B)** (right side) illustrates that by applying a negative 6 V potential, the FRR increased from 84.74% to a maximum value of 99.94%, while the FDR decreased significantly to a minimum value of <1%. These results indicate that the ECM1 membrane experienced no fouling with SA/$CaCl_2$ as the applied cathodic potential was increased from 0 to 6 V. In addition to the benefits of the electric field in reducing membrane fouling, we also observed a high flux recovery rate for membranes subjected to a negative voltage after membrane washing. Similarly, **Figure 2.18(C)** (left side) shows a substantial reduction in the fouling propensity of the ECM1 under the negative voltages (2, 4, 6, and 8 V) during the filtration of a BSA solution. Additionally, applying an 8 V electric field in the electrochemical cell (**Figure 2.18C))** resulted in >99% FRR and an almost negligible FDR, indicating the exceptional protein fouling resistance of MXene-modified membranes.

Overall, **Figure 2.18** indicates that the initial stage involves a rapid decline in flux within the first five minutes, followed by a subsequent phase where the flux decline stabilizes into a steady-state pattern. This two-stage fouling mechanism suggests a dynamic fouling process where an immediate and intense fouling effect takes place initially, likely due to the accumulation of larger particles or the formation of a surface layer. This is then succeeded by a more gradual fouling process that establishes a consistent flux reduction rate. The primary fouling mechanism can be inferred from this observation. The abrupt flux decline in the early stage implies that particulate fouling, where larger particles block the membrane pores or attach to its surface, might be the dominant mechanism during this period. As the flux decline stabilizes in the later stage, it could indicate that a secondary fouling mechanism, such as cake formation or concentration polarization, starts to play a more substantial role in contributing to the flux reduction.

The observed enhancement in fouling resistance can be attributed to multiple factors. Firstly, the strong electrostatic repulsion between the membrane and the foulants, along with the occurrence of electrochemical reactions, play significant roles, as will be elaborated later. The negatively charged contaminants in the water, including HA, SA/$CaCl_2$, and BSA, are effectively repelled from the membrane surface due to the negative charge on the cathode surface, resulting in high effective electrostatic repulsion forces. Moreover, the potential direct and indirect electrochemical reactions occurring on the membrane surface might also contribute to the degradation of organic matter and reduce its adherence to the membrane surface, primarily by diminishing hydrophobic attraction. Additionally, the fabricated membranes exhibit remarkable superhydrophilic properties, as indicated by WCA results. Consequently, when immersed in aqueous solutions, a hydration layer forms on the surface of ECM1 due to the affinity of water molecules. This hydration layer further minimizes interactions between the membrane surface and foulants, thereby enhancing fouling resistance.

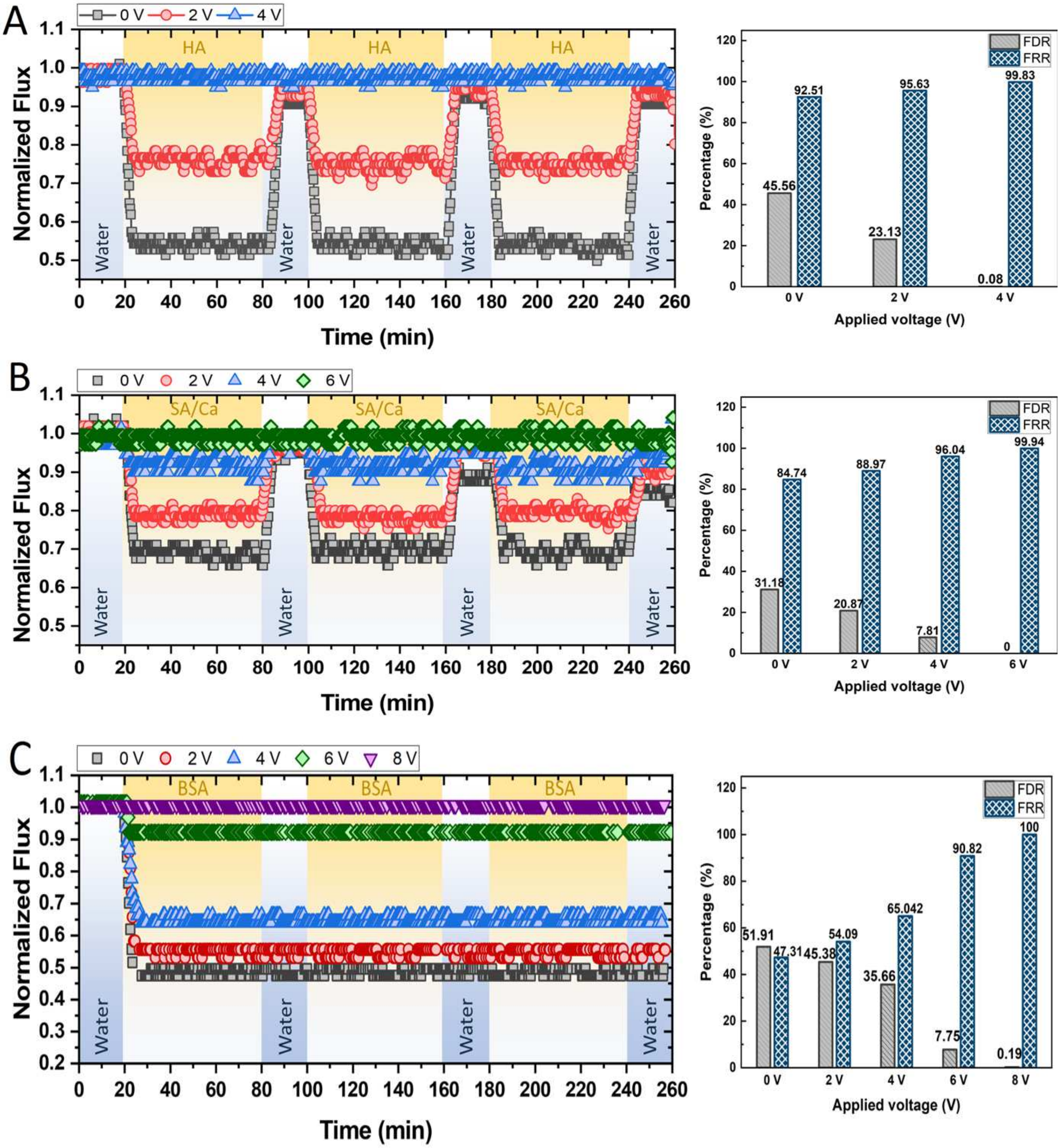

Figure 2.18. Variation of normalized water flux versus time for prepared ECM1 with different applied voltages using various foulant solutions (left side) with corresponding FDR and FRR values (right side): (A) HA solution (200 ppm HA, pH~7), (B) SA/CaCl$_2$ solution (200 ppm SA and 0.5 mM CaCl$_2$), and (C) BSA (200 ppm).

All mentioned factors, either due to inherent static membrane properties (e.g., wettability) or due to applied potential (e.g., electrochemical reactions), collectively contribute to the observed enhancement in fouling resistance. They showcase the intricate interplay between high electrostatic repulsion forces, possible negligible electrochemical reactions, and the superhydrophilic properties of the fabricated membranes, ultimately leading to improved fouling resistance.

2.3.4 Surface free energy

In fouling experiments, the deposition of foulants on the membrane surface is typically influenced by both hydrodynamic and physicochemical interactions between the foulant macromolecule and the membrane surface [182]. However, the physicochemical interactions are found to be more influential in the membrane fouling phenomenon [173,183]. The surface tension components of a membrane provide valuable insights into the energy associated with the affinity between the membrane surface and foulants with varying chemistry and molecular structures. To determine these surface tension components, contact angle analyses were performed using three probe liquids with different polarities: water, glycerol, and diiodomethane. The recorded contact angles for these liquids were 0°, 18°, and 0°, respectively. The obtained surface tension components, as shown in **Table 2.7**, indicate that all the studied foulants and the membrane possess high electron donor monopolarity and negligible electron acceptor components [184]. This finding aligns with the characteristics of polymeric membranes, which are often characterized by high electron donor monopolarity [173]. Also, the monopolar surface properties of all model foulants observed in this study are in line with previous findings reported by Subramani et al. [185].

The free energy of adhesion represents the energy per unit area between the membrane surface and foulants when submerged in a solvent, such as water. If $\Delta G_{mlf}^{TOT} > 0,$ the membrane surface is considered hydrophilic and exhibits a higher affinity for water than foulants. Conversely, if $\Delta G_{mlf}^{TOT} < 0,$ the attachment of foulant molecules is more favorable [186]. **Table 2.7** shows that ECM1 has a higher electron donor compared to electron acceptor surface tension components, suggesting that the basic component of the acid-base (AB) interactions control the polar contribution of the surface free energy. Additionally, for ECM1, the nonpolar components contribute significantly to the total surface tension. Given the relatively large negative values of the foulants, these materials are expected to exhibit repulsive behavior when deposited on the membrane surface [187]. The significantly high positive value of ΔG_{mlf}^{TOT} (13.54 mJ/m^2) for HA reported in **Table 2.7** indicates that the interactions between the membrane and HA molecules are expected to be strongly repulsive. Also, based on the calculated ΔG_{mlf}^{TOT} values for SA and BSA, it is expected that these foulants exhibit relatively stronger adhesion to the membrane surface compared to HA, as the interfacial adhesion energy between the membrane and SA or BSA foulants is lower than that of HA.

In conclusion, by applying an external electric potential, the loosely attached HA foulants to the membrane surface can be effectively removed after washing, restoring the water permeation performance to its initial value. The membrane fouling behaviors depicted in **Figure 2.18** confirm the findings of this study, where a complete antifouling performance was observed during lower cathodic potential applications in the HA experiments. It's important to note that while the thermodynamics described by ΔG provides insights into the potential adhesion strength, other factors such as the kinetics of the adhesion process, fouling dynamics, and the presence of external factors (e.g., flow rate, shear forces) should also be considered to obtain a comprehensive understanding of fouling behavior.

Table 2.7. Surface energy parameters (mJ/m^2) of ECM1 and studied foulants.

Membrane/ Foulants	γ^{LW}	γ^{+}	γ^{-}	γ^{AB}	γ^{TOT}	ΔG_{mlf}^{LW}	ΔG_{mlf}^{AB}	ΔG_{mlf}^{TOT}
ECM1	37.68	0.76	34.44	10.23	47.91	-	-	-
HA*	47	0.3	43	-2	40	-6.42	19.97	13.54
SA/CaCl$_2$*	46	2.1	40	-4	15	-6.21	16.55	10.33
BSA*	49	2.4	27	-6	7	-6.85	6.95	0.10

* ***Note.*** Adapted from **"**Assessment of physicochemical interactions in hollow fiber ultrafiltration membrane by contact angle analysis **",** by Nashida Subhi et al., Journal of Membrane Science, 403-404 [182].

2.3.5 Mechanisms of fouling mitigation in Ti$_3$C$_2$-MXene modified membranes

Electrostatic repulsive forces play a significant role in mitigating fouling between the negatively charged membrane and negatively charged foulants. Since all the studied foulants possess a negative intrinsic surface charge [188], applying an external potential to increase the negative charge on the membrane surface enhances the electrostatic repulsion between the membrane surface and foulants, thereby minimizing foulant attachment. Previous studies have demonstrated that manipulating surface charge can effectively regulate organic fouling by reducing pore blocking and gel formation [189]. Observations indicate that the repulsive force between the membrane surface and foulants increases as the cathodic potential increases. Consequently, foulant attachment to the membrane is further reduced, improving overall antifouling performance. Moreover, the application of an electric field between external electrodes has been shown to enhance the antifouling propensity of the membrane [190]. This can be attributed to the electrophoresis phenomenon, where charged foulant particles in water experience movement under the influence of the electric field toward the electrode with the opposite charge, preventing foulant deposition and cake layer formation on the membrane surface.

Gas bubbling represents another effective mechanism for controlling membrane fouling [191]. During conventional reduction/oxidation processes on inert electrodes, water electrolysis can occur, leading to the hydrogen evolution reaction (HER) and oxygen evolution reaction (OER) on the electrode surfaces. The HER involves the oxidation of water molecules to form oxygen gas on the anode surface (**Equation**2.12). Additionally, water electrolysis generates hydrogen bubbles on the cathode surface (**Equation 2.13**). By increasing the electric potential, the production of hydrogen gas on the electrode surface can be augmented, which mitigates the fouling rate.

$$2H_2O \rightarrow O_2 + 4H^+ + 4e^- \qquad 2.12$$

$$2H_2O + 2e^- \rightarrow H_2 + 2OH^- \qquad 2.13$$

Furthermore, electrochemical reactions may occur on the membrane surface regardless of the process configuration. Electrochemical reduction involves two cathodic processes. The first process, known as direct electron transfer (DET), involves the transfer of electrons from the cathode surface to the foulants. However, based on the CV results, the observed antifouling performance of the fabricated Ti_3C_2 MXene multilayered membranes cannot be attributed to the DET mechanism, as no corresponding reduction peak was observed within the applied potential range. The second process is an indirect electrochemical reduction mechanism induced by atomic hydrogen (H^*) adsorbed on the cathode surface. By applying a cathodic potential, atomic hydrogen might also be generated on the membrane surface (cathode) through the electrochemical reduction of protons (H^+) in the electrolyte (**Equation 2.14**) [192]. In the indirect electro-reduction process, the adsorbed atomic hydrogen interacts with the foulants, leading to their reduction. The adsorption of atomic hydrogen on the membrane surface can facilitate foulant reduction through various mechanisms. One possible mechanism involves the reaction of atomic hydrogen with foulants present in the electrolyte, breaking their chemical structure. This reaction, known as hydrogenolysis, involves the cleavage of chemical bonds in foulant molecules by atomic hydrogen, leading to the formation of smaller, less complex molecules that can be easily removed from the system [193,194].

$$H_2O + e^- \rightarrow H^* + OH^- \qquad 2.14$$

Another mechanism for mitigating fouling is the generation of superactive reagents, such as hydroxyl radicals ($^{\bullet}OH$), which can attack the chemical bonds of organic compounds near the membrane surface. This process reduces the molecular size of organic foulants and weakens their attachment to the membrane surface by diminishing hydrophobic interactions [195]. Also, during the cathodic reaction, electrons are transferred from the cathode to dissolved oxygen molecules in the surrounding solution. In acidic solutions, this results in the reduction of O_2 to form hydrogen peroxide, H_2O_2, at the cathode surface (**Equation 2.15**) [196,197]. In neutral pH solutions, the reaction still occurs but at a slower rate compared to acidic media. In alkaline solutions, electrons are transferred from the cathode to oxygen molecules in the solution, leading to the reduction of O_2 and the formation of hydroperoxide ions (HO_2^-) and hydroxide ions (OH^-) (**Equation 2.16**) [197].

$$O_2 + 2H^+ + 2e^- \rightarrow H_2O_2 \qquad 2.15$$

$$O_2 + H_2O + 2e^- \rightarrow HO_2^- + OH^- \qquad 2.16$$

2.4 Conclusion

This study presented a method to develop physically stable electro-conductive membranes with great robustness in vigorous stirring conditions. Specific weight ratios of MXene and CMC were co-deposited onto PAI support using pressurized air force to make electroconductive membranes that could respond to changes in an electric field. The modified Ti_3C_2-MXene membranes exhibited a notable enhancement in separation performance, particularly in removal of negatively charged dyes. Specifically, the rejections of reactive red 120 (RR120), reactive black (RB), and methyl orange (MO) dyes significantly increased from 45.2%, 40.81%, and 33.65% to 99.71%, 97.95%, and 68.91%, respectively. This remarkable enhancement in dye rejection was primarily attributed to the electrostatic repulsive interactions between the modified membrane surface and the negatively charged dyes.

The fouling performance of the ECM1 membrane, modified with Ti_3C_2-MXene, was evaluated under an electric potential using three different foulant solutions (HA, SA/$CaCl_2$, and BSA). In the case of the HA solution, applying a 4 V cathodic potential resulted in a remarkable FRR of 99.83% and a negligible decrease in FDR, while without any applied voltage, the FRR and FDR were considerably lower at 92.51% and 45.56%, respectively. Similarly, for the SA/$CaCl_2$ foulant, applying a 6 V cathodic potential increased the FRR from 84.74% to 94.4% while reducing the FDR to almost zero percent. Furthermore, when BSA was used as the model protein foulant, applying an 8 V potential to the Ti_3C_2-MXene membranes resulted in complete flux recovery (FRR of 100%) and no detectable flux decline. The observed antifouling properties of the ECM1 membranes can be mostly attributed to mechanisms such as strong electrostatic repulsive interactions and hydrogen gas bubbling through water electrolysis. These mechanisms work together to mitigate fouling and enhance the membrane's resistance to fouling.

The findings of this study provide valuable insights into the design and development of electro-conductive membranes with improved separation performance and fouling resistance. Such membranes hold promise for applications in various fields, including water treatment and filtration systems, where fouling is a critical concern. By addressing fouling challenges and offering sustainable solutions, these membranes contribute to the advancement of membrane technology and provide the potential for more efficient and environmentally friendly approaches to water treatment.

Chapter 3

Developing Electrically-Conductive Silver-Coated Polyamide-imide membranes for Sustainable Dye Removal and Antifouling Performance

3.1 Introduction

Water treatment technologies must be innovative and efficient, as water contamination andcarcity are major global issues [131–133]. Despite their widespread use, conventional polymeric membranes frequently suffer from fouling, instability, and decreasing separation efficiency over time [139,140]. Electroconductive membranes (ECMs) are being investigated in the search for improved membranes as they might be able to reduce fouling issues and open up possibilities for controlled processes by applying external electric potentials [72]. The introduction of electroconductive membranes has emerged as an innovative approach for addressing challenges concerning stability, antifouling properties, and separation efficiency in the pursuit of developing membrane-based technologies for water treatment processes [72].

ECMs present various capabilities, including electrophoretic mixing, joule heating, resistance to fouling, antimicrobial features, and the prevention of scaling. These attributes collectively enhance the performance of membrane filtration processes in applications related to water treatment [72]. There are various approaches to fabricating ECMs, ranging from incorporating conductive materials/polymers into the membrane to altering the membrane's surface by surface modification. However, creating an electrically conductive membrane through surface modification can pose some challenges, as it may amplify the intricate trade-off between flux and rejection. Additionally, the stability of the modified surface, encompassing electrochemical, mechanical, and physical aspects, is crucial to upholding durability across different operational conditions [198].

Silver, a noble metal known for its exceptional electrical conductivity, has attracted attention in exploring cutting-edge materials for electrochemical wastewater treatment applications [199]. The dual attributes of inherent conductivity and intrinsic antimicrobial properties of silver make it an excellent candidate for improving membrane performance in the context of fouling mitigation. The electrochemical performance of membranes has been demonstrated to be significantly enhanced by the incorporation of silver nanoparticles.

Research by Yi et al. showed that a thin film composite polyamide-imide membrane decorated with silver nanoparticles significantly improved dye removal efficiency and fouling performance [200]. Concurrently addressing multiple challenges, integrating silver nanoparticles improved the membrane’s electrical conductivity and added to its antimicrobial properties. Silver nanoparticles were immobilized on graphene oxide sheets in a study by Zhang et al., resulting in a hybrid material with strong antibacterial characteristics. Silver’s versatility in multifunctional membrane design for wastewater treatment applications is demonstrated by the synergistic effects of graphene oxide and silver, which not only enhanced the membrane’s electrical conductivity but also provided its antimicrobial functionality [201]. The review by Smith et al. provides a thorough analysis of the various applications, synthesis techniques, and mechanisms of antimicrobial performance of silver nanoparticles, with a focus on their potential in electrochemical processes for water treatment applications [202]. This study highlights silver's multifaceted role in addressing the challenges related to dye removal and fouling in water treatment processes, in addition to its role as a conductive element. Despite the remarkable advantages, it is important to note that silver’s stability under physical, mechanical, and electrochemical stresses in a range of operating conditions needs to be carefully considered. In order to improve the stability of silver-based materials, Gupta and Rai evaluated the function of citrate in the biogenic synthesis of silver nanoparticles [203]. This insight becomes especially important when designing silver-coated membranes to ensure sustained long-term performance over extended periods.

Building on the foundation laid by previous studies, recent research by Wang et al. focused on the development of silver-coated membranes with a specific emphasis on sustainable wastewater treatment. The study investigated the long-term performance of these membranes, considering factors such as stability, durability, and overall system efficiency. The results exhibited the potential of silver-coated membranes as an effective and long-lasting option for addressing the challenges of electrochemical wastewater treatment processes [204]. Understanding the mechanisms behind the enhanced electrochemical performance of silver-incorporated membranes is important for optimizing their design. Dhibar et al. investigated the electrochemical performance of membranes functionalized with silver. According to this study, silver increased the redox reaction effects during electrochemical processes for the degradation of organic pollutants in wastewater by facilitating electron transfer [205]. The electrochemical properties of silver are also essential for increasing oxidation and reduction mechanisms on the membrane surface. Zhou et al. investigated the electrocatalytic properties of silver-based membranes, demonstrating their ability to facilitate the electrochemical degradation of pollutants. Silver actively participates in redox reactions in various oxidation states, contributing to the organic compound's breakdown and removingollutants from wastewater [206].

This study provides a comprehensive study of a new type of electroconductive membrane, specifically an Ag-coated polyamide-imide (PAI) membrane that was fabricated via a facile 'spray and cure' coating technique. The membrane can function as a cathode material by applying an electrical field, actively participating in electrochemical reactions. In addition, the membrane showed antifouling performance via strong electrostatic repulsion between the membrane surface and foulants, gas bubbling through water electrolysis, and possible electrochemical reactions. Fabrication and characterization of Ag-coated PAI membrane provide insightful details about its unique characteristics and highlight its potential for implementation in environmentally friendly water treatment applications. Innovative approaches, such as the Ag-coated PAI membrane, indicate promise in addressing water-related issues and improving membrane-based water treatment technologies.

3.2 Experimental methodology

3.2.1 Chemical and Reagents

Aqueous-based conductive ink with 52% silver loading (SPI 508) was purchased from Novacentrix company (USA). N,N-dimethylacetamide (DMAc, >99.9%), calcium chloride ($CaCl_2$), sulfuric acid (H_2SO_4), and acetone were provided by Fisher Scientific. Additionally, hydrochloric acid (HCl) was supplied by Anachemica. Also, polyvinylpyrrolidone (PVP, 360 kDa), poly (ethylene glycol) (PEG), sodium alginate (SA), glacial acetic acid (ReagentPlus, 99.0%), and potassium hexacyanoferrate (III) ($K_4Fe(CN)_6$), and sodium hydroxide (NaOH) were purchased from Sigma-Aldrich. Polyamide-imide (PAI, Torlon 4000 THV) was supplied by Solvay Advanced Polymers. Reactive red 120 (RR120, MW: 1774.15 Da) and reactive black (RB, MW: 991.82 Da) dyes were acquired from Sigma-Aldrich and utilized as organic contaminants for dye removal experiments. Deionized water was used throughout this research.

3.2.2 Electro-conductive Ag-coated PAI membrane fabrication

3.2.2.1 Fabrication of PAI support layer

The fabrication of PAI support layers was conducted by applying the non-solvent-induced phase inversion (NIPS) technique. In this process, the utilized polymer was PAI, specifically Torlon 4000 THV, which is recognized for its outstanding attributes in terms of thermal, mechanical, and chemical resistance, in addition to its remarkable hydrophilicity. Supplementary additives such as PVP and PEG were incorporated to enhance membrane porosity, and the solvent employed throughout this procedure was DMAc. To obtain a uniform polymer solution, a mixture of 9 wt% PAI and appropriate amounts of additives was dissolved in DMAc and stirred at 350 rpm while being maintained at a temperature of 40 $^{\circ}$c for 24 hours. The homogenous solution was then left undisturbed in a vacuum oven for 10-15 minutes to eliminate any trapped air bubbles.

Finally, the PAI supports were synthesized by the large-scale membrane fabrication casting device using a film applicator to cast the solution onto a non-woven polyester fabric. The casting process was operated at a speed of 20 mm/s, with a constant gap height of 120 µm. Lastly, the cast film was immersed in a coagulation bath containing deionized water, where it remained overnight to ensure the complete removal of the solvent from the polymer matrix.

3.2.2.2 Preparation of silver ink-coated PAI membrane

Following PAI membrane synthesis, an Ag-coated PAI membrane was prepared using a facile spray coating method. This approach utilized an airbrush equipped with a 1 mm diameter nozzle to spray the Ag ink under an air pressure of 25 psi. During the spraying process, a total volume of 3 ml of silver ink was evenly distributed onto the PAI membrane with a surface area of 1000 cm^2. A consistent distance of 25 cm was maintained between the membrane and the airbrush to ensure uniform coverage and prevent the formation of large droplets. After applying the silver ink on top of the PAI membrane surface, the coated membrane proceeded through a curing step to ensure the adhesion and stability of the silver coating on top of the PAI membrane surface. In this curing process, the silver-coated PAI membrane, known as Ag-PAI, was positioned inside an oven and exposed to a temperature of 80°C for a duration of 20 minutes. After the completion of the curing process, the Ag-PAI membrane was allowed to naturally cool down to room temperature, thereby finalizing the fabrication of the electroconductive Ag-PAI process.

Employing commercially accessible silver ink on the membrane surface and curing the prepared coated membrane provided a straightforward and effective approach for preparing the PAI membrane with a conductive silver coating layer. This process resulted in the fabrication of Ag-PAI membranes with electroconductive properties, suitable for a wide range of applications, indicating its viability as a feasible solution in different fields such a water treatment through membrane-based technologies. Therefore, this prepared Ag-PAI membrane sets the stage for subsequent evaluations and performance assessments, which will be evaluated in the following sections.

3.2.3 Characterizations of Ag-PAI membranes

The surface wettability of both pristine PAI membrane and Ag-coated PAI membrane was evaluated by measuring the contact angles utilizing a drop shape analyzer (DSA 100E, KRÜSS GmbH, Germany). To prepare the samples, they were initially cleaned using ethanol, followed by a 5-min wash with deionized water, and subsequent drying using nitrogen gas. During each measurement, a 2 ± 0.1 μL droplet was carefully deposited onto the membrane surface, and the contact angle was recorded across the membrane surface. For both samples, contact angles were measured at five different positions on the surface for all samples, and the average value was reported.

The morphology of pristine PAI membrane and Ag-coated PAI membrane was examined using Field-emission scanning electron microscopy (FESEM, Zeiss Sigma 300 VP) equipped with an Energy Dispersive X-ray (EDX) spectrometer. For cross-section images, the membrane layer was separated from the polyester support and carefully fractured after being immersed in liquid nitrogen. To enhance conductivity and minimize charging effects during imaging, samples were sputter-coated with a thin layer of gold (2 nm thick) before SEM imaging. The top and cross-section SEM images were captured at different magnifications.

The surface zeta potential for the membranes was then measured utilizing the Surpass^{TM} 3 Electrokinetic analyzer (Anton Paar, Graz, Austria). Zeta potential values were assessed within the pH range of 4-9 at a temperature of 25 °C, employing a 1mM KCl solution and based on the streaming potential measurements. The pH of the electrolyte solution was adjusted using HCl and NaOH solutions to achieve the desired pH levels for the analysis.

The sheet resistivity of the membranes was also measured using a four-point probe resistivity measurement device (PRO4-4000) connected to a Keithley 2601A power source meter. A total of 10 measurements were taken from various locations on each membrane, and the electrical conductivity (measured in S/cm) of the membranes was subsequently calculated using **Equation 3.1**.

$$\text{Conductivity} = \frac{1}{\text{Resistivity}} \tag{3.1}$$

To evaluate the stability of the Ag-coated PAI membrane, it was subjected to varying pH conditions, especially pH of 2, 7, and 10, over a duration of 48 hours. Additionally, measurements of water contact angle and electrical conductivity were taken to comprehend any changes in morphology and coating stability induced by the applied chemical stress.

Cyclic voltammetry (CV) investigations were carried out on the Ag-PAI membrane using the Ossila Potentiostat, employing a scan rate of 40 mV/sec. The analysis was performed within a three-electrode electrochemical cell comprising a working electrode represented by the Ag-PAI membrane, a counter electrode composed of platinum wire, and a reference electrode using the SCE (Saturated Calomel Electrode). The applied voltage was varied within the range of -1V to 0V, and the electrolyte solution was thoroughly saturated with nitrogen gas (N_2) to observe the electrode's response under N_2 conditions. Background electrolyte solutions utilized in these experiments included mixtures of potassium hexacyanoferrate (0.01M $K_4Fe(CN)_6$) and sodium nitrate (0.1M $NaNO_3$), as well as solutions containing 20 ppm of RR 120 and 20 ppm of RB. Nitrogen gas was introduced into the three-electrode cell for a duration of 10 minutes to eliminate any saturated oxygen from the electrolyte solution.

The cathodic electro-reduction (CER) reactions were carried out by connecting the top surface of the Ag-PAI membrane to the cathode output of a DC power supply. A rectangular piece of stainless steel (7.45 cm^2) smaller than the membrane (cathode) was used as the anode, and a distance of 1.4 mm was adjusted between the anode and the cathode. The electroactivity of the coated membrane was evaluated by applying different electric potentials to the membrane surface.

The performances of pristine PAI membrane and Ag-PAI membrane were quantified with cross-flow filtration setup at the pressure of 20 psi and feed flow rate of 2.4 L.min^{-1}. The filtration setup was equipped with a circulating water bath (Iso temp3013, Fisher Scientific) to control the feed temperature.

3.2.4 Membrane permeability, dye rejection, and fouling experiments

To evaluate the dye rejection performance of the membrane in presence of the electrical potential, 20 ppm of RR120 and RB were filtered while the electrical potential was applied between the stainless-steel electrode (anode) and the Ag-PAI membrane surface (cathode). The volumetric permeate flux, J_w, and dye rejection was determined by **Equations 3.2** and **Equation 3.3.**

$$J_w = \frac{\Delta m}{\rho A_m \Delta t} \tag{3.2}$$

Where Δm is the mass difference, ρ is the membrane permeate density, A_m is the membrane surface area (20.25 cm^2), and Δt is the filtration time.

$$R(\%) = \left(1 - \frac{C_p}{C_f}\right) \times 100 \tag{3.3}$$

Where C_p and C_f represent the dye concentration in permeate and feed solutions, respectively, which were measured by UV–Vis spectrophotometer.

The antifouling experiments tests were also conducted based on the following procedure. A three-step experimental approach was used to evaluate the fouling performance of the membranes with an applied electric potential. First, a deionized pure DI water filtration experiment was performed for 20 min, and the permeate flux was allowed to stabilize before the foulant was added to the feed solution. The water that passed through the membrane was collected on a digital balance (ME4002, Mettler Toledo), and the data was then automatically recorded on a computer at 15-second intervals. After measuring the pure deionized water flux, the feed solution was replaced with a 200 mg.L^{-1} foulant solution, and the permeate flux of the foulant solution (J_{wf}) was measured for almost 5 hours. Following the fouling step, the membrane surface was washed by stirring with distilled water for 10 minutes at the same operational flow rate used during the fouling step, with no applied pressure. It should be noted that, during the cleaning step, the membrane surface was subjected to the same DC electrical potential applied during the fouling step. Ultimately, the pure water flux of the cleaned membrane (J_{w2}) was recorded after cleaning the membrane surface with deionized water. To evaluate the antifouling property of the membranes, the total flux decline ratio (FDR) and flux recovery ratio (FRR) were determined as **Equation 3.4** and **Equation 3.5**.

$$FDR = 1 - \frac{J_{wf}}{J_{w1}} \qquad 3.4$$

$$FRR = \frac{J_{w2}}{J_{w1}} \qquad 3.5$$

3.3 Results and discussions

3.3.1 Characterization of fabricated membranes

Coating hydrophilic nanomaterials onto membranes can contribute to the alleviation of organic substances with hydrophobic properties adhering to the membranes. This is possible through two effects: increased roughness and enhanced hydrophilicity. Both properties enhance the passage of water through the membrane and establish a hydration layer that prevents foulants from attaching to the membrane surface [207,208]. The surface hydrophilicity of the membranes was examined via water contact angle (WCA) testing. As illustrated in **Figure 3.1**, it is evident that there was a 12-degree reduction in the WCA of the pristine PAI membrane, shifting from 55° to 43° following the application of silver nanoparticles as a coating on the membrane surface. The reduced WCA of the modified membrane indicates that the newly fabricated membrane's surface is hydrophilic, enhancing its antifouling properties.

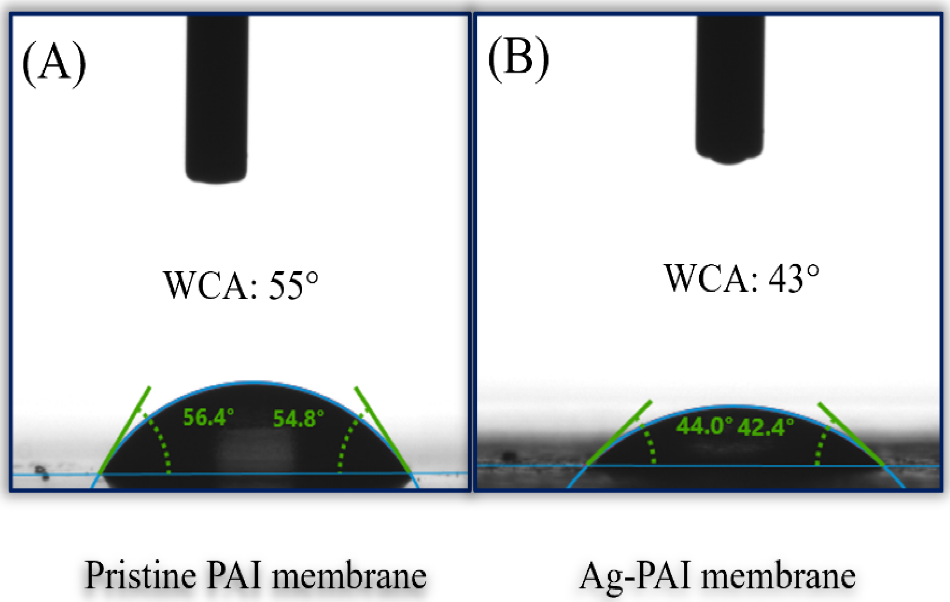

Figure 3.1. Water contact angle for (A) pristine PAI membrane (M0), and (B) Ag-coated PAI membrane (ECM)

The changes in the surface and cross-section morphology of the membranes before and after Ag-coating were analyzed using FESEM. **Figure 3.2** present the top surface and cross sectional view of both pristine PAI membrane and Ag-coated PAI membrane. The images provide a clear representation of the porous structure of the PAI membrane. Significantly, when examining the Ag-modified membrane, we observed not only a homogenous, bright layer but also a notable reduction in the size of these pores, which can be directly attributed to the silver nanoparticle coating on the membrane surface [209]. Furthermore, it is evident that the deposition of Ag-coating did not completely block the surface pores, as these pores were still clearly observable in the top surface image. To demonstrate the formation of the coating layer on the PAI support, the cross-sectional morphology was observed via FESEM. A distinct layer of Ag-coating with a thickness of 0.54 μm could be observed on the membrane surface, indicating a well-dispersed and homogenous layer of silver.

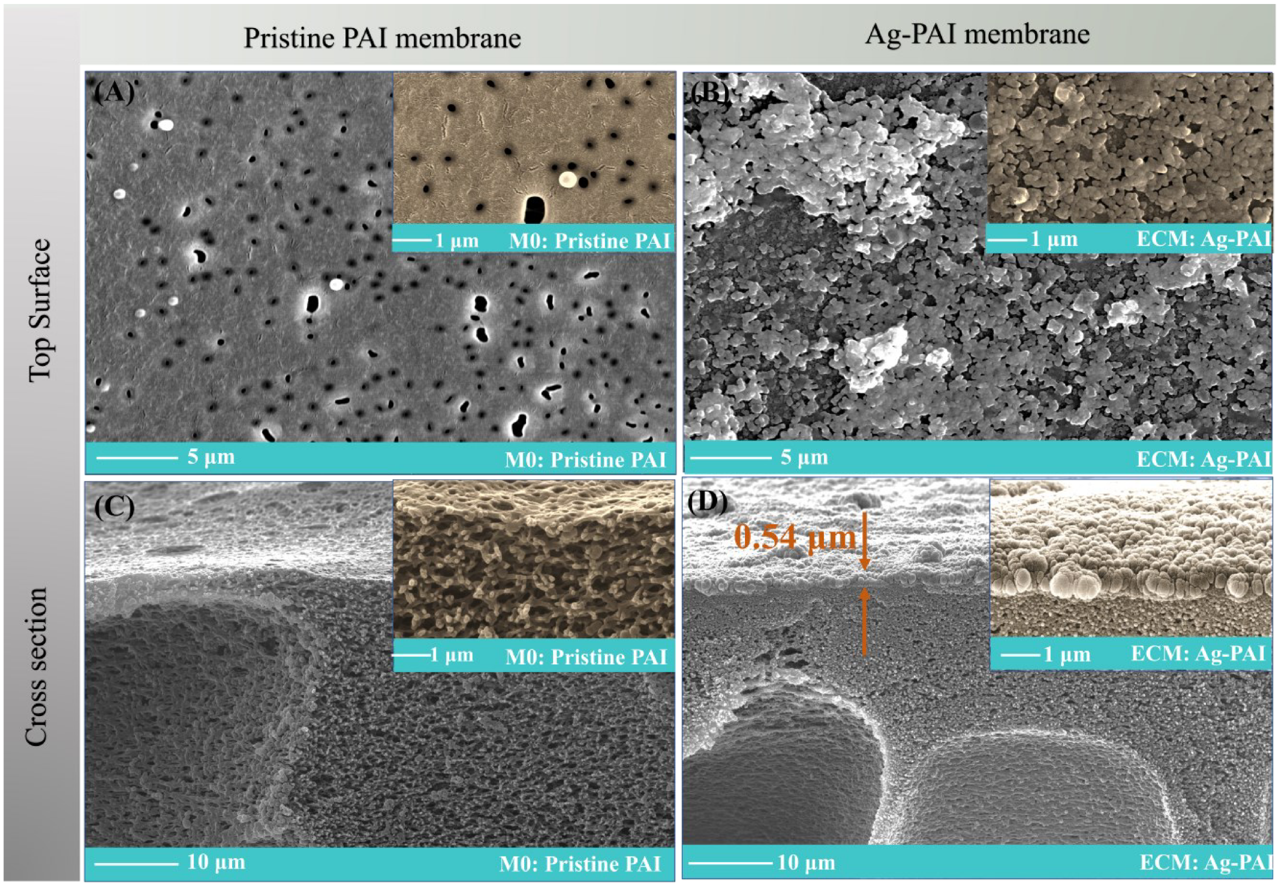

Figure 3.2. (A) The top surface FESEM image from the prepared pristine PAI support layer (M0), (B) top surface FESEM image from Ag-coated PAI membrane (ECM), (C) cross-sectional FESEM image from M0, and (D) cross-sectional FESEM image from ECM.

EDX mapping provided additional confirmation of the presence of Ag on the membrane's surface. As demonstrated in **Figure 3.3(C)**, the average loading of Ag, calculated from the EDX analysis, was up to 96% by weight on the Ag-coated membrane. **Figure 3.3** clearly represents the EDX scan obtained from the top and cross-sectional view of the silver-modified membrane. The images clearly demonstrate that while the cross-section of the membrane contains more C and O elements, the top surface is predominantly covered by Ag. This indicates the successful deposition of silver on the membrane's top surface.

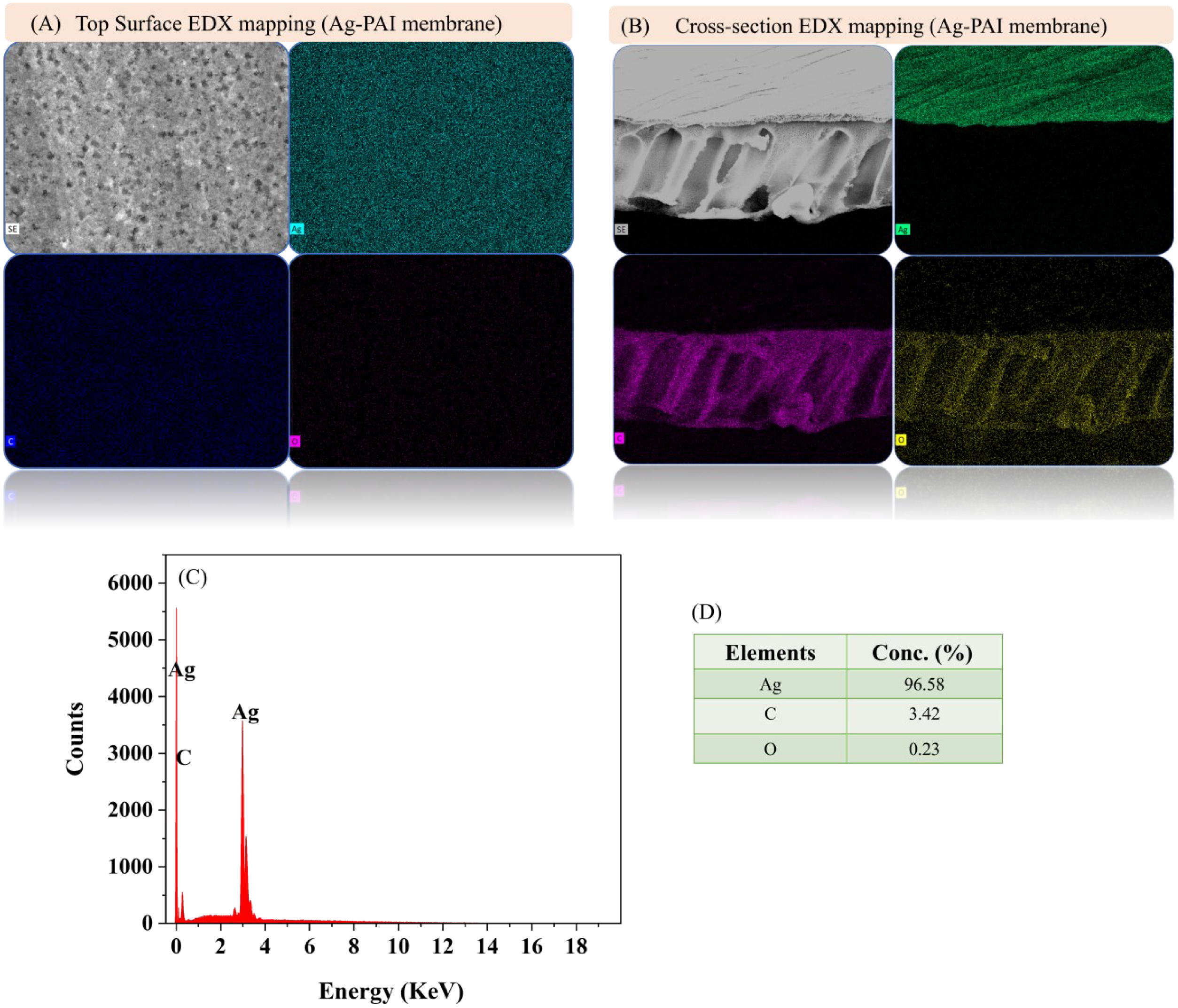

(D)

Elements	**Conc. (%)**
Ag	96.58
C	3.42
O	0.23

Figure 3.3. (A) STEM-EDX maps of the Ag coating layer (top surface view), (B) STEM-EDX maps of Ag coating layer (cross-section view), (C and D) elemental compositions of Ag-coated membrane (96.58% silver)

Figure 3.4 displays the surface charge analysis results for uncoated pristine PAI and Ag-coated PAI membranes, which were examined using a zeta potential analyzer. The recorded data revealed that both membranes exhibited a negative charge across the entire pH range examined, which extended from 4 to 9. Furthermore, the magnitude of this negative charge increases with rising pH values. While the pristine PAI exhibited a slight reduction in charge with only a 6 mV fluctuation, the Ag-coated membrane displayed an isoelectric point (IEP) at pH 4.5 and a notable reduction in its negative potential, reaching -15 mV at pH 9. This effect can be attributed to the presence of the Ag-coating layer. Given the challenging nature of measuring the externally voltage-induced zeta potential and the complexity associated with modeling, we were unable to provide data concerning these aspects. However, an increase in applied voltage is expected to leato an elevated surface charge density and a more negatively charged surface of the membrane [210]. Furthermore, due to the inherently non-conductive nature of the PAI polymer, the pristine PAI membrane exhibited a low electrical conductivity of 2.215E-5 S/cm. In contrast, the Ag-coated membrane displayed a significantly high value of 56,497 S/cm. This substantial increase in electrical conductivity can be attributed to the metallic nature of silver nanoparticles, which serve as channels for electrons to migrate, facilitating rapid transfer across the membrane. Consequently, coating the PAI support with silver nanoparticles offers a significant advantage in enhancing its electrical conductivity, suggesting its potential as an electrode for providing electrical assistance in future antifouling experiments [211].

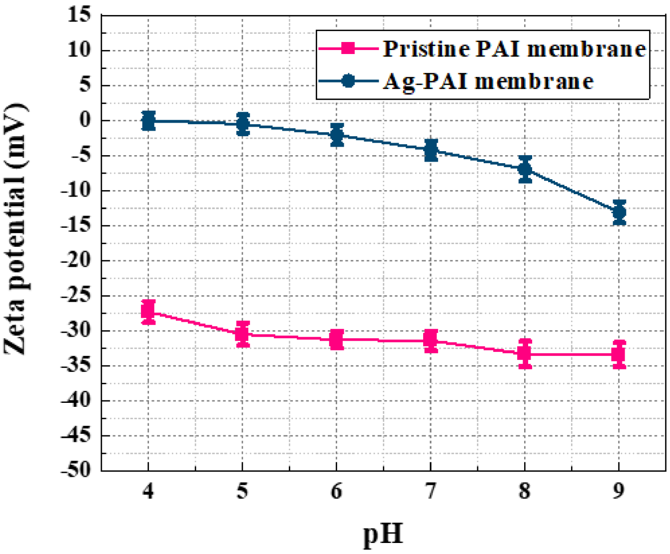

Figure 3.4. The zeta potential of Pristine PAI membrane and Ag-coated PAI membrane as a function of solution pH

Electrically conductive membranes developed for water filtration processes show great potential, yet encounter challenges related to stability when exposed to dynamic operational modes and the rigorous physical and chemical conditions inherent to wastewater treatment. Despite their exceptional antifouling and antimicrobial performance, these membranes fail to be adopted by large-scale production applications because of their low inherent stability [198]. Various research investigations have delved into the complex chemistry of grafting [212] and crosslinking

[213,214] to enhance the stability of the coating layers by strengthening the adhesion between the membrane and its coating layer. In our pursuit of a more straightforward solution, we have opted to utilize an aqueous-based silver ink known for its advantageous properties, including robust adhesion, resilient coatings, resistance to water, flexibility, and crease resistance. The WCA, measured after subjecting the membrane to various chemical stressors, exhibits minimal changes and remains consistent at around 44 °C, consistent with the measurement obtained before conducting the tests, as illustrated in **Figure 3.5(A)**. Similarly, as depicted in **Figure 3.5(B)**, the electrical conductivity of the Ag-PAI membrane is measured at approximately 55,000 S/cm following the chemical stability tests. It is worth noting that the Ag-PAI membrane demonstrates cathodic stability while displaying anodic instability when subjected to positive electric potential. This anodic instability arises from the rapid oxidation of Ag nanoparticles, leading to a peeling-off effect of the Ag coating and consequent reduction in the membrane's electrical conductivity. It is significant to highlight that a similar phenomenon has been documented for carbon nanotube (CNT) coatings, which exhibit instability during anodic operation modes due to CNT oxidation.

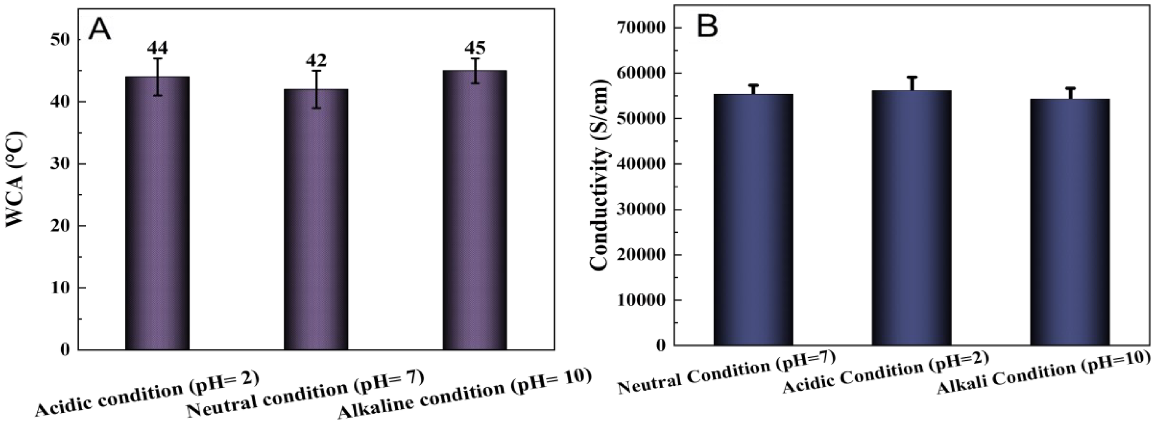

Figure 3.5. Stability tests: (A) WCA measurement and (B) electrical conductivity measurement after stability test (48 hours immersion in solutions with various pH)

Cyclic voltammetry (CV) tests were also employed to examine the electrochemical behavior of the Ag-modified membrane in reduction and oxidation processes. The potential of the membrane surface was assessed in specific background electrolytes, including $K_4Fe(CN)_6/NaNO_3$, SA/$CaCl_2$, RR120, and RB solutions. The assessment covered a range of applied cell potentials from -1 V to 0 V, referenced to the saturated calomel electrode (SCE). Generally, the appearance of redox peaks in a CV spectrum suggests that the electrode responds strongly to the electrolyte solutions, confirming the occurrence of a redox reaction. However, in this experiment, a different observation was made. As shown in **Figure 3.7,** when the Ag-coated membrane was exposed to the Potassium hexacyanoferrate electrolyte solution, it did not display any discernible signal related to the reduction or oxidation reaction. Further investigations involved exposing the modified membrane to a model foulant solution and two dye solutions to study its electrochemical behavior.

As depicted in **Figure 3.7,** based on depicted voltammograms obtained for RR 120, RB, and SA/$CaCl_2$, a negligible current density of approximately 0.2 mA/cm² was measured for a membrane with an applied surface potential ranging from -1 V to 0 V vs. SCE. This current level is considered too low for an electrochemical reaction, indicating that the electrochemical reaction has a negligible influence on the subsequent antifouling alleviation. However, the hydrogen evolution reaction (HER) might be responsible to a very low extent considering the low current density values.

The image provided in **Figure 3.10** represents a water-splitting cell, allowing for the clear observation of the generation of H_2 and O_2 bubbles. Compared to the sophisticated methods required for preparing electrocatalysts aimed at antifouling improvement, the HER attributed to the presence of silver nanoparticles offers a facile, easily scalable deposition approach [215,216]. This demonstrates a distinct advantage over other methods.

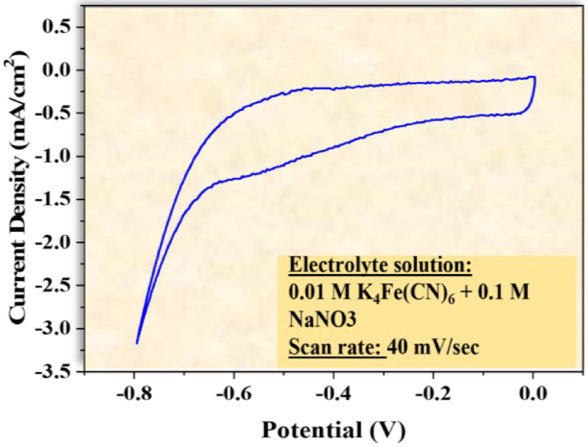

Figure 3.6. CV analysis for $K_4Fe(CN)_6$/$NaNO_3$ solution with a potential range from –0.8 V to 0 V vs. SCE, with a scan rate of 40 mV/sec.

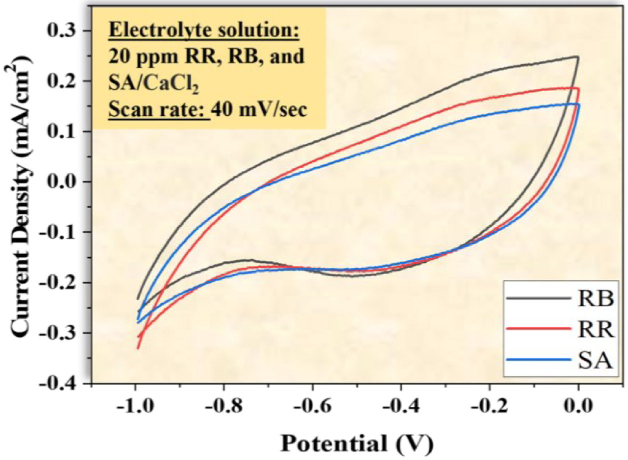

Figure 3.7. CV analysis for RR, RB, SA/CaCl$_2$ solutions with a potential range from –1 V to 0 V vs. SCE, with a scan rate of 40 mV/sec.

3.3.2 Dye separation performance of Ag-coated PAI membranes

The filtration performance of the PAI and electroconductive Ag-PAI membranes was assessed using a two-electrode cross-flow filtration setup, focusing on key parameters of dye rejection as determining factors in the evaluation of membrane performance in the presence of electric potentials. In this setup, the Ag-PAI membrane served as the cathode, while stainless steel was used as the anode. To assess the influence of electrical assistance on the modified membrane, two negatively charged dyes, RB (MW: 991.82 Da) and RR120 (MW: 1774.15 Da), were filtered at incremental potentials ranging from 0 to 7 V. Upon coating the PAI membrane surface by silver ink, the membrane water flux reduced substantially by a factor of 8**,** dropping from 1300 in pristine PAI membrane to 100 LMH. This observation can be attributed to the blockage of the membrane surface due to the presence of silver nanoparticles, resulting in a reduced membrane pore size and a decline in water flux.

Figure 3.8 shows the filtration performance of the Ag-coated membrane for RR120 and RB as a function of applied voltage. It was observed that the dye rejection performance exhibited a linear dependence on the applied potential range for both dyes, increasing by 14% and 32% for RR120 and RB, respectively, from their initial values. However, increasing the potential had almost no effect on the permeation flux, as it remained unchanged at around 90 to 100 LMH**.** This suggests that the induced external voltage positively improved the rejection without decreasing the permeation flux. The possible explanation for this enhancement can be attributed to the reduced pore size caused by silver coating in the newly developed membrane, as evidenced by the water flux data. Moreover, the results were consistent with the obtained CV curves. As discussed earlier, no electrochemical reaction occurred on the surface of the Ag-coated membrane when exposed to the RR120 and RB solutions. This indicates that no redox reaction disrupted permeability or rejection. Instead, electrical repulsion caused by the external voltage played a crucial role in enhancing filtration. In this process, the membrane surface is anticipated to become more negatively charged when an electric potential is generated between the modified membrane (cathode) and the anode. This creates an electrostatic repulsive force between the membrane surface and the negatively charged dyes, leading to increased rejection of these dyes [119].

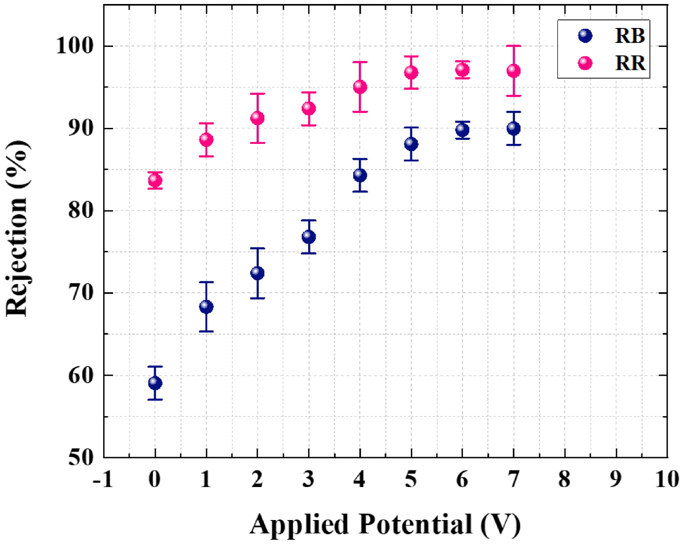

Figure 3.8. Dye rejection performance of the Ag-coated PAI membrane with electrochemical assistance, using RR120 and RB as dye solutions.

3.3.3 Antifouling behavior of modified Ag-coated PAI in the electrochemical cell

To evaluate the antifouling performance of the pristine PAI and modified Ag-PAI membranes, the flux decline rate (FDR) for the aqueous solution of SA/$CaCl_2$ was monitored for six hours using the same dynamic cross–flow filtration setup. Afterward, the feed solution was replaced with deionized (DI) water, and the membrane underwent a 30-minute cleaning process. Following this cleaning step, the corresponding flux recovery ratio (FRR) was assessed by determining the recovered water flux after washing using **Equation 3.5**. Similar to the filtration experiment, the membrane was exposed to an external voltage ranging from 0 to 7 V with an increment of 2 V. The normalized fluxes versus time are summarized in **Figure 3.9(A)**. Initially, the flux of foulant in the pristine PAI membrane decreased more sharply than the modified Ag-coated membrane. Moreover, the modified membrane experienced a milder flux decline as the applied voltage increased. It is demonstrated that during the organic fouling test, the pristine PAI membrane lost approximately 60% of its initial flux, while the Ag-coated membrane experienced a lower flux decline, reaching a minimum of 43% at 7 V. Simultaneously, the FRR values increased with rising the electrical potential in the modified Ag-coated PAI membrane. Compared to the pristine PAI membrane with an FRR of around 49%, the Ag-coated membrane exhibited an increased FRR, ranging from 43% to 80%. These results confirm the enhanced antifouling properties of the electroconductive membrane.

Overall, the enhancement of antifouling behavior can likely be attributed to a combination of phenomena: (1) the increased negative surface charge of both the membrane surface and the foulants, which leads to electrostatic repulsion, hindering foulants from migrating to the similarly charged membrane surface; (2) the generation of gas bubbles on the electroconductive membrane surface due to water electrolysis, effectively eliminating the cake layer; and (3) improved hydrophilicity, which directly results in the formation of a hydration barrier preventing foulant attachment [66,210].

Applying voltage to the electroconductive membrane increases their negative charge density, especially at higher voltages when the pH near the electrode may change, reducing foulant attachment to the membrane surface. This phenomenon is known as electrophoresis, a process in which the electric field repels foulants in the feed solution away from the surface of the conductive membrane, significantly reducing the possibility of foulant absorption [217].

Figure 3.10 presents the gas bubbles produced by the Ag-coated electroconductive membrane when a voltage is applied in an electrochemical cell, including the background electrolyte solution and also in the experimental cell.

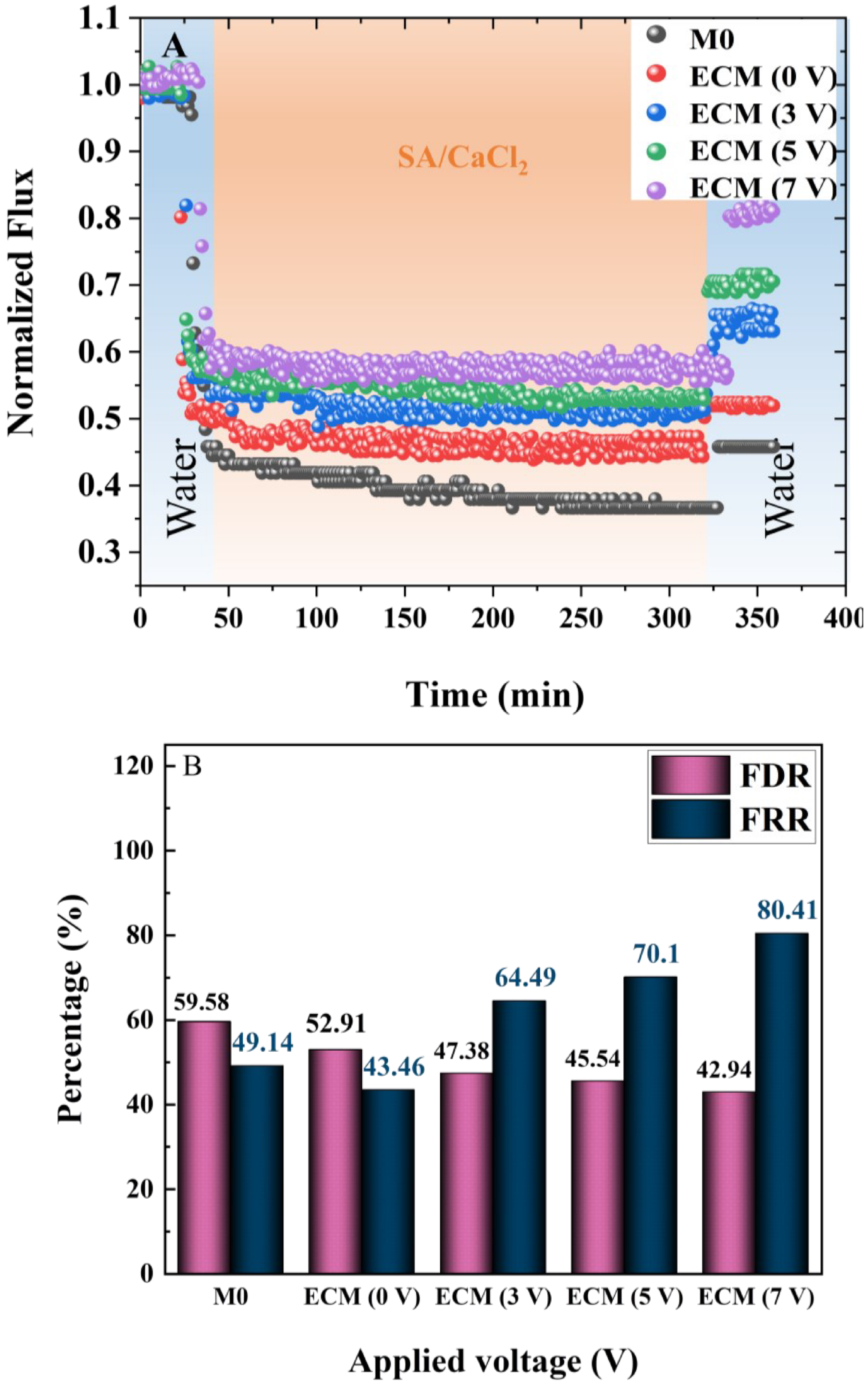

Figure 3.9. (A) Fouling of Ag-PAI membranes by applying various potentials using SA/CaCl2 as model foulant over time and (B) Comparison of the fouling characteristics membranes. FDR is the total flux decline ratio, and FRR is the flux recovery ratio.

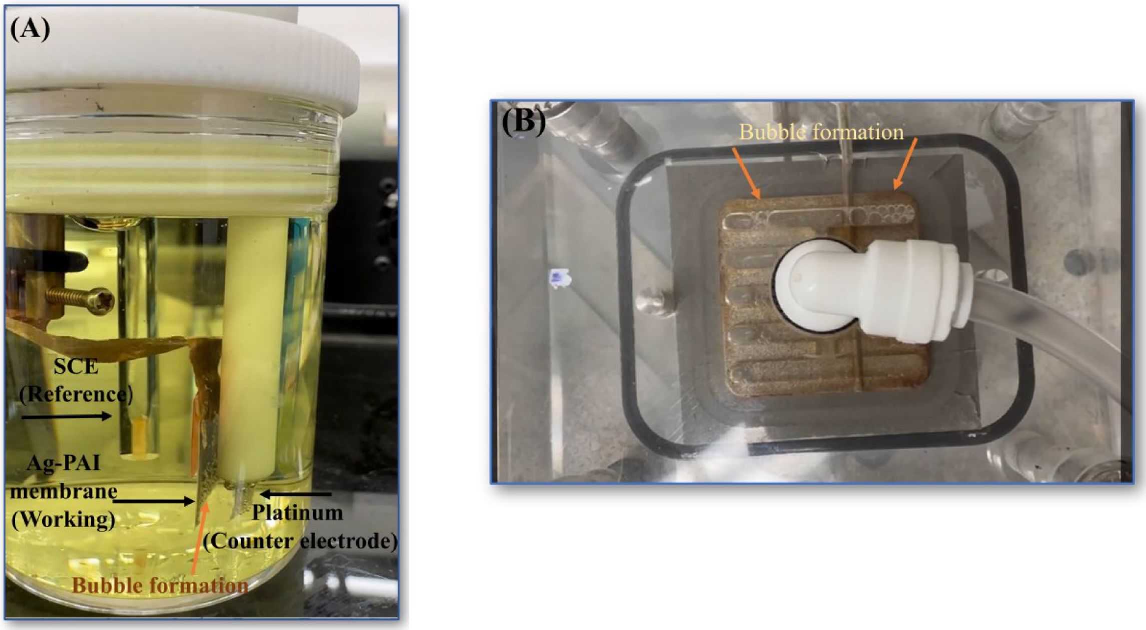

Figure 3.10. Formation of gas bubbles on the surface of Ag-PAI membrane (A) in electrochemical CV cell (B) in electrochemical filtration cell.

During water electrolysis, hydrogen gas is produced at the cathode (electroconductive Ag-PAI membrane), called hydrogen evolution reaction (HER), while oxygen is produced at the anode, called oxygen evolution reaction (OER), as shown in the equations below.

$$2H_2O \rightarrow O_2 + 4H^+ + 4e^- \qquad \text{(HER)} \qquad 3.6$$

$$2H_2O + 2e^- \rightarrow H_2 + 2OH^- \qquad \text{(OER)} \qquad 3.7$$

It is important to note that applied voltage influences both the energy balance and the rate of the hydrogen evolution reaction. Higher applied voltages lead to an increased rate of hydrogen evolution, which, in turn, is expected to minimize membrane fouling due to the scouring effect of increased gas bubble generation at the electrode surface. These hydrogen bubbles can effectively dislodge fouling materials deposited on the membrane surface. Furthermore, when these bubbles are formed in-situ on the cathode, they can enhance the cleaning efficiency of the fouled membrane by reducing the interaction between foulants and the membrane. This, in turn, leads to the removal of the fouled layer and facilitates flux recovery [218]. Therefore, the proposed electrically enhanced approach for reducing fouling propensity is a straightforward strategy that eliminates the need for chemicals and consumes low energy.

3.4 Conclusion

In conclusion, the given study proposes a unique Ag-coated PAI membrane with improved electro-conductive and antifouling properties that was developed by employing a facile 'spray-cure' coating process. The electroconductive performance of the membrane, obtained through incorporating an aqueous-based conductive ink with a high silver loading, provides outstanding stability and electrical conductivity to the pristine PAI support membrane. The combined use of PAI as a substrate and silver nanoparticles as a conductive coating material provides a strong foundation for a variety of applications, particularly in the water treatment processes. The Ag-PAI membrane's characterizations, encompassing surface wettability, morphologies, zeta potential, and electrical conductivity, reveal its specific characteristics and highlight its potential as an electroconductive membrane. Notably, the membrane has a hydrophilic surface as well as a uniform silver coating layer with a thickness of 0.54 μm, resulting in an electrical conductivity of 56,000 S/cm, making it a promising candidate for a wide range of electrochemical applications. The electrochemical properties of the Ag-PAI membrane were evaluated by utilizing cyclic voltammetry (CV), which indicates no significant redox peaks throughout diverse electrolyte solutions. Also, it should be noted that while the membrane exhibited anodic instability in the presence of positive electric potential, it illustrated cathodic stability, making it ideal for applications requiring reduction mechanisms.

An external electric potential applied to the Ag-PAI membrane during filtration experiments elucidated its substantial effect on the rejection of negatively charged dyes and the antifouling performance of the membrane. The dye rejection experiments displayed a linear correlation with the applied potential range for RR120 and RB dyes. Specifically, there was a 14% increase for RB and a 32% increase for RR120 from their initial dye rejection values. The capability of the membrane to reject negatively charged dyes, as revealed by the electro-assisted filtration process, highlights its potential for improved separation efficiency.

Furthermore, the membrane exhibits outstanding antifouling behavior, with a flux decline rate of 43% and a corresponding flux recovery ratio (FRR) of up to 80% with an application of 7V cathodic potential, compared to 60% FDR and 49% FRR (zero applied electric potential), demonstrating the 17% and 31% improvement in FDR and FRR, respectively.

It is important to highlight that although the primary process identified in this investigation involves robust electrostatic repulsion between the membrane surface and negatively charged dyes and contaminants, the enhanced antifouling and dye separation performance might also be influenced by gas generation and low potential electrochemical reactions as side reactions.

With its specific combination of stability, antifouling, and electroconductive properties, the proposed Ag-PAI membrane opens new avenues in water treatment applications. This study offers significant insights into the development of electroconductive membranes, supporting the ongoing efforts towards overcoming challenges in the field of water treatment technologies. The Ag-PAI membrane’s demonstrated electrochemical and antifouling capabilities make it an appealing candidate for scalable and environmentally friendly water treatment techniques, representing an achievement in the ongoing search for novel approaches to the world's water-related issues.

Chapter 4

Conclusion and future works

4.1 Conclusion

The thesis revolves around experimental research on the fabrication and characterization of smart electro-conductive membranes and their application for wastewater treatment. The research was carried out in a structured sequence of two chapters, each considering the main objective: developing high-performance electro-conductive nanocomposite membrane with enhanced capabilities in terms of permeation, dye separation and fouling resistance properties achieved through the electrochemical assistance methods.

In the first part of the thesis, Ti_3C_2 MXene nanosheets were employed for the first time in the fabrication of electroconductive nanocomposite membranes using the NIPS fabrication method to fabricate the PAI membrane support and pressure-assisted filtration technique to coat the Ti_3C_2 MXene/CMC on top of the PAI membrane surface. The antifouling performance of the synthesized membranes by MXene nanosheets was subsequently evaluated in terms of fouling performance by applying various electrical potentials to the membrane surface, compared with the scenario without any applied potential. The introduction of Ti_3C_2-MXene had discernible effects on the membrane properties, including enhancements in electrical conductivity, hydrophilicity, and negative surface charge. The results obtained from contact angle and zeta potential measurements indicated the formation of more hydrophilic and negatively charged MXene-PAI nanocomposite membranes. In the presence of applied electrical potential, MXene-modified PAI nanocomposite membranes exhibited superior antifouling performance compared to the zero applied potential cases. Fouling measurement results revealed that fouling was mitigated due to the improved membrane surface properties of the membranes and the application of electric potential. Specifically, the use of Ti_3C_2-MXene nanosheets and CMC binder at an optimum loading of 80 mg and 4 mg, respectively, yielded the maximum electrical conductivity of 174 ± 0.16 S/m. This Ti_3C_2-modified membrane displayed significantly enhanced antifouling properties, showcasing a 45%, 31%, and 51% reduction in FDR when subjected to 4V,6V, and 8V potentials, using various foulants such as HA, SA/CaCl2, and BSA as foulants, respectively, as compared to cases with zero applied potential. Moreover, the results of FRR measurements indicated a complete recovery of the membrane under these abovementioned specified potentials and foulants. In this study, we employed an extended DLVO (XDLVO) interaction energy analysis alongside fouling experiments to investigate the fouling behavior of various organic foulants on the membrane surface. The XDLVO analysis allowed us to assess the fundamental interactions, including van der Waals forces, electrostatic forces, and acid-base interactions, that control organic fouling. Surface tension parameters were derived from contact angle measurements and were used to calculate the free energy of adhesion between the membrane and model foulants. Our findings revealed that acid-base interaction energies between the foulants and the membrane's surface were the most substantial factor in the total energy of interaction. This investigation demonstrated that assessing surface free energy components for membranes is a reliable method for predicting the fouling behavior of organic substances on the membrane surface.

In the second part of this thesis, a thin layer of silver (Ag ink) was introduced onto a polyamide-imide (PAI) membrane support. Using the electrical conductivity of the fabricated membranes, we reduced organic fouling by applying an external electric field. The electrical conductivity of the pristine PAI membrane was measured at 2.21×10^{-5} S/cm, while by coating the appropriate amount of silver, it was significantly enhanced to 56,497 S/cm. Moreover, the performed physical stability tests demonstrated the remarkable durability of the silver coating layer, as the electrical conductivity remained largely unchanged even after immersing the membrane for 48 hours in both acidic and alkali solutions.

We applied cathodic potentials across varying ranges on the surface of prepared Ag-coated PAI membranes when the feed water contained 20 ppm of different dyes, including RR120 and RB. The obtained results for the range of applied cathodic potentials illustrated the higher dye removal by applying higher electrical potential for Ag-modified PAI membrane, as it illustrated the dye removal improvement of 15% and 31% for RR120 and RB dyes by applying the 7V cathodic potential as compared to the zero applied potential case. Antifouling tests further indicated that the membrane's antifouling performance, using SA/$CaCl_2$ foulant, led to about 17% reduction in FDR and a 31% increase in flux recovery when a 7 V cathodic potential was applied as compared to the unmodified pristine PAI membrane. Notably, by incrementally increasing the applied voltage from 1 V to 7 V, the antifouling propensity of the membrane increased dramatically in the cathode setting. The observed antifouling performance can be attributed to several factors, including the presence of large gas bubbles and electroreduction reactions.

ECMs have shown promising antifouling potential that can be extended to various applications, such as the separation of bacteria, viruses, colloidal substances, and metals. They have become a highly researched topic recently due to their fouling mitigation potential; however, their surface instabilities necessitate the development of more stable membranes suitable for industrial adoption in real-world applications.

4.2 Possible Future works

ECMs have demonstrated promising antifouling capabilities that can be extended to a wide range of applications, such as the separation of bacteria, viruses, colloidal substances, and metals.

MXenes, a fascinating group of 2D transition-metal compounds, exhibit various physicochemical properties such as metallic conductivity, hydrophilicity, and redox activity, making them suitable for several applications. However, while the potential applications of MXene signify their brilliant futuristic scope, some challenges still need to be addressed to harness their emerging potential fully.

Given the known and well-documented challenge of MXene oxidation over time and the resultant loss of conductivity, an intriguing future direction arises. Therefore, a fascinating avenue for the future is the adoption of sacrificial polymers to mitigate the oxidation rate of MXenes, thereby preserving their conductivity over time. Building upon the foundation laid in this research, these innovative approaches hold great promise in advancing the field of electro-conductive membranes and their applications in water treatment and beyond. In summary, it is important to embark on research endeavors aimed at increasing the conductivity of electro-conductive membranes, as such conductivity improvements can yield further reductions in energy consumption, aligning with the ongoing pursuit of more efficient and sustainable desalination and water treatment processes.

Furthermore, in addition to the insights gained from this study on electro-conductive membranes incorporating MXene and silver to enhance organic antifouling properties and dye removal under applied potential, several compelling directions for future research emerge. One prospective project could delve into evaluating the antibacterial performance of these silver or MXene-coated nanofiltration (NF) membranes. Investigating their ability to resist and deter bacterial adhesion and growth is crucial for addressing biofouling challenges in water treatment.

Moreover, the surface instabilities of ECMs necessitate the development of more stable membranes suitable for industrial adoption in real-world applications. The stability of ECMs, encompassing electrochemical, physical, and mechanical properties, is essential for expanding their applications beyond the lab scale. While ECMs have demonstrated cathodic stability, they are notably anodically unstable under low voltages. The drop in their electrochemical conductance was attributed to the oxidation of conductive elements under such potentials. Therefore, the introduction of sacrificial polymers like glutaraldehyde enhances the resilience of the networks against anodic oxidation potential.

In addition to the antifouling and dye removal applications explored in this thesis using ECMs under applied potential, it is worth highlighting that ECMs also offer several advantageous characteristics for desalination and enhanced ion transport. Leveraging their electrical conductivity, ECMs have the potential to significantly enhance ion transport, making them well-suited for processes such as electrodialysis and capacitive deionization in desalination processes. Furthermore, ECMs have shown the capacity to enhance energy efficiency in desalination by allowing for the application of electrical fields to facilitate separation processes, potentially reducing overall energy consumption. These characteristics underscore the vast potential for ECMs to not only address fouling and dye removal challenges but also to play a pivotal role in increasing the efficiency, sustainability, and overall performance of desalination processes.

Consequently, all the above-mentioned future avenues for enhancing the efficiency, sustainability, and overall performance of ECMs hold significant potential, perfectly aligned with the growing global demand for freshwater resources. The investigation of these future prospects signifies not only our dedication to advancing water treatment technologies but also our proactive response to the pressing global challenge of securing a consistent and sustainable source of clean water for an ever-growing population.

References

[1] U.N. Water, Sustainable Development Goal 6 synthesis report on water and sanitation, Published by the United Nations New York, New York. 10017 (2018).

[2] B.K. Mishra, S. Chakraborty, P. Kumar, C. Saraswat, Water Science and Technology Library Sustainable Solutions for Urban Water Security Innovative Studies, n.d. http://www.springer.com/series/6689.

[3] M. Kummu, J.H.A. Guillaume, H. De Moel, S. Eisner, M. Flörke, M. Porkka, S. Siebert, T.I.E. Veldkamp, P.J. Ward, The world's road to water scarcity: Shortage and stress in the 20th century and pathways towards sustainability, Sci Rep. 6 (2016). https://doi.org/10.1038/srep38495.

[4] A. Boretti, L. Rosa, Reassessing the projections of the World Water Development Report, NPJ Clean Water. 2 (2019). https://doi.org/10.1038/s41545-019-0039-9.

[5] J. Rose, Water and the Environment, CRC Press, 2017.

[6] J.B. Brown, J.M. Conder, J.A. Arblaster, C.P. Higgins, Assessing Human Health Risks from Per-And Polyfluoroalkyl Substance (PFAS)-Impacted Vegetable Consumption: A Tiered Modeling Approach, Environ Sci Technol. 54 (2020) 15202–15214. https://doi.org/10.1021/acs.est.0c03411.

[7] A. Mukherjee, B.R. Scanlon, A. Aureli, S. Langan, H. Guo, A.A. McKenzie, Global groundwater: source, scarcity, sustainability, security, and solutions, Elsevier, 2020.

[8] C. Santhosh, V. Velmurugan, G. Jacob, S.K. Jeong, A.N. Grace, A. Bhatnagar, Role of nanomaterials in water treatment applications: A review, Chemical Engineering Journal. 306 (2016) 1116–1137. https://doi.org/10.1016/j.cej.2016.08.053.

[9] M.A. Shannon, P.W. Bohn, M. Elimelech, J.G. Georgiadis, B.J. Marĩas, A.M. Mayes, Science and technology for water purification in the coming decades, Nature. 452 (2008) 301–310. https://doi.org/10.1038/nature06599.

[10] N. Wang, T. Zheng, G. Zhang, P. Wang, A review on Fenton-like processes for organic wastewater treatment, J Environ Chem Eng. 4 (2016) 762–787. https://doi.org/10.1016/j.jece.2015.12.016.

[11] C. V. Rekhate, J.K. Srivastava, Recent advances in ozone-based advanced oxidation processes for treatment of wastewater- A review, Chemical Engineering Journal Advances. 3 (2020). https://doi.org/10.1016/j.ceja.2020.100031.

[12] M.B. Asif, Z. Zhang, Ceramic membrane technology for water and wastewater treatment: A critical review of performance, full-scale applications, membrane fouling and prospects, Chemical Engineering Journal. 418 (2021). https://doi.org/10.1016/j.cej.2021.129481.

[13] A. Lee, J.W. Elam, S.B. Darling, Membrane materials for water purification: Design, development, and application, Environ Sci (Camb). 2 (2016) 17–42. https://doi.org/10.1039/c5ew00159e.

[14] P.R. Gogate, A.B. Pandit, A review of imperative technologies for wastewater treatment I: Oxidation technologies at ambient conditions, Advances in Environmental Research. 8 (2004) 501–551. https://doi.org/10.1016/S1093-0191(03)00032-7.

[15] C. Byrne, G. Subramanian, S.C. Pillai, Recent advances in photocatalysis for environmental applications, J Environ Chem Eng. 6 (2018) 3531–3555. https://doi.org/10.1016/j.jece.2017.07.080.

[16] A. Yusuf, A. Sodiq, A. Giwa, J. Eke, O. Pikuda, G. De Luca, J.L. Di Salvo, S. Chakraborty, A review of emerging trends in membrane science and technology for sustainable water treatment, J Clean Prod. 266 (2020). https://doi.org/10.1016/j.jclepro.2020.121867.

[17] D.L. Shaffer, L.H. Arias Chavez, M. Ben-Sasson, S. Romero-Vargas Castrillón, N.Y. Yip, M. Elimelech, Desalination and reuse of high-salinity shale gas produced water: Drivers, technologies, and future directions, Environ Sci Technol. 47 (2013) 9569–9583. https://doi.org/10.1021/es401966e.

[18] X. Zhang, J. Ma, J. Zheng, R. Dai, X. Wang, Z. Wang, Recent advances in nature-inspired antifouling membranes for water purification, Chemical Engineering Journal. 432 (2022). https://doi.org/10.1016/j.cej.2021.134425.

[19] E. Drioli, F. Macedonio, E. Tocci, Membrane Science and membrane Engineering for a sustainable industrial development, Sep Purif Technol. 275 (2021). https://doi.org/10.1016/j.seppur.2021.119196.

[20] M. Khraisheh, S. Elhenawy, F. Almomani, M. Al-Ghouti, M.K. Hassan, B.H. Hameed, Recent progress on nanomaterial-based membranes for water treatment, Membranes (Basel). 11 (2021). https://doi.org/10.3390/membranes11120995.

[21] D. Rana, T. Matsuura, Surface modifications for antifouling membranes, Chem Rev. 110 (2010) 2448–2471. https://doi.org/10.1021/cr800208y.

[22] W. Gao, H. Liang, J. Ma, M. Han, Z. lin Chen, Z. shuang Han, G. bai Li, Membrane fouling control in ultrafiltration technology for drinking water production: A review, Desalination. 272 (2011) 1–8. https://doi.org/10.1016/j.desal.2011.01.051.

[23] X. Shi, G. Tal, N.P. Hankins, V. Gitis, Fouling and cleaning of ultrafiltration membranes: A review, Journal of Water Process Engineering. 1 (2014) 121–138. https://doi.org/10.1016/j.jwpe.2014.04.003.

[24] N.U. Barambu, M.R. Bilad, M.A. Bustam, K.A. Kurnia, M.H.D. Othman, N.A.H.M. Nordin, Development of membrane material for oily wastewater treatment: A review, Ain Shams Engineering Journal. 12 (2021) 1361–1374. https://doi.org/10.1016/j.asej.2020.08.027.

[25] Y.R. Chang, Y.J. Lee, D.J. Lee, Membrane fouling during water or wastewater treatments: Current research updated, J Taiwan Inst Chem Eng. 94 (2019) 88–96. https://doi.org/10.1016/j.jtice.2017.12.019.

[26] L.D. Tijing, Y.C. Woo, J.S. Choi, S. Lee, S.H. Kim, H.K. Shon, Fouling and its control in membrane distillation-A review, J Memb Sci. 475 (2015) 215–244. https://doi.org/10.1016/j.memsci.2014.09.042.

[27] G. Van Eygen, B. Van der Bruggen, A. Buekenhoudt, P. Luis Alconero, Efficient membrane-based affinity separations for chemical applications: A review, Chemical Engineering and Processing - Process Intensification. 169 (2021). https://doi.org/10.1016/j.cep.2021.108613.

[28] H. Al Abdulgader, V. Kochkodan, N. Hilal, Hybrid ion exchange - Pressure driven membrane processes in water treatment: A review, Sep Purif Technol. 116 (2013) 253–264. https://doi.org/10.1016/j.seppur.2013.05.052.

[29] B. Van Der Bruggen, C. Vandecasteele, T. Van Gestel, W. Doyen, R. Leysen, A review of pressure-driven membrane processes in wastewater treatment and drinking water production, Environmental Progress. 22 (2003) 46–56. https://doi.org/10.1002/ep.670220116.

[30] W. Suwaileh, D. Johnson, N. Hilal, Membrane desalination and water re-use for agriculture: State of the art and future outlook, Desalination. 491 (2020). https://doi.org/10.1016/j.desal.2020.114559.

[31] I.C. Escobar, B. Van Der Bruggen, Microfiltration and ultrafiltration membrane science and technology, J Appl Polym Sci. 132 (2015). https://doi.org/10.1002/app.42002.

[32] S. Al Aani, T.N. Mustafa, N. Hilal, Ultrafiltration membranes for wastewater and water process engineering: A comprehensive statistical review over the past decade, Journal of Water Process Engineering. 35 (2020). https://doi.org/10.1016/j.jwpe.2020.101241.

[33] R.W. Baker, Membrane technology and applications, John Wiley & Sons, 2024.

[34] M.M. Pendergast, E.M.V. Hoek, A review of water treatment membrane nanotechnologies, Energy Environ Sci. 4 (2011) 1946–1971. https://doi.org/10.1039/c0ee00541j.

[35] B. Ladewig, M.N.Z. Al-Shaeli, B. Ladewig, M.N.Z. Al-Shaeli, Fundamentals of membrane processes, Fundamentals of Membrane Bioreactors: Materials, Systems and Membrane Fouling. (2017) 13–37.

[36] J. Wilcox, J. Wilcox, Membrane technology, Carbon Capture. (2012) 177–218.

[37] M. Mulder, Basic principles of membrane technology, Springer science & business media, 1996.

[38] H. Darcy, Les fontaines publiques de la ville de Dijon: exposition et application des principes à suivre et des formules à employer dans les questions de distribution d'eau, Victor dalmont, 1856.

[39] J.L. Poiseuille, Recherches expérimentales sur le mouvement des liquides dans les tubes de très-petits diamètres, Imprimerie Royale, 1844.

[40] W. Guo, H.H. Ngo, J. Li, A mini-review on membrane fouling, Bioresour Technol. 122 (2012) 27–34. https://doi.org/10.1016/j.biortech.2012.04.089.

[41] B. Li, B. Qi, Z. Guo, D. Wang, T. Jiao, Recent developments in the application of membrane separation technology and its challenges in oil-water separation: A review, Chemosphere. 327 (2023). https://doi.org/10.1016/j.chemosphere.2023.138528.

[42] A. Basile, A. Cassano, N.K. Rastogi, Advances in membrane technologies for water treatment: materials, processes and applications, Elsevier, 2015.

[43] A.S. Al-Amoudi, Factors affecting natural organic matter (NOM) and scaling fouling in NF membranes: A review, Desalination. 259 (2010) 1–10. https://doi.org/10.1016/j.desal.2010.04.003.

[44] R. Zhang, Y. Liu, M. He, Y. Su, X. Zhao, M. Elimelech, Z. Jiang, Antifouling membranes for sustainable water purification: Strategies and mechanisms, Chem Soc Rev. 45 (2016) 5888–5924. https://doi.org/10.1039/c5cs00579e.

[45] S.P. Bera, M. Godhaniya, C. Kothari, Emerging and advanced membrane technology for wastewater treatment: A review, J Basic Microbiol. 62 (2022) 245–259. https://doi.org/10.1002/jobm.202100259.

[46] F. Meng, S.R. Chae, A. Drews, M. Kraume, H.S. Shin, F. Yang, Recent advances in membrane bioreactors (MBRs): Membrane fouling and membrane material, Water Res. 43 (2009) 1489–1512. https://doi.org/10.1016/j.watres.2008.12.044.

[47] D. Li, H. Wang, Recent developments in reverse osmosis desalination membranes, J Mater Chem. 20 (2010) 4551–4566. https://doi.org/10.1039/b924553g.

[48] L.Y. Ng, A.W. Mohammad, C.P. Leo, N. Hilal, Polymeric membranes incorporated with metal/metal oxide nanoparticles: A comprehensive review, Desalination. 308 (2013) 15–33. https://doi.org/10.1016/j.desal.2010.11.033.

[49] W. Salim, W.W. Ho, Recent developments on nanostructured polymer-based membranes, Curr Opin Chem Eng. 8 (2015) 76–82. https://doi.org/10.1016/j.coche.2015.03.003.

[50] X. Qu, P.J.J. Alvarez, Q. Li, Applications of nanotechnology in water and wastewater treatment, Water Res. 47 (2013) 3931–3946. https://doi.org/10.1016/j.watres.2012.09.058.

[51] C.H. Ahn, Y. Baek, C. Lee, S.O. Kim, S. Kim, S. Lee, S.H. Kim, S.S. Bae, J. Park, J. Yoon, Carbon nanotube-based membranes: Fabrication and application to desalination, Journal of Industrial and Engineering Chemistry. 18 (2012) 1551–1559. https://doi.org/10.1016/j.jiec.2012.04.005.

[52] D. Li, Y. Yan, H. Wang, Recent advances in polymer and polymer composite membranes for reverse and forward osmosis processes, Prog Polym Sci. 61 (2016) 104–155. https://doi.org/10.1016/j.progpolymsci.2016.03.003.

[53] K.P. Lee, T.C. Arnot, D. Mattia, A review of reverse osmosis membrane materials for desalination-Development to date and future potential, J Memb Sci. 370 (2011) 1–22. https://doi.org/10.1016/j.memsci.2010.12.036.

[54] A.W. Mohammad, Y.H. Teow, W.L. Ang, Y.T. Chung, D.L. Oatley-Radcliffe, N. Hilal, Nanofiltration membranes review: Recent advances and future prospects, Desalination. 356 (2015) 226–254. https://doi.org/10.1016/j.desal.2014.10.043.

[55] R.P. Pandey, P.A. Rasheed, T. Gomez, R.S. Azam, K.A. Mahmoud, A fouling-resistant mixed-matrix nanofiltration membrane based on covalently cross-linked Ti3C2TX (MXene)/cellulose acetate, J Memb Sci. 607 (2020). https://doi.org/10.1016/j.memsci.2020.118139.

[56] A. Dashtbozorg, E. Saljoughi, S.M. Mousavi, S. Kiani, High-performance and robust polysulfone nanocomposite membrane containing 2D functionalized MXene nanosheets for the nanofiltration of salt and dye solutions, Desalination. 527 (2022). https://doi.org/10.1016/j.desal.2022.115600.

[57] P. Wang, B. He, Y. Du, B. Wang, J. Gao, S. Liu, Q. Ye, F. Zhou, Functionalized Ti3C2Tx-based nanocomposite coatings for anticorrosion and antifouling applications, Chemical Engineering Journal. 448 (2022). https://doi.org/10.1016/j.cej.2022.137668.

[58] T. Liu, X. Liu, N. Graham, W. Yu, K. Sun, Two-dimensional MXene incorporated graphene oxide composite membrane with enhanced water purification performance, J Memb Sci. 593 (2020). https://doi.org/10.1016/j.memsci.2019.117431.

[59] AWWA, Recent Advances and Research Need in Membrane Fouling. , AWWA. (2005).

[60] J. Kim, B. Van Der Bruggen, The use of nanoparticles in polymeric and ceramic membrane structures: Review of manufacturing procedures and performance improvement for water treatment, Environmental Pollution. 158 (2010) 2335–2349. https://doi.org/10.1016/j.envpol.2010.03.024.

[61] J.F. Li, Z.L. Xu, H. Yang, L.Y. Yu, M. Liu, Effect of TiO 2 nanoparticles on the surface morphology and performance of microporous PES membrane, Appl Surf Sci. 255 (2009) 4725–4732. https://doi.org/10.1016/j.apsusc.2008.07.139.

[62] J.B. Li, J.W. Zhu, M.S. Zheng, Morphologies and properties of poly(phthalazinone ether sulfone ketone) matrix ultrafiltration membranes with entrapped TiO2 nanoparticles, J Appl Polym Sci. 103 (2007) 3623–3629. https://doi.org/10.1002/app.25428.

[63] M.L. Liu, L. Li, Y.X. Sun, Z.J. Fu, X.L. Cao, S.P. Sun, Scalable conductive polymer membranes for ultrafast organic pollutants removal, J Memb Sci. 617 (2021). https://doi.org/10.1016/j.memsci.2020.118644.

[64] M. Rezakazemi, A. Dashti, H. Riasat Harami, N. Hajilari, Inamuddin, Fouling-resistant membranes for water reuse, Environ Chem Lett. 16 (2018) 715–763. https://doi.org/10.1007/s10311-018-0717-8.

[65] L. Xu, S. Shahid, A.K. Holda, E.A.C. Emanuelsson, D.A. Patterson, Stimuli responsive conductive polyaniline membrane: In-filtration electrical tuneability of flux and MWCO, J Memb Sci. 552 (2018) 153–166. https://doi.org/10.1016/j.memsci.2018.01.070.

[66] A. Karkooti, M. Rastgar, N. Nazemifard, M. Sadrzadeh, Graphene-based electro-conductive anti-fouling membranes for the treatment of oil sands produced water, Science of the Total Environment. 704 (2020). https://doi.org/10.1016/j.scitotenv.2019.135365.

[67] M. Rastgar, A. Bozorg, A. Shakeri, M. Sadrzadeh, Substantially improved antifouling properties in electro-oxidative graphene laminate forward osmosis membrane, Chemical Engineering Research and Design. 141 (2019) 413–424. https://doi.org/10.1016/j.cherd.2018.11.010.

[68] B. Anne Braghetta, F.A. DiGiano, W.P. BalV Member, NANOFILTRATION OF NATURAL ORGANIC MATTER: pH AND IONIC STRENGTH EFFECTS, n.d.

[69] N. Mameda, K.H. Choo, Electrochemical membrane technology for fouling control, in: Electrochemical Membrane Technology for Water and Wastewater Treatment, Elsevier, 2022: pp. 195–225. https://doi.org/10.1016/B978-0-12-824470-8.00007-3.

[70] K.L. Jones, C.R. O'melia, Protein and humic acid adsorption onto hydrophilic membrane surfaces: effects of pH and ionic strength, 2000.

[71] C. Li, X. Guo, X. Wang, S. Fan, Q. Zhou, H. Shao, W. Hu, C. Li, L. Tong, R.R. Kumar, J. Huang, Membrane fouling mitigation by coupling applied electric field in membrane system: Configuration, mechanism and performance, Electrochim Acta. 287 (2018) 124–134. https://doi.org/10.1016/j.electacta.2018.06.150.

[72] N.H. Barbhuiya, U. Misra, S.P. Singh, Synthesis, fabrication, and mechanism of action of electrically conductive membranes: A review, Environ Sci (Camb). 7 (2021) 671–705. https://doi.org/10.1039/d0ew01070g.

[73] Z. Wang, Y. Zhang, K. Li, J. Guo, C. Yang, H. Liu, J. Wang, In situ coupling of electrochemical oxidation and membrane filtration processes for simultaneous decontamination and membrane fouling mitigation, Sep Purif Technol. 290 (2022). https://doi.org/10.1016/j.seppur.2022.120918.

[74] F. Ahmed, B.S. Lalia, V. Kochkodan, N. Hilal, R. Hashaikeh, Electrically conductive polymeric membranes for fouling prevention and detection: A review, Desalination. 391 (2016) 1–15. https://doi.org/10.1016/j.desal.2016.01.030.

[75] C. Trellu, B.P. Chaplin, C. Coetsier, R. Esmilaire, S. Cerneaux, C. Causserand, M. Cretin, Electro-oxidation of organic pollutants by reactive electrochemical membranes, Chemosphere. 208 (2018) 159–175. https://doi.org/10.1016/j.chemosphere.2018.05.026.

[76] L. Dumée, J.L. Campbell, K. Sears, J. Schütz, N. Finn, M. Duke, S. Gray, The impact of hydrophobic coating on the performance of carbon nanotube bucky-paper membranes in membrane distillation, Desalination. 283 (2011) 64–67. https://doi.org/10.1016/j.desal.2011.02.046.

[77] F. Li, M. Scampicchio, S. Mannino, Carbon Nanotube-Adsorbed Electrospun Nanofibrous Membranes as Coating for Electrochemical Sensors for Sulfhydryl Compounds, Electroanalysis. 23 (2011) 1773–1775. https://doi.org/10.1002/elan.201100068.

[78] T. V. Shishkanova, P. Matějka, V. Král, I. Šeděnková, M. Trchová, J. Stejskal, Optimization of the thickness of a conducting polymer, polyaniline, deposited on the surface of poly(vinyl chloride) membranes: A new way to improve their potentiometric response, Anal Chim Acta. 624 (2008) 238–246. https://doi.org/10.1016/j.aca.2008.07.001.

[79] W. Hu, S. Chen, Z. Yang, L. Liu, H. Wang, Flexible electrically conductive nanocomposite membrane based on bacterial cellulose and polyaniline, Journal of Physical Chemistry B. 115 (2011) 8453–8457. https://doi.org/10.1021/jp204422v.

[80] I.-H. Loh, R.A. Moody, J.C. Huang, ELECTRICALLY CONDUCTIVE MEMBRANES: SYNTHESIS AND APPLICATIONS, 1990.

[81] X. Zhu, D. Jassby, Electroactive Membranes for Water Treatment: Enhanced Treatment Functionalities, Energy Considerations, and Future Challenges, Acc Chem Res. 52 (2019) 1177–1186. https://doi.org/10.1021/acs.accounts.8b00558.

[82] Q. Zhang, C.D. Vecitis, Conductive CNT-PVDF membrane for capacitive organic fouling reduction, J Memb Sci. 459 (2014) 143–156. https://doi.org/10.1016/j.memsci.2014.02.017.

[83] J. Huang, Z. Wang, J. Zhang, X. Zhang, J. Ma, Z. Wu, A novel composite conductive microfiltration membrane and its anti-fouling performance with an external electric field in membrane bioreactors, Sci Rep. 5 (2015). https://doi.org/10.1038/srep09268.

[84] C. Wang, H. Song, Q. Zhang, B. Wang, A. Li, Parameter optimization based on capacitive deionization for highly efficient desalination of domestic wastewater biotreated effluent and the fouled electrode regeneration, Desalination. 365 (2015) 407–415. https://doi.org/10.1016/j.desal.2015.03.025.

[85] J. Liu, L. Liu, B. Gao, F. Yang, Integration of bio-electrochemical cell in membrane bioreactor for membrane cathode fouling reduction through electricity generation, J Memb Sci. 430 (2013) 196–202. https://doi.org/10.1016/j.memsci.2012.11.046.

[86] A. Holder, J. Weik, J. Hinrichs, A study of fouling during long-term fractionation of functional peptides by means of cross-flow ultrafiltration and cross-flow electro membrane filtration, J Memb Sci. 446 (2013) 440–448. https://doi.org/10.1016/j.memsci.2013.06.017.

[87] S. Wang, S. Liang, P. Liang, X. Zhang, J. Sun, S. Wu, X. Huang, In-situ combined dual-layer CNT/PVDF membrane for electrically-enhanced fouling resistance, J Memb Sci. 491 (2015) 37–44. https://doi.org/10.1016/j.memsci.2015.05.014.

[88] K.C. Ho, Y.H. Teow, A.W. Mohammad, W.L. Ang, P.H. Lee, Development of graphene oxide (GO)/multi-walled carbon nanotubes (MWCNTs) nanocomposite conductive membranes for electrically enhanced fouling mitigation, J Memb Sci. 552 (2018) 189–201. https://doi.org/10.1016/j.memsci.2018.02.001.

[89] J.H. Jhaveri, Z.V.P. Murthy, A comprehensive review on anti-fouling nanocomposite membranes for pressure driven membrane separation processes, Desalination. 379 (2016) 137–154. https://doi.org/10.1016/j.desal.2015.11.009.

[90] L. Dumée, K. Sears, J. Schütz, N. Finn, M. Duke, S. Gray, Carbon nanotube based composite membranes for water desalination by membrane distillation, Desalination Water Treat. 17 (2010) 72–79. https://doi.org/10.5004/dwt.2010.1701.

[91] A. Mansourizadeh, I. Rezaei, W.J. Lau, M.Q. Seah, A.F. Ismail, A review on recent progress in environmental applications of membrane contactor technology, J Environ Chem Eng. 10 (2022). https://doi.org/10.1016/j.jece.2022.107631.

[92] B. Mi, M. Elimelech, Chemical and physical aspects of organic fouling of forward osmosis membranes, J Memb Sci. 320 (2008) 292–302. https://doi.org/10.1016/j.memsci.2008.04.036.

[93] H. Li, W. Shi, Y. Su, H. Zhang, X. Qin, Preparation and characterization of carboxylated multiwalled carbon nanotube/polyamide composite nanofiltration membranes with improved performance, J Appl Polym Sci. 134 (2017). https://doi.org/10.1002/app.45268.

[94] Y. Li, S. Huang, S. Zhou, A.G. Fane, Y. Zhang, S. Zhao, Enhancing water permeability and fouling resistance of polyvinylidene fluoride membranes with carboxylated nanodiamonds, J Memb Sci. 556 (2018) 154–163. https://doi.org/10.1016/j.memsci.2018.04.004.

[95] H. Zhao, S. Qiu, L. Wu, L. Zhang, H. Chen, C. Gao, Improving the performance of polyamide reverse osmosis membrane by incorporation of modified multi-walled carbon nanotubes, J Memb Sci. 450 (2014) 249–256. https://doi.org/10.1016/j.memsci.2013.09.014.

[96] J. Li, C. Xu, J. Long, Z. Ding, R. Yuan, Z. Li, Lamellar MXene Nanofiltration Membranes for Electrostatic Modulation of Molecular Permeation: Implications for Fine Separation, ACS Appl Nano Mater. 5 (2022) 7373–7381. https://doi.org/10.1021/acsanm.2c01304.

[97] L. Qian, C. Yuan, X. Wang, H. Zhang, L. Du, G. Wei, S. Chen, Conductive MXene ultrafiltration membrane for improved antifouling ability and water quality under electrochemical assistance, RSC Adv. 13 (2023) 15872–15880. https://doi.org/10.1039/d3ra01116j.

[98] C.E. Ren, M. Alhabeb, B.W. Byles, M.Q. Zhao, B. Anasori, E. Pomerantseva, K.A. Mahmoud, Y. Gogotsi, Voltage-gated ions sieving through 2d mxene ti3c2txmembranes, ACS Appl Nano Mater. 1 (2018) 3644–3652. https://doi.org/10.1021/acsanm.8b00762.

[99] J. Kim, E.T. Yun, L. Tijing, H.K. Shon, S. Hong, Mitigation of fouling and wetting in membrane distillation by electrical repulsion using a multi-layered single-wall carbon nanotube/polyvinylidene fluoride membrane, J Memb Sci. 653 (2022). https://doi.org/10.1016/j.memsci.2022.120519.

[100] C. Hu, Z. Liu, X. Lu, J. Sun, H. Liu, J. Qu, Enhancement of the Donnan effect through capacitive ion increase using an electroconductive rGO-CNT nanofiltration membrane, J Mater Chem A Mater. 6 (2018) 4737–4745. https://doi.org/10.1039/c7ta11003k.

[101] E.L. Subtil, J. Gonçalves, H.G. Lemos, E.C. Venancio, J.C. Mierzwa, J. dos Santos de Souza, W. Alves, P. Le-Clech, Preparation and characterization of a new composite conductive polyethersulfone membrane using polyaniline (PANI) and reduced graphene oxide (rGO), Chemical Engineering Journal. 390 (2020). https://doi.org/10.1016/j.cej.2020.124612.

[102] Y. Zhang, T. Wang, J. Meng, J. Lei, X. Zheng, Y. Wang, J. Zhang, X. Cao, X. Li, X. Qiu, J. Xue, A novel conductive composite membrane with polypyrrole (PPy) and stainless-steel mesh: Fabrication, performance, and anti-fouling mechanism, J Memb Sci. 621 (2021). https://doi.org/10.1016/j.memsci.2020.118937.

[103] W. Duan, A. Ronen, S. Walker, D. Jassby, Polyaniline-Coated Carbon Nanotube Ultrafiltration Membranes: Enhanced Anodic Stability for in Situ Cleaning and Electro-Oxidation Processes, ACS Appl Mater Interfaces. 8 (2016) 22574–22584. https://doi.org/10.1021/acsami.6b07196.

[104] F.G.F. Qin, J. Mawson, X.A. Zeng, Experimental study of fouling and cleaning of sintered stainless steel membrane in electro-microfiltration of calcium salt particles, Membranes (Basel). 1 (2011) 119–131. https://doi.org/10.3390/membranes1020119.

[105] L.L. Xu, K.P. Wang, K.L. Li, S.Y. Zhao, J. Wang, Development and performance of stable PANI/MWNT conductive membrane for contaminants degradation and anti-fouling behavior, Sep Purif Technol. 282 (2022). https://doi.org/10.1016/j.seppur.2021.120112.

[106] F.R. Omi, M.R. Choudhury, N. Anwar, A.R. Bakr, M.S. Rahaman, Highly Conductive Ultrafiltration Membrane via Vacuum Filtration Assisted Layer-by-Layer Deposition of Functionalized Carbon Nanotubes, Ind Eng Chem Res. 56 (2017) 8474–8484. https://doi.org/10.1021/acs.iecr.7b00847.

[107] S.F. Anis, B.S. Lalia, A. Lesimple, R. Hashaikeh, N. Hilal, Electrically conductive membranes for contemporaneous dye rejection and degradation, Chemical Engineering Journal. 428 (2022). https://doi.org/10.1016/j.cej.2021.131184.

[108] Y. Zhang, W. Yu, R. Li, Y. Xu, L. Shen, H. Lin, B.Q. Liao, G. Wu, Novel conductive membranes breaking through the selectivity-permeability trade-off for Congo red removal, Sep Purif Technol. 211 (2019) 368–376. https://doi.org/10.1016/j.seppur.2018.10.008.

[109] X. Wang, H. Zhang, X. Wang, S. Chen, H. Yu, X. Quan, Electroconductive RGO-MXene membranes with wettability-regulated channels: improved water permeability and electro-enhanced rejection performance, Front Environ Sci Eng. 17 (2023). https://doi.org/10.1007/s11783-023-1601-8.

[110] N. Li, T.J. Lou, W. Wang, M. Li, L.C. Jing, Z.X. Yang, R.Y. Chang, J. Li, H.Z. Geng, MXene-PANI/PES composite ultrafiltration membranes with conductive properties for anti-fouling and dye removal, J Memb Sci. 668 (2023). https://doi.org/10.1016/j.memsci.2022.121271.

[111] Y. Zhao, W. Yu, R. Li, Y. Xu, Y. Liu, T. Sun, L. Shen, H. Lin, Electric field endowing the conductive polyvinylidene fluoride (PVDF)-graphene oxide (GO)-nickel (Ni) membrane with high-efficient performance for dye wastewater treatment, Appl Surf Sci. 483 (2019) 1006–1016. https://doi.org/10.1016/j.apsusc.2019.04.054.

[112] G. Yi, L. Du, G. Wei, H. Zhang, H. Yu, X. Quan, S. Chen, Selective molecular separation with conductive MXene/CNT nanofiltration membranes under electrochemical assistance, J Memb Sci. 658 (2022). https://doi.org/10.1016/j.memsci.2022.120719.

[113] A.K. Thakur, S.P. Singh, C. Thamaraiselvan, M.N. Kleinberg, C.J. Arnusch, Graphene oxide on laser-induced graphene filters for antifouling, electrically conductive ultrafiltration membranes, J Memb Sci. 591 (2019). https://doi.org/10.1016/j.memsci.2019.117322.

[114] A. Niu, Y. Han, J. Wu, N. Yu, Q. Xu, Synthesis of one-dimensional carbon nanomaterials wrapped by silver nanoparticles and their antibacterial behavior, Journal of Physical Chemistry C. 114 (2010) 12728–12735. https://doi.org/10.1021/jp104720w.

[115] Z. Hanif, Z.A. Khan, M.F. Siddiqui, S. Park, S.J. Park, Polypyrrole-based Conducting and Antibacterial Hybrid Cellulose Membranes: A study on the effect of UV exposure on the conductivity and formation of silver nanoparticles, Sensors and Materials. 31 (2019) 1927–1938. https://doi.org/10.18494/SAM.2019.2310.

[116] C.Y. Foong, M.D.H. Wirzal, M.A. Bustam, A review on nanofibers membrane with amino-based ionic liquid for heavy metal removal, J Mol Liq. 297 (2020). https://doi.org/10.1016/j.molliq.2019.111793.

[117] J.P. John, T.E. Mary Nancy, T.K. Bindu Sharmila, A comprehensive review on the environmental applications of graphene-carbon nanotube hybrids: Recent progress, challenges and prospects, Mater Adv. 2 (2021) 6816–6838. https://doi.org/10.1039/d1ma00324k.

[118] Y. Zhang, S. Zhang, T.S. Chung, Nanometric Graphene Oxide Framework Membranes with Enhanced Heavy Metal Removal via Nanofiltration, Environ Sci Technol. 49 (2015) 10235–10242. https://doi.org/10.1021/acs.est.5b02086.

[119] H. Zhang, X. Quan, X. Fan, G. Yi, S. Chen, H. Yu, Y. Chen, Improving Ion Rejection of Conductive Nanofiltration Membrane through Electrically Enhanced Surface Charge Density, Environ Sci Technol. 53 (2019) 868–877. https://doi.org/10.1021/acs.est.8b04268.

[120] Y. He, L. Qin, H. Huang, Calcium-enhanced retention of humic substances by carbon nanotube membranes: Mechanisms and implication, J Memb Sci. 629 (2021). https://doi.org/10.1016/j.memsci.2021.119273.

[121] P. Formoso, E. Pantuso, G. De Filpo, F.P. Nicoletta, Electro-conductive membranes for permeation enhancement and fouling mitigation: A short review, Membranes (Basel). 7 (2017). https://doi.org/10.3390/membranes7030039.

[122] L.L. Xu, Y. Xu, L. Liu, K.P. Wang, D.A. Patterson, J. Wang, Electrically responsive ultrafiltration polyaniline membrane to solve fouling under applied potential, J Memb Sci. 572 (2019) 442–452. https://doi.org/10.1016/j.memsci.2018.11.026.

[123] Z.-K. Xu, X.-J. Huang, L.-S. Wan, Surface engineering of polymer membranes, Springer Science & Business Media, 2009.

[124] B. Díez, R. Rosal, A critical review of membrane modification techniques for fouling and biofouling control in pressure-driven membrane processes, Nanotechnology for Environmental Engineering. 5 (2020). https://doi.org/10.1007/s41204-020-00077-x.

[125] A. Kerr, T. Hodgkiess, M.J. Cowling, C.M. Beveridge, M.J. Smith, A.C.S. Parr, A novel technique to prevent bacterial fouling, using imposed surface potential, J Appl Microbiol. 85 (1998) 1067–1072.

[126] C. Cano-Raya, Z.Z. Denchev, S.F. Cruz, J.C. Viana, Chemistry of solid metal-based inks and pastes for printed electronics – A review, Appl Mater Today. 15 (2019) 416–430. https://doi.org/10.1016/j.apmt.2019.02.012.

[127] M. Naguib, V.N. Mochalin, M.W. Barsoum, Y. Gogotsi, 25th anniversary article: MXenes: A new family of two-dimensional materials, Advanced Materials. 26 (2014) 992–1005. https://doi.org/10.1002/adma.201304138.

[128] P. Bhol, S. Yadav, A. Altaee, M. Saxena, P.K. Misra, A.K. Samal, Graphene-Based Membranes for Water and Wastewater Treatment: A Review, ACS Appl Nano Mater. 4 (2021) 3274–3293. https://doi.org/10.1021/acsanm.0c03439.

[129] X. Fan, G. Wei, X. Quan, Carbon nanomaterial-based membranes for water and wastewater treatment under electrochemical assistance, Environ Sci Nano. 10 (2022) 11–40. https://doi.org/10.1039/d2en00545j.

[130] Y. Zhang, L. Liu, F. Yang, A novel conductive membrane with RGO/PVDF coated on carbon fiber cloth for fouling reduction with electric field in separating polyacrylamide, J Appl Polym Sci. 133 (2016). https://doi.org/10.1002/app.43597.

[131] M. Rastgar, J. Fleck, R. Graessner, A. Taghipour, M. Sadrzadeh, Smart harvesting and in-situ application of piezoelectricity in membrane filtration systems, J Memb Sci. 660 (2022). https://doi.org/10.1016/j.memsci.2022.120819.

[132] M. Rastgar, A. Karkooti, A. Sohrabi, P. Karami, N. Nazemifard, M. Sadrzadeh, Osmotic dewatering accelerates inherent sluggish kinetics of electro-Fenton process: Toward sustainable removal of organic contaminants, Chemical Engineering Journal. 394 (2020). https://doi.org/10.1016/j.cej.2020.125043.

[133] M. Dadashi Firouzjaei, E. Zolghadr, S. Ahmadalipour, N. Taghvaei, F. Akbari Afkhami, S. Nejati, M.A. Elliott, Chemistry, abundance, detection and treatment of per- and polyfluoroalkyl substances in water: a review, Environ Chem Lett. 20 (2022) 661–679. https://doi.org/10.1007/s10311-021-01340-6.

[134] M.D. Firouzjaei, S.F. Seyedpour, S.A. Aktij, M. Giagnorio, N. Bazrafshan, A. Mollahosseini, F. Samadi, S. Ahmadalipour, F.D. Firouzjaei, M.R. Esfahani, A. Tiraferri, M. Elliott, M. Sangermano, A. Abdelrasoul, J.R. McCutcheon, M. Sadrzadeh, A.R. Esfahani, A. Rahimpour, Recent advances in functionalized polymer membranes for biofouling control and mitigation in forward osmosis, J Memb Sci. 596 (2020). https://doi.org/10.1016/j.memsci.2019.117604.

[135] M. Dadashi Firouzjaei, M. Pejman, M.S. Gh, S.A. Aktij, E. Zolghadr, A. Rahimpour, M. Sadrzadeh, A.A. Shamsabadi, A. Tiraferri, M. Elliott, Functionalized polyamide membranes yield suppression of biofilm and planktonic bacteria while retaining flux and selectivity, Sep Purif Technol. 282 (2022). https://doi.org/10.1016/j.seppur.2021.119981.

[136] M. Elimelech, W.A. Phillip, The Future of Seawater Desalination: Energy, Technology, and the Environment, 2011. www.sciencemag.org.

[137] M.; Z.A.R.; M.H.R.; S.H.; N.H.R. Rastgar, Photocatalytic/Adsorptive Removal of Methylene Blue Dye by Electrophoretic Nanostructured TiO2/Montmorillonite Composite Films. Journal of Advanced Oxidation Technologies 2013, Journal of Advanced Oxidation Technologies . 16 (2013) 292–297.

[138] W.J. Lau, S. Gray, T. Matsuura, D. Emadzadeh, J. Paul Chen, A.F. Ismail, A review on polyamide thin film nanocomposite (TFN) membranes: History, applications, challenges and approaches, Water Res. 80 (2015) 306–324. https://doi.org/10.1016/j.watres.2015.04.037.

[139] N. Bazrafshan, M. Dadashi Firouzjaei, M. Elliott, A. Moradkhani, A. Rahimpour, Preparation and modification of low-fouling ultrafiltration membranes for cheese whey treatment by membrane bioreactor, Case Studies in Chemical and Environmental Engineering. 4 (2021). https://doi.org/10.1016/j.cscee.2021.100137.

[140] S. Mohammad Nejad, S.F. Seyedpour, S. Aghapour Aktij, M. Dadashi Firouzjaei, M. Elliott, A. Tiraferri, M. Sadrzadeh, A. Rahimpour, Loose nanofiltration membranes functionalized with in situ-synthesized metal organic framework for water treatment, Mater Today Chem. 24 (2022). https://doi.org/10.1016/j.mtchem.2022.100909.

[141] N. Hilal, O.O. Ogunbiyi, N.J. Miles, R. Nigmatullin, Methods employed for control of fouling in MF and UF membranes: A comprehensive review, Sep Sci Technol. 40 (2005) 1957–2005. https://doi.org/10.1081/SS-200068409.

[142] M. Pejman, M. Dadashi Firouzjaei, S. Aghapour Aktij, E. Zolghadr, P. Das, M. Elliott, M. Sadrzadeh, M. Sangermano, A. Rahimpour, A. Tiraferri, Effective strategy for UV-mediated grafting of biocidal Ag-MOFs on polymeric membranes aimed at enhanced water ultrafiltration, Chemical Engineering Journal. 426 (2021). https://doi.org/10.1016/j.cej.2021.130704.

[143] P. Karami, S.A. Aktij, B. Khorshidi, M.D. Firouzjaei, A. Asad, M. Elliott, A. Rahimpour, J.B.P. Soares, M. Sadrzadeh, Nanodiamond-decorated thin film composite membranes with antifouling and antibacterial properties, Desalination. 522 (2022). https://doi.org/10.1016/j.desal.2021.115436.

[144] M. Pejman, M. Dadashi Firouzjaei, S. Aghapour Aktij, P. Das, E. Zolghadr, H. Jafarian, A. Arabi Shamsabadi, M. Elliott, M. Sadrzadeh, M. Sangermano, A. Rahimpour, A. Tiraferri, In Situ Ag-

MOF Growth on Pre-Grafted Zwitterions Imparts Outstanding Antifouling Properties to Forward Osmosis Membranes, ACS Appl Mater Interfaces. 12 (2020) 36287–36300. https://doi.org/10.1021/acsami.0c12141.

[145] M. Pejman, M.D. Firouzjaei, S.A. Aktij, P. Das, E. Zolghadr, H. Jafarian, A.A. Shamsabadi, M. Elliott, M.R. Esfahani, M. Sangermano, M. Sadrzadeh, E.K. Wujcik, A. Rahimpour, A. Tiraferri, Improved antifouling and antibacterial properties of forward osmosis membranes through surface modification with zwitterions and silver-based metal organic frameworks, J Memb Sci. 611 (2020). https://doi.org/10.1016/j.memsci.2020.118352.

[146] L. Zhu, H. Song, G. Wang, Z. Zeng, Q. Xue, Symmetrical polysulfone/poly(acrylic acid) porous membranes with uniform wormlike morphology and pH responsibility: Preparation, characterization and application in water purification, J Memb Sci. 549 (2018) 515–522. https://doi.org/10.1016/j.memsci.2017.12.052.

[147] J. Liu, L.J. Yu, G. Yue, N. Wang, Z. Cui, L. Hou, J. Li, Q. Li, A. Karton, Q. Cheng, L. Jiang, Y. Zhao, Thermoresponsive Graphene Membranes with Reversible Gating Regularity for Smart Fluid Control, Adv Funct Mater. 29 (2019). https://doi.org/10.1002/adfm.201808501.

[148] J. Liu, N. Wang, L.J. Yu, A. Karton, W. Li, W. Zhang, F. Guo, L. Hou, Q. Cheng, L. Jiang, D.A. Weitz, Y. Zhao, Bioinspired graphene membrane with temperature tunable channels for water gating and molecular separation, Nat Commun. 8 (2017). https://doi.org/10.1038/s41467-017-02198-5.

[149] X. Hou, Y. Hu, A. Grinthal, M. Khan, J. Aizenberg, Liquid-based gating mechanism with tunable multiphase selectivity and antifouling behaviour, Nature. 519 (2015) 70–73. https://doi.org/10.1038/nature14253.

[150] Z. Sheng, H. Wang, Y. Tang, M. Wang, L. Huang, L. Min, H. Meng, S. Chen, L. Jiang, X. Hou, Liquid gating elastomeric porous system with dynamically controllable gas/liquid transport, 2018. https://www.science.org.

[151] K. Huang, P. Rowe, C. Chi, V. Sreepal, T. Bohn, K.G. Zhou, Y. Su, E. Prestat, P.B. Pillai, C.T. Cherian, A. Michaelides, R.R. Nair, Cation-controlled wetting properties of vermiculite membranes and its promise for fouling resistant oil–water separation, Nat Commun. 11 (2020). https://doi.org/10.1038/s41467-020-14854-4.

[152] A. Feng, J. Yuan, Smart nanocontainers: Progress on novel stimuli-responsive polymer vesicles, Macromol Rapid Commun. 35 (2014) 767–779. https://doi.org/10.1002/marc.201300866.

[153] J. Liu, X. Xu, Y. Lei, M. Zhang, Z. Sheng, H. Wang, M. Cao, J. Zhang, X. Hou, Liquid Gating Meniscus-Shaped Deformable Magnetoelastic Membranes with Self-Driven Regulation of Gas/Liquid Release, Advanced Materials. 34 (2022). https://doi.org/10.1002/adma.202107327.

[154] Z. Sheng, M. Zhang, J. Liu, P. Malgaretti, J. Li, S. Wang, W. Lv, R. Zhang, Y. Fan, Y. Zhang, X. Chen, X. Hou, Reconfiguring confined magnetic colloids with tunable fluid transport behavior, Natl Sci Rev. 8 (2021). https://doi.org/10.1093/nsr/nwaa301.

[155] R. Tabassian, J.H. Oh, S. Kim, D. Kim, S. Ryu, S.M. Cho, N. Koratkar, I.K. Oh, Graphene-coated meshes for electroactive flow control devices utilizing two antagonistic functions of repellency and permeability, Nat Commun. 7 (2016). https://doi.org/10.1038/ncomms13345.

[156] L. Jiang, M. Rastgar, C. Wang, S. Ke, L. He, X. Chen, Y. Song, C. He, J. Wang, M. Sadrzadeh, Robust PANI-entangled CNTs Electro-responsive membranes for enhanced In-situ generation of H2O2 and effective separation of charged contaminants, Sep Purif Technol. 303 (2022). https://doi.org/10.1016/j.seppur.2022.122274.

[157] D. Liu, X. Chen, B. Bian, Z. Lai, Y. Situ, Dual-Function Conductive Copper Hollow Fibers for Microfiltration and Anti-biofouling in Electrochemical Membrane Bioreactors, Front Chem. 6 (2018). https://doi.org/10.3389/fchem.2018.00445.

[158] D. Bell, R. Sengpiel, M. Wessling, Metallized hollow fiber membranes for electrochemical fouling control, J Memb Sci. 594 (2020). https://doi.org/10.1016/j.memsci.2019.117397.

[159] K.P. Katuri, N.M.S. Bettahalli, X. Wang, G. Matar, S. Chisca, S.P. Nunes, P.E. Saikaly, A Microfiltration Polymer-Based Hollow-Fiber Cathode as a Promising Advanced Material for Simultaneous Recovery of Energy and Water, Advanced Materials. 28 (2016) 9504–9511. https://doi.org/10.1002/adma.201603074.

[160] B. Khorshidi, J. Hajinasiri, G. Ma, S. Bhattacharjee, M. Sadrzadeh, Thermally resistant and electrically conductive PES/ITO nanocomposite membrane, J Memb Sci. 500 (2016) 151–160. https://doi.org/10.1016/j.memsci.2015.11.015.

[161] B. Khorshidi, S.A. Hosseini, G. Ma, M. McGregor, M. Sadrzadeh, Novel nanocomposite polyethersulfone- antimony tin oxide membrane with enhanced thermal, electrical and antifouling properties, Polymer (Guildf). 163 (2019) 48–56. https://doi.org/10.1016/j.polymer.2018.12.058.

[162] L. Du, X. Quan, X. Fan, G. Wei, S. Chen, Conductive CNT/nanofiber composite hollow fiber membranes with electrospun support layer for water purification, J Memb Sci. 596 (2020). https://doi.org/10.1016/j.memsci.2019.117613.

[163] C. Cuevas, D. Kim, K.P. Katuri, P. Saikaly, S.P. Nunes, Electrochemically active polymeric hollow fibers based on poly(ether-b-amide)/carbon nanotubes, J Memb Sci. 545 (2018) 323–328. https://doi.org/10.1016/j.memsci.2017.09.052.

[164] M.J. Larocque, D.R. Latulippe, C.F. de Lannoy, Formation of electrically conductive hollow fiber membranes via crossflow deposition of carbon nanotubes – Addressing the conductivity/permeability trade-off, J Memb Sci. 620 (2021). https://doi.org/10.1016/j.memsci.2020.118859.

[165] M. Naguib, O. Mashtalir, J. Carle, V. Presser, J. Lu, L. Hultman, Y. Gogotsi, M.W. Barsoum, Two-dimensional transition metal carbides, ACS Nano. 6 (2012) 1322–1331. https://doi.org/10.1021/nn204153h.

[166] K. Rasool, R.P. Pandey, P.A. Rasheed, S. Buczek, Y. Gogotsi, K.A. Mahmoud, Water treatment and environmental remediation applications of two-dimensional metal carbides (MXenes), Materials Today. 30 (2019) 80–102. https://doi.org/10.1016/j.mattod.2019.05.017.

[167] J. Gao, Y. Feng, W. Guo, L. Jiang, Nanofluidics in two-dimensional layered materials: Inspirations from nature, Chem Soc Rev. 46 (2017) 5400–5424. https://doi.org/10.1039/c7cs00369b.

[168] J. Gao, A.R. Koltonow, K. Raidongia, B. Beckerman, N. Boon, E. Luijten, M. Olvera De La Cruz, J. Huang, Kirigami nanofluidics, Mater Chem Front. 2 (2018) 475–482. https://doi.org/10.1039/c7qm00620a.

[169] J. Lao, R. Lv, J. Gao, A. Wang, J. Wu, J. Luo, Aqueous Stable Ti 3 C 2 MXene Membrane with Fast and Photoswitchable Nanofluidic Transport, ACS Nano. 12 (2018) 12464–12471. https://doi.org/10.1021/acsnano.8b06708.

[170] K. Raidongia, J. Huang, Nanofluidic ion transport through reconstructed layered materials, J Am Chem Soc. 134 (2012) 16528–16531. https://doi.org/10.1021/ja308167f.

[171] C.J. Van Oss, Second Edition Interfacial Forces in Aqueous Media, n.d.

[172] A. Maiti, M. Sadrezadeh, S. Guha Thakurta, D.J. Pernitsky, S. Bhattacharjee, Characterization of boiler blowdown water from steam-assisted gravity drainage and silica-organic coprecipitation during acidification and ultrafiltration, Energy and Fuels. 26 (2012) 5604–5612. https://doi.org/10.1021/ef300865e.

[173] J.A. Brant, A.E. Childress, Assessing short-range membrane-colloid interactions using surface energetics, 2002.

[174] M. Rastgar, A. Shakeri, A. Bozorg, H. Salehi, V. Saadattalab, Highly-efficient forward osmosis membrane tailored by magnetically responsive graphene oxide/Fe 3 O 4 nanohybrid, Appl Surf Sci. 441 (2018) 923–935. https://doi.org/10.1016/j.apsusc.2018.02.118.

[175] L.P. Yu, L. Lu, X.H. Zhou, L. Xu, Current Understanding of the Wettability of MXenes, Adv Mater Interfaces. 10 (2023). https://doi.org/10.1002/admi.202201818.

[176] Z. Ling, C.E. Ren, M.Q. Zhao, J. Yang, J.M. Giammarco, J. Qiu, M.W. Barsoum, Y. Gogotsi, Flexible and conductive MXene films and nanocomposites with high capacitance, Proc Natl Acad Sci U S A. 111 (2014) 16676–16681. https://doi.org/10.1073/pnas.1414215111.

[177] A. Sarycheva, Y. Gogotsi, Raman Spectroscopy Analysis of the Structure and Surface Chemistry of Ti3C2T xMXene, Chemistry of Materials. 32 (2020) 3480–3488. https://doi.org/10.1021/acs.chemmater.0c00359.

[178] J. Halim, K.M. Cook, M. Naguib, P. Eklund, Y. Gogotsi, J. Rosen, M.W. Barsoum, X-ray photoelectron spectroscopy of select multi-layered transition metal carbides (MXenes), Appl Surf Sci. 362 (2016) 406–417. https://doi.org/10.1016/j.apsusc.2015.11.089.

[179] M.R. Lukatskaya, J. Halim, B. Dyatkin, M. Naguib, Y.S. Buranova, M.W. Barsoum, Y. Gogotsi, Room-Temperature Carbide-Derived Carbon Synthesis by Electrochemical Etching of MAX Phases, Angewandte Chemie. 126 (2014) 4977–4980. https://doi.org/10.1002/ange.201402513.

[180] S. Myhra, J.A.A. Crossley, M.W. Barsoum, Crystal-chemistry of the Ti 3 AlC 2 and Ti 4 AlN 3 layered carbide/ nitride phasesÐcharacterization by XPS, n.d. www.elsevier.nl/locate/jpcs.

[181] S. Yamamoto, H. Bluhm, K. Andersson, G. Ketteler, H. Ogasawara, M. Salmeron, A. Nilsson, In situ x-ray photoelectron spectroscopy studies of water on metals and oxides at ambient conditions, Journal of Physics Condensed Matter. 20 (2008). https://doi.org/10.1088/0953-8984/20/18/184025.

[182] N. Subhi, A.R.D. Verliefde, V. Chen, P. Le-Clech, Assessment of physicochemical interactions in hollow fibre ultrafiltration membrane by contact angle analysis, J Memb Sci. 403–404 (2012) 32–40. https://doi.org/10.1016/j.memsci.2012.02.007.

[183] S. Hong, M. Elimelech, Chemical and physical aspects of natural organic matter (NOM) fouling of nanofiltration membranes, 1997.

[184] S. Kim, E.M.V. Hoek, Interactions controlling biopolymer fouling of reverse osmosis membranes, Desalination. 202 (2007) 333–342. https://doi.org/10.1016/j.desal.2005.12.072.

[185] A. Subramani, X. Huang, E.M.V. Hoek, Direct observation of bacterial deposition onto clean and organic-fouled polyamide membranes, J Colloid Interface Sci. 336 (2009) 13–20. https://doi.org/10.1016/j.jcis.2009.03.063.

[186] E. Soheyli, D. Azad, R. Sahraei, A.A. Hatamnia, A. Rostamzad, M. Alinazari, Synthesis and optimization of emission characteristics of water-dispersible ag-in-s quantum dots and their bactericidal activity, Colloids Surf B Biointerfaces. 182 (2019). https://doi.org/10.1016/j.colsurfb.2019.110389.

[187] J.A. Brant, A.E. Childress, Colloidal adhesion to hydrophilic membrane surfaces, J Memb Sci. 241 (2004) 235–248. https://doi.org/10.1016/j.memsci.2004.04.036.

[188] R. Beckett, N.P. Le, The Role of Organic Matter and Ionic Composition in Determining the Surface Charge of Suspended Particles in Natural Waters, 1990.

[189] J.S. Park, H.J. Lee, S.J. Choi, K.E. Geckeler, J. Cho, S.H. Moon, Fouling mitigation of anion exchange membrane by zeta potential control, J Colloid Interface Sci. 259 (2003) 293–300. https://doi.org/10.1016/S0021-9797(02)00095-4.

[190] G.C.C. Yang, C.J. Li, Electrofiltration of silica nanoparticle-containing wastewater using tubular ceramic membranes, Sep Purif Technol. 58 (2007) 159–165. https://doi.org/10.1016/j.seppur.2007.07.019.

[191] T.M. Qaisrani, W.M. Samhaber, Impact of gas bubbling and backflushing on fouling control and membrane cleaning, Desalination. 266 (2011) 154–161. https://doi.org/10.1016/j.desal.2010.08.019.

[192] Z. Zhang, G. Huang, Y. Li, X. Chen, Y. Yao, S. Ren, M. Li, Y. Wu, C. An, Electrically conductive inorganic membranes: A review on principles, characteristics and applications, Chemical Engineering Journal. 427 (2022). https://doi.org/10.1016/j.cej.2021.131987.

[193] Q. Gu, T.C.A. Ng, Y. Bao, H.Y. Ng, S.C. Tan, J. Wang, Developing better ceramic membranes for water and wastewater Treatment: Where microstructure integrates with chemistry and functionalities, Chemical Engineering Journal. 428 (2021). https://doi.org/10.1016/j.cej.2021.130456.

[194] Y. Liu, Y. Ren, S. You, Electrified carbon nanotube membrane technology for water treatment, in: Electrochemical Membrane Technology for Water and Wastewater Treatment, Elsevier, 2022: pp. 111–140. https://doi.org/10.1016/B978-0-12-824470-8.00013-9.

[195] G. V. Buxton, C.L. Greenstock, W.P. Helman, A.B. Ross, Critical Review of rate constants for reactions of hydrated electrons, hydrogen atoms and hydroxyl radicals (·OH/·O− in Aqueous Solution, J Phys Chem Ref Data. 17 (1988) 513–886. https://doi.org/10.1063/1.555805.

[196] A.M.M.M. E. BRILLAS, Electrochemical extraction of oxygen from air via hydroperoxide ion, J Appl Electrochem. (1997) 83–92.

[197] E. Brillas, I. Sirés, M.A. Oturan, Electro-fenton process and related electrochemical technologies based on fenton's reaction chemistry, Chem Rev. 109 (2009) 6570–6631. https://doi.org/10.1021/cr900136g.

[198] M.A. Halali, M. Larocque, C.F. de Lannoy, Investigating the stability of electrically conductive membranes, J Memb Sci. 627 (2021). https://doi.org/10.1016/j.memsci.2021.119181.

[199] R.K. Sharma, S. Yadav, S. Dutta, H.B. Kale, I.R. Warkad, R. Zboril, R.S. Varma, M.B. Gawande, Silver nanomaterials: Synthesis and (electro/photo) catalytic applications, Chem Soc Rev. 50 (2021) 11293–11380. https://doi.org/10.1039/d0cs00912a.

[200] M. Yi, L. Tian, Y. Liu, L. Shen, C. Ding, T. Zhu, X. Yu, Y. Wang, Thin-Film Composite Polyamide Membranes with In Situ Attached Ag Nanoparticles for Fouling-Mitigated Wastewater

Treatment, ACS ES and T Water. 1 (2021) 1901–1910. https://doi.org/10.1021/acsestwater.1c00139.

[201] Q. Bao, D. Zhang, P. Qi, Synthesis and characterization of silver nanoparticle and graphene oxide nanosheet composites as a bactericidal agent for water disinfection, J Colloid Interface Sci. 360 (2011) 463–470. https://doi.org/10.1016/j.jcis.2011.05.009.

[202] H. Zhang, J.A. Smith, V. Oyanedel-Craver, The effect of natural water conditions on the anti-bacterial performance and stability of silver nanoparticles capped with different polymers, Water Res. 46 (2012) 691–699. https://doi.org/10.1016/j.watres.2011.11.037.

[203] M. Rai, S. Birla, A.P. Ingle, I. Gupta, A. Gade, K. Abd-Elsalam, P.D. Marcato, N. Duran, Nanosilver: An inorganic nanoparticle with myriad potential applications, Nanotechnol Rev. 3 (2014) 281–309. https://doi.org/10.1515/ntrev-2014-0001.

[204] L. Huang, S. Zhao, Z. Wang, J. Wu, J. Wang, S. Wang, In situ immobilization of silver nanoparticles for improving permeability, antifouling and anti-bacterial properties of ultrafiltration membrane, J Memb Sci. 499 (2016) 269–281. https://doi.org/10.1016/j.memsci.2015.10.055.

[205] S. Dhibar, C.K. Das, Electrochemical performances of silver nanoparticles decorated polyaniline/graphene nanocomposite in different electrolytes, J Alloys Compd. 653 (2015) 486–497. https://doi.org/10.1016/j.jallcom.2015.08.158.

[206] Q. Li, Q. Zhang, L. Ding, D. Zhou, H. Cui, Z. Wei, J. Zhai, Synthesis of silver/multi-walled carbon nanotubes composite and its application for electrocatalytic reduction of bromate, Chemical Engineering Journal. 217 (2013) 28–33. https://doi.org/10.1016/j.cej.2012.12.005.

[207] K. Wang, D. Hou, J. Wang, Z. Wang, B. Tian, P. Liang, Hydrophilic surface coating on hydrophobic PTFE membrane for robust anti-oil-fouling membrane distillation, Appl Surf Sci. 450 (2018) 57–65. https://doi.org/10.1016/j.apsusc.2018.04.180.

[208] Y.S. Guo, X.D. Weng, B. Wu, Y.F. Mi, B.K. Zhu, Y.L. Ji, Q.F. An, C.J. Gao, Construction of nonfouling nanofiltration membrane via introducing uniformly tunable zwitterionic layer, J Memb Sci. 583 (2019) 152–162. https://doi.org/10.1016/j.memsci.2019.04.055.

[209] M.S.S.A. Saraswathi, D. Rana, S. Alwarappan, S. Gowrishankar, P. Vijayakumar, A. Nagendran, Polydopamine layered poly (ether imide) ultrafiltration membranes tailored with silver

nanoparticles designed for better permeability, selectivity and antifouling, Journal of Industrial and Engineering Chemistry. 76 (2019) 141–149. https://doi.org/10.1016/j.jiec.2019.03.014.

[210] W. Yu, Y. Liu, Y. Xu, R. Li, J. Chen, B.Q. Liao, L. Shen, H. Lin, A conductive PVDF-Ni membrane with superior rejection, permeance and antifouling ability via electric assisted in-situ aeration for dye separation, J Memb Sci. 581 (2019) 401–412. https://doi.org/10.1016/j.memsci.2019.03.083.

[211] X. Fang, R. Li, Z. Zhang, X. Zhang, F. Li, Y. Liu, Electrically Conductive PVDF Ultrafiltration Membrane with in Situ Formation of a Ag NP Coating Layer for Perm-Selectivity Enhancement and Fouling Mitigation, ACS ES and T Water. 2 (2022) 2706–2715. https://doi.org/10.1021/acsestwater.2c00476.

[212] P. Salarizadeh, M. Javanbakht, S. Pourmahdian, M.S.A. Hazer, K. Hooshyari, M.B. Askari, Novel proton exchange membranes based on proton conductive sulfonated PAMPS/PSSA-TiO2 hybrid nanoparticles and sulfonated poly (ether ether ketone) for PEMFC, Int J Hydrogen Energy. 44 (2019) 3099–3114. https://doi.org/10.1016/j.ijhydene.2018.11.235.

[213] C.F. de Lannoy, D. Jassby, D.D. Davis, M.R. Wiesner, A highly electrically conductive polymer-multiwalled carbon nanotube nanocomposite membrane, J Memb Sci. 415–416 (2012) 718–724. https://doi.org/10.1016/j.memsci.2012.05.061.

[214] A. V. Dudchenko, J. Rolf, K. Russell, W. Duan, D. Jassby, Organic fouling inhibition on electrically conducting carbon nanotube-polyvinyl alcohol composite ultrafiltration membranes, J Memb Sci. 468 (2014) 1–10. https://doi.org/10.1016/j.memsci.2014.05.041.

[215] A. Thamilselvan, P. Manivel, V. Rajagopal, N. Nesakumar, V. Suryanarayanan, Improved electrocatalytic activity of Au@Fe 3 O 4 magnetic nanoparticles for sensitive dopamine detection, Colloids Surf B Biointerfaces. 180 (2019) 1–8. https://doi.org/10.1016/j.colsurfb.2019.04.034.

[216] Y. Xiang, M.B. Camarada, Y. Wen, H. Wu, J. Chen, M. Li, X. Liao, Simple voltammetric analyses of ochratoxin A in food samples using highly-stable and anti-fouling black phosphorene nanosensor, Electrochim Acta. 282 (2018) 490–498. https://doi.org/10.1016/j.electacta.2018.06.055.

[217] G. Bargeman, G.-H. Koopsb, J. Houwing, I. Breebaartb, H.C. Van Der Horsta, M. Wesslingb, The development of electro-membrane filtration for the isolation of bioactive peptides: the effect of membrane selection and operating parameters on the transport rate, 2002.

[218] T.H.J.A. Sleutels, A. Ter Heijne, C.J.N. Buisman, H.V.M. Hamelers, Bioelectrochemical systems: An outlook for practical applications, ChemSusChem. 5 (2012) 1012–1019. https://doi.org/10.1002/cssc.201100732.